JAYSON TESSIER

# MULTIVARIATE STATISTICAL ANALYSIS OF HALL-HÉROULT REDUCTION CELLS

## Investigation and monitoring of factors affecting performance

Thèse présentée
à la Faculté des études supérieures de l'Université Laval
dans le cadre du programme de doctorat en Génie Chimique
pour l'obtention du grade de Philosophiae Doctor (Ph.D.)

DÉPARTEMENT DE GÉNIE CHIMIQUE
FACULTÉ DES SCIENCES ET GÉNIE
UNIVERSITÉ LAVAL
QUÉBEC

2010

# Résumé

Les cuves d'électrolyse utilisées pour la production aluminium sont soumises à des variations de la qualité des matières premières, à des perturbations diverses encourues en cours de production ou en cours de démarrage. Il est connu que ces perturbations ont un impact sur la durée de vie des cuves ainsi que sur l'efficacité de production, métallurgique et énergétique. L'amélioration des performances passe nécessairement par une meilleure compréhension des sources de variations. Plusieurs travaux ont été présentés jusqu'à présent par le biais d'études univariées entre les différents facteurs et les performances. Cependant, dans ces études, le comportement des cuves n'est pas étudié de manière multivariée, ce qui ne permet pas d'étudier les interactions entre les différentes variables. Cette thèse propose d'étudier les facteurs affectant les performances des cuves d'électrolyse, précisément la duré de vie, le rendement Faraday et la consommation énergétique, par le biais de méthodes statistiques multivariées (PCA et PLS). Premièrement, il est démontré que la durée de vie des cuves est expliquée à 72% en utilisant l'information provenant des préchauffages, des démarrages et de l'opération transitoire, démontrant ainsi l'effet de ces étapes sur la durée de vie des cuves. Cette étude est suivie d'une analyse des facteurs affectant l'efficacité de courant et la consommation énergétique des cuves. L'effet de la qualité de l'alumine, des anodes, des variables manipulées, et des variables d'états des cuves permet d'expliquer 50% des variations des performances. Cette étude démontre l'importance du contrôle de la hauteur de bain. Ainsi, une étude approfondie des facteurs affectant la hauteur de bain est effectuée. La composition du produit de recouvrement des anodes a un impact majeur sur la hauteur de bain. Malheureusement, il est présentement impossible de bien effectuer le suivi et le contrôle de cette composition puisque seulement quelques échantillons sont analysés quotidiennement. Afin de palier à ce manque, cette thèse présente une nouvelle approche, basée sur l'analyse d'image, pour prédire la composition du produit de recouvrement. Cette application faciliterait le suivi et le contrôle de la composition, ce qui améliorerait le contrôle de la hauteur de bain permettant ainsi d'améliorer les performances des cuves.

# Abstract

Aluminum reduction cells are submitted to raw materials quality variations and process upsets, from the operation or from deficient control strategies, different preheating, start-up and early operation behaviour. It is known that these factors have an impact on cells potlife, current efficiency and energy consumption. However, improving these performance indicators requires a good understanding of the variables affecting them. So far, many authors have reported the impact of individual variables on performance instead of considering the cell behaviour as a whole multivariate process. In this thesis, an attempt is made at finding the combinations of raw material properties and process variables having an impact on potlife, current efficiency and energy consumption using different multivariate statistical analysis techniques (PCA and PLS), in order to gain a better understanding of variables interactions. First, the impact of preheating, start-up and early operation on potlife is investigated. It is demonstrated that these steps account for about 72% of the potlife variance, thus highlighting their great impact. An investigation of the factors affecting current efficiency and energy consumption is then presented. Alumina and anode quality are combined with pot manipulated and state variables in order to develop a multivariate regression model between these variables and current efficiency and energy consumption. From this study, only 50% of current efficiency and energy consumption is explained highlighting the fact that some pieces of the puzzle are missing and that more information has to be measured to better understand performance variations. An in-depth study of bath level control is therefore presented as it was previously highlighted important for current efficiency and energy consumption variations. The variable having the greatest effect on bath level is anode cover product composition, which unfortunately is measured on a limited number of samples, thus not known on a pot-to-pot basis. Finally, this thesis presents a novel machine vision solution to predict anode cover product composition within errors compatible with process application. Such a device would enable a better control of anode cover product composition, which in turn would facilitate bath level control and thus improve pot performance.

# Forewords

The work presented in this thesis was performed at the Alcoa Deschambault smelter (Deschambault, QC, Canada) and at the Alcoa Technical Center (Alcoa Center, PA, USA). All results were generated using industrial data.

Following the introduction and two background chapters, the core of this thesis consists of four chapters: one paper submitted to *Metallurgical and Materials Transactions B*, one manuscript in preparation, one consisting of unpublished material and one paper published in *Chemical Engineering Science*. The candidate performed data collection and analysis, wrote the various computer codes and all publication materials under the supervision of his supervisor. The work performed through this thesis also led to four conference papers and one patent. These are presented next with their contribution to the discipline of aluminum reduction.

The first part of this thesis consists of using the information hidden in industrial aluminum smelter databases to highlight and investigate possible causes of variations leading to performance fluctuations.

- At a plant level, variables interactions were investigated to highlight how anodes and alumina quality and pot manipulated variables behaviour combined together led to a performance drop in the potroom area. This paper showed that this particular performance drift was related to the simultaneous degradation of some alumina and anode quality variables concurrently happening with a decrease in bath level.

  [1] Tessier, J., Duchesne, C., Tarcy, G.P., Gauthier, C., Dufour, G., Analysis of a potroom performance drift, from a multivariate point of view, *Proceedings of TMS 2008, Light Metals 2008 Volume 2: Aluminum Reduction Technology*, New Orleans, LA, USA, March 2008, pp 319-324.

- Reduction cells have a limited lifespan due to the degradation of their materials from continuous operation in a highly aggressive environment. The impact of reduction cells preheating, start-up and early operation quality was investigated with respect to cells operating time. This work showed that after only 60 days of

operation, enough information is available to predict potlife within 84 days. Considering that these cells are operated for more than 2000 days, this paper demonstrated that preheating, start-up and early operation have a strong impact on potlife. Therefore, key variables are identified and multivariate statistical process monitoring and control strategies are presented to better monitor them.

[2] Tessier, J., Duchesne, C., Tarcy, G.P., Gauthier, C., Dufour, G., Increasing potlife of Hall-Héroult reduction cells through multivariate on-line monitoring of preheating, start-up and early operation, submitted to *Metallurgical and Materials Transactions B* (Manuscript E-TP-09-195-B, June 23rd, 2009).

[3] Tessier, J., Duchesne, C., Tarcy, G.P., Gauthier, C., Dufour, G., Investigation of the impact of pre-heating, start-up and early operation on potlife *Proceedings of TMS 2010, Light Metals 2010: Electrode Technology,* Submitted on September 15th, 2009.

- Finally, the influence of alumina and anode quality, as well as pot state and manipulated variables were studied with respect to current efficiency and energy consumption variations over complete pot life cycles, from start-up to death. This paper builds on the findings of the paper presented at TMS 2008 [1], but covers them more deeply while focusing on a pot basis instead of a plant basis. It is shown that many variables have an impact on performance and the relative importance of these variables is also highlighted. Again, a multivariate statistical monitoring strategy is presented in order to efficiently monitor the process variables affecting current efficiency and energy consumption.

[4] Tessier, J., Duchesne, C., Tarcy, G.P., Gauthier, C., Dufour, G., Multivariate analysis and monitoring of the performance of aluminum reduction cells, submitted to *Metallurgical and Materials Transactions B* (E-TP-09-335-B, November 24th, 2009)

**Tessier, J.**, Duchesne, C., Tarcy, G.P., Gauthier, C., Dufour, G., 2009, Multivariate Analysis and Monitoring of the Performance of Aluminum Reduction Cells, *Metallurgical and Materials Transactions B*, Soumis le 24 novembre 2009.

Some of these studies have pointed out the fact that bath level control had an important impact on current efficiency and energy consumption. Hence, a chapter investigates the variables contributing the most to bath level variations, which in turns lead to different operational problems negatively affecting pot performance. It is demonstrated that bath level is heavily affected by anode cover material composition, which is not properly controlled. This is presented in a chapter of unpublished materials.

In the second part of this work, the use of image analysis to predict anode cover material composition is presented.

- At first, different image analysis algorithms were investigated on hand-made anode cover material samples covering a wide alumina composition range. Different color and textural image analysis algorithms were investigated. Results demonstrated that it is possible to predict anode cover material composition based on textural features extracted from images captured by a conventional off-the-shelf color (RGB) digital camera.

  [5] Tessier, J., Duchesne, C., Gauthier, C., Dufour, G., 2008, Estimation of alumina content of anode cover material using multivariate image analysis technique, *Chemical Engineering Science*, Vol. 63, March 2008, pp. 1370-1380

- Following this study, an image acquisition set-up was constructed, using a better camera and lightning set-up to ensure constant lightning conditions. This set-up was used to fine-tune the image analysis algorithm based on hand-made and industrial samples of anode cover material. Industrial samples were grabbed from 12 reductions cells over a period of three months. Using the industrial samples, it was shown that it is possible to predict anode cover material composition with a root

mean squared error of prediction of 0.9 % $Al_2O_3$ and that 83.3% of the predictions fall within the laboratory confidence interval.

[6] Tessier, J., Duchesne, C., Gauthier, C., Dufour, G., Anode cover material estimation using image analysis in primary aluminum production, *Preprints of the 12th IFAC Symposium on Automation in Mining, Mineral and Metal Processing*, Quebec City, QC, Canada, August, 2007. pp. 483-489.

[7] Tessier, J., Duchesne, C., Gauthier, C., Dufour, G., Image analysis for the estimation of anode cover material composition, *Proceedings of TMS 2008, Light Metals 2008 Volume 2: Aluminum Reduction Technology*, New Orleans, LA, USA, March 2008, pp. 293-298

[8] Tessier, J., Duchesne, C., Gauthier, C., Dufour, G., *Methods, Systems and Apparatus for Determining Composition of Feed Material of Metal Electrolysis Cells*, U.S. Patent Application publication No. 2009/0107840 A1, filed on October 24th, 2008, published on April 30th, 2009.

# Acknowledgements

Over the past few years, I spend a lot of time working on this thesis. During this time, I have been blessed to be surrounded by many good people who have played a role in this work. This work was made possible through the funding of Alcoa, the Natural Sciences and Engineering Research Council of Canada Industrial Postgraduate Scholarships (NSERC IPS) and the REGAL aluminum research centre.

First, many thanks to Prof. Carl Duchesne. At any time during this work, Carl took the time to wisely step-back and think about the problems I was facing. Thanks for your guidance, support and dedication. A special thanks to Gilles Dufour at Alcoa. In fall 2005, I presented him what I wanted to do for my Ph.D. and he stepped in, fortunately, and directed me to the right folks within the Alcoa network. Without his enthusiasm, this work would not have been possible.

I have been lucky to work during the past four years, and before as an undergrad student, with great people. I would like to thanks the Alcoa Deschambault Potroom, Electrode and Laboratory technical staff. I asked a lot of questions and some of your time and you never said no. A special thanks also to Patrice Doiron for many technical and non-technical discussions and to Claude Gauthier, for his support, time spent during coffee breaks and technical discussions. The time spent traveling with Claude was always a blast. I also travelled to different Alcoa smelters around the world and I spent summer 2007 at the Alcoa Technical Center. Thanks to Gary P. Tarcy, Jay N. Bruggeman, the Hall Process Improvement folks and other Alcoans met during my many trips for sharing their time and knowledge with me.

I would like to express my deepest gratitude to my Mom and Dad, Lorraine and Yves. You two never stopped me from doing what I wanted to do and always stick around no matter what was going on. Thank you for all your help, support and encouragement.

Finally, thanks to Lorrie, my wife, for her endless support, encouragement, dedication, and understanding. Thank you for taking care of Kimi and Axelle when I was away from home for a day or two or for some weeks. I love you all...

*To Lorrie, Kimi, Axelle and David*

# Table of contents

# Table list

# Figure list

# 1 Introduction

Although, it makes up to only about 8% of the Earth's solid weight (Encyclopoedia Britannica (a)) aluminum (Al) is the third most abundant element on Earth, after oxygen (O) and silicon (Si). It is now widely used across the world in many day-to-day applications:

- Transportation : cars, aircrafts, trains, trucks and bicycles parts
- Construction : doors, windows, sidings and electrical wires
- Packaging : cans, containers and wrapping foils
- Electrical transmission lines : cables and towers components
- Powder aluminum : paints, pyrotechnics and rocket fuels

However, aluminum is too chemically reactive to occur in nature as native metal and is found combined in different minerals including bauxite, which is the most common mineral used to extract aluminum. Bauxite contains 40 to 60% alumina ($Al_2O_3$), mainly under gibbsite, böhmite and/or diaspore forms. Hence, aluminum has to be dissociated and as it is not found in native state. Aluminum is a *young* metal when compared to; gold (6000 B.C.), copper (4200 B.C.), silver (4000 B.C.), lead (3500 B.C.), tin (1750 B.C.) or iron (1500 B.C.) used by the Mesopotamians, Egyptians, Greeks and the Romans during the Metal Age. Nevertheless, back in the late 1700, Antoine Laurent de Lavoisier (1743-1794), a French chemist, started to study alumina and noted the affinity of aluminum, a yet undiscovered metal, to oxygen is so strong that it cannot be reduced by carbon or any known reducing agent. In 1825, a Danish chemist, Hans Christian Ørsted (1777-1851) produced small amounts of aluminum from aluminum chloride ($AlCl_3$). Later in 1855, at the Universal Exposition in Paris, the French chemist Henri Etienne Sainte-Claire Deville (1818-1881) presented aluminum plates produced from clay. Deville's researches were financially supported by Napoleon III (1808-1873), emperor of France, who saw a potential for aluminum as a light weight armor material for the French troops. However, the extraction process used by Deville was so expensive and unpromising that aluminum was

considered as a precious metal with more value than gold. Napoleon III once gave a banquet at which the members of the Royal family and the most honoured guests had the privilege to eat with aluminum utensils, while the other ordinary guests had to use gold ones (Venetski, 1969).

However, aluminum was *downgraded* from precious metal to light metal around the beginning of the 20$^{th}$ century when Charles Martin Hall (1863-1914), an American engineer and Louis-Paul Toussaint Héroult (1863-1914), a French scientist, both independently and almost simultaneously filed a patent for a cheaper way of producing aluminum through an electrolytic process, now known as the Hall-Héroult process. Héroult filed a French patent on April 23$^{rd}$, 1886 and in the United States on May 22$^{nd}$, 1886, while Hall submitted his documents to the Unites States Patent Office on July 9$^{th}$, 1886 (Edwards, 1955). Hall later founded the Pittsburgh Reduction Company, now Alcoa, while Héroult created the backbones of Aluminum Pechiney, latter bought by Alcan, now Rio Tinto Alcan.

More than a century later, the Hall-Héroult process is still the only economically viable industrial process for producing aluminum even though scientists and aluminum companies' have worked on major process upgrade like the inert anodes (Welch, 2009), wetted and drained cathodes (Welch, 1999; Keniry, 2001; Thonstad et *al.*, 2001; Li et *al.*, 2008), or on totally different processes like the Alcoa Smelting Process involving $AlCl_3$ production and electrolysis (Thonstad et *al.*, 2001) or the carbothermic process (Bruno, 2003; Choate and Green, 2006; Liu et *al.*, 2009). This latter process should have energy, capital and operating costs below those of Hall-Héroult. However, no industrial plants have been built and aluminum producers are still building and planning for greenfield aluminum reduction smelters for the years to come.

In the Hall-Héroult process, alumina powder, obtained from bauxite through the Bayer process (Grjotheim and Kvande, 1993) named after the Austrian chemist Karl Josef Bayer (1847-1904), is dissolved in molten cryolite ($Na_3AlF_6$), known as bath, and is electrochemically dissociated into aluminum and oxygen using a dissociation voltage of 2.21 V (Grjotheim and Kvande, 1993). However, in order to save on electrical energy, the Hall-Héroult process uses carbon anode, thus lowering the dissociation voltage to 1.2 V (Thonstad et *al.*, 2001). Therefore, the global reaction is:

$$2\ Al_2O_{3(diss)} + 3\ C_{(s)} = 4\ Al_{(l)} + 3\ CO_{2(g)} \qquad [1.1]$$

A drawing of Hall's metallurgical reactors used to produce aluminum is presented in Figure 1.1, courtesy of Alcoa. This drawing presents the electrolytic cells, called pots, set-up in the Pittsburgh Reduction Company plant, now Alcoa, on Smallman Street in Pittsburgh, Pennsylvania. This was the first large-scale aluminum production plant. It shows the cast iron pots and the carbon anodes suspended by copper rods and some ingot moulds are also drawn on the plant's floor between the cells. In January 1889, the plant was operated in the 1700-1800 amperes (A) range and the start-up of a second cell boosted the production capacity to 50 pounds a day at a market price of $8.00 a pound.

Figure 1.1: Drawing of Hall's original electrolytic cells.

Since then, many primary aluminum smelters have been built and closed around the world. Active smelters now produce between 14 000 to 950 000 metric tons of molten aluminum per annum and their combined output was close to 38 000 000 metric tons in 2008. Figure 1.2 presents the world primary aluminum production for the period of 1886 to 2008.

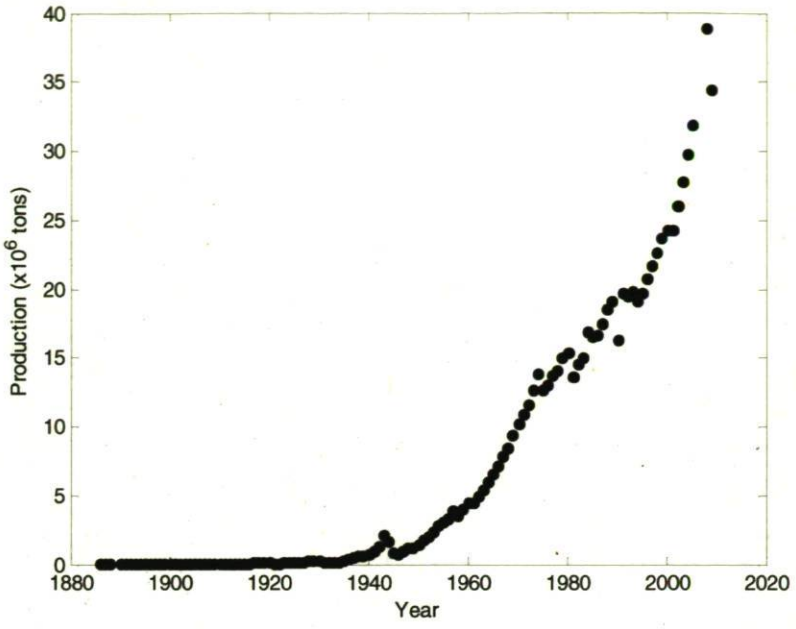


Figure 1.2: World primary aluminum production. Sources: Aluminum Association of Canada www.aia.aluminum.qc.ca (1886-2005) and Alcoa annual reports (2006-2009).

However, modern pots are quite different than those of the Pittsburgh Reduction Company plant; pots and anodes are bigger, electrolytic bath chemistry is optimized to maximize production and applied electrical current could be as high as 500 kA (Benkhala et *al.*, 2008, 2009). Pot design, once made by intuition, trials and errors, is now carefully performed using finite element modelling to select the best materials specifications and configuration in order to achieve high current efficiency, low electrical consumption and high pot life. Haupin (2003) reported that the plant operated at Smallman Street performed at around 31 kWh/kg and 80% current efficiency, significantly less efficient compared to the performances achieved presently by modern smelters in the 13 to 15 kWh/kg and 95% current efficiency. These improvements also came through the development of process control, which were fine tuned and optimized over time (Bearne, 1999; Homsi et *al.*, 2000; Moore at *al.*, 2001; Yurkov et *al.*, 2004; Stevens McFadden et *al.*, 2006), better pot designs and also from the use of pot computer simulators to help predict pot behaviour after set point changes (Tabsh et *al.*, 1996, 1997; Yurkov and Mann, 2005).

As a consequence of these improvements, most of nowadays pots are operated well above their nominal production capacity, thus boosting up smelters production using already existing assets. Major research and investments programs helped producing more and more metal with the same equipments. Therefore, many smelters performed load creeps, close to 20% (Proulx et *al.*, 2006) through better pot designs, improved magnetic compensation and advanced pot control algorithms. Nevertheless, these pots are operated within a smaller operational window and the margin left for error shrunk over time as pot robustness is often compromised. For example, at a plant start-up say 20 years ago, a well designed pot technology that was very robust to operational upsets is now operated over its nominal design and might now heavily be affected by these operational upsets. Unfortunately, it is known that some coke and alumina quality properties, the Hall-Héroult raw materials, are degrading (Lindsay, 2005; Adams et *al.*, 2009; Baron et *al.*, 2009; Wilkening, 2009). As a result, keeping good performance becomes an issue faced by many plant operators around the world.

This thesis aims at identifying and understanding the different sources of variations having an impact on pot performance. Here, pot performance is defined as current efficiency (CE), energy efficiency (EC) and potlife. Identifying parameters having the greatest impact on performance should help develop, implement and perform a good monitoring and control of these few variables therefore ensuring and sustaining good pot performance. Over the years, many authors have investigated pot performance and many studies have been published in the open literature. Several of these have been presented at the TMS annual conference (The Minerals, Metals and Materials Society) or at the Australasian Aluminum Smelter Technology Conference and Workshop held every three years. So far, many studies were performed in laboratory cells, investigating parameters using the one at the time approach. Some other works were based on industrial cells, but again often carried-out in a piece-wise fashion, as parameters were studied one after the other, without fully investigating cells as multivariate processes. As proposed in this thesis, it is advantageous to study this process as a whole and to take into account, simultaneously, all available information to better understand performances variations. To achieve this goal, multivariate statistical methods are used throughout this thesis to better understand aluminum reduction cell performance variations, but also to obtain new information or measurements that could

be useful to better control aluminum reduction cells through multivariate process monitoring tools.

This thesis consists of eight chapters, including this introduction. The links between the chapters are illustrated in Figure 1.3. Chapters in light blue have been submitted or accepted in scientific journals while the others correspond to manuscripts in preparation. Background on aluminum reduction and Multivariate Statistical Methods, also known as Latent Variable Methods, are found in chapter 2 and 3, respectively. Chapter 4 presents the investigation of factors having an impact on potlife variations, while factors having an impact on pot current efficiency and energy consumption are presented in chapter 5. From the discussions arising in both of these chapters, it is demonstrated that controlling bath level is important. Therefore, the most important variables influencing bath level are presented in chapter 6, where it is demonstrated that the current bath level monitoring strategy is insufficient for control purposes. In chapter 7, a novel machine vision approach is proposed to estimate alumina content within the anode cover material, the variable contributing the most to bath level variations. Finally, conclusions are drawn and future works are discussed in chapter 8.

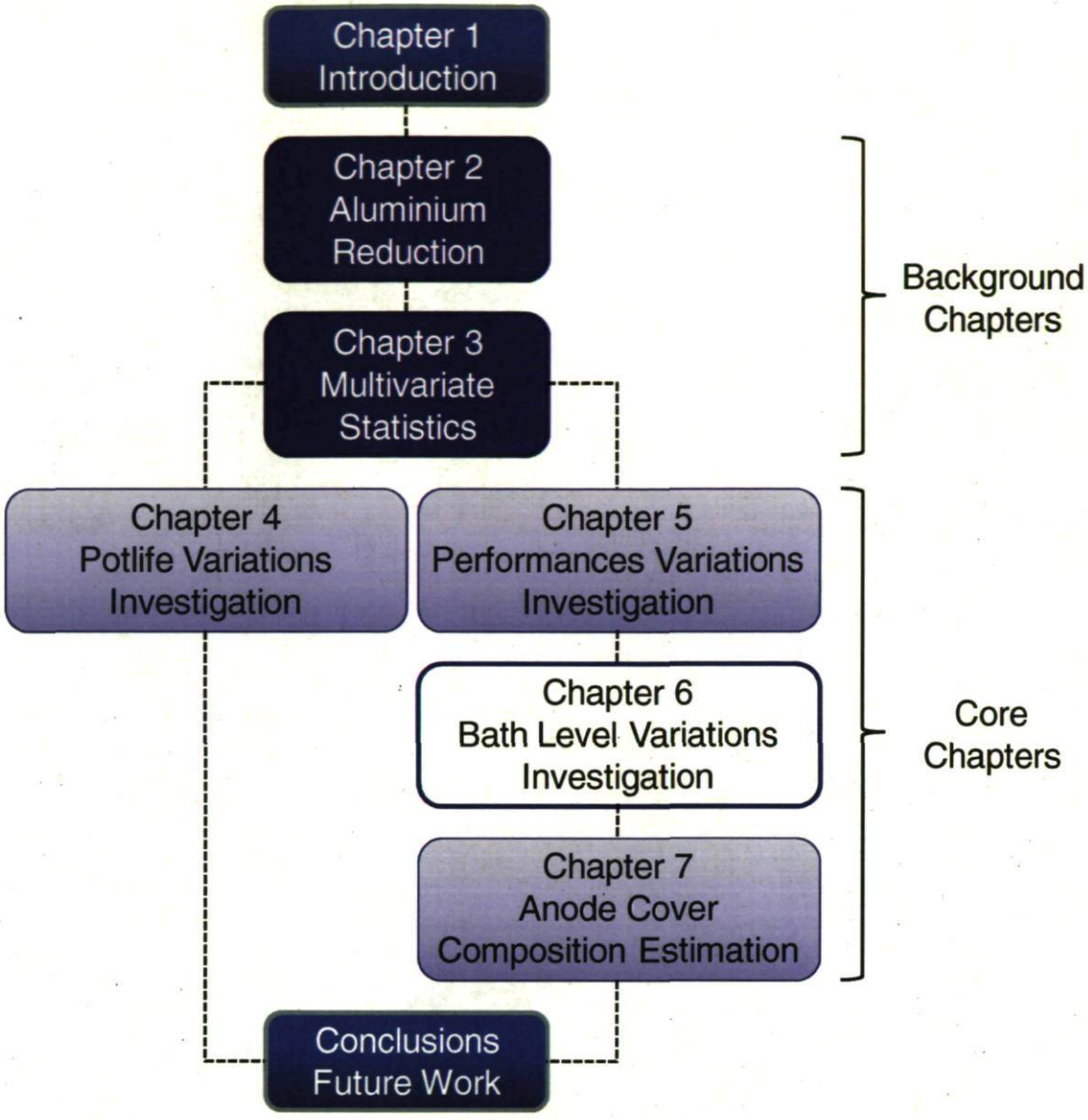


Figure 1.3: Organisation of the thesis.

# 2 Aluminum Reduction Background

The Hall-Héroult process takes place in metallurgical reactors called pots or cells. In such a reactor, alumina is fed and dissolved in a hot molten electrolytic bath consisting mainly of cryolite ($Na_3AlF_6$), aluminum fluoride ($AlF_3$) and calcium fluoride ($CaF_2$). Other additives such as lithium fluoride (LiF), magnesium fluoride ($MgF_2$) or potassium fluoride (KF) are sometimes added to modify the bath electrophysical properties (Haupin and Kvande, 1993; Kvande, 1994; Thonstad et *al.*, 2001). The bath is kept at a temperature of 940 to 970°C by the heat generated by the resistance to the passage of a high continuous electric current and alumina is electrochemically dissociated into aluminum and oxygen through Eq. [1.1]. Oxygen further reacts with carbon anodes to produce gaseous carbon dioxide ($CO_2$) and liquid aluminum settles at the bottom of the pot. This chapter presents the basis of the Hall-Héroult process and the problems covered through this thesis. The reader is referred to the books of Grjotheim and Kvande (1993) and Thonstad et *al.* (2001), and to the paper of Haupin (1995) for more information on the Hall-Héroult process.

## 2.1 The Reactor

Two types of Hall-Héroult reactors are used for industrial production of aluminum. Pictures of different pot technologies are presented in Figure 2.1 to illustrate their evolution over the last century.

The first type of pot is the Söderberg, named after a Norwegian engineer, C.W. Söderberg (1876-1955). It uses a continuous self baking carbon anode. The extra heat added to the pot, discussed later in this chapter, is used to pyrolyze the coke and pitch mixture placed on top of the pot. As the lower part of the anode is consumed by the reaction (Eq. [1.1]), more material is added on top of the anode. As coke and pitch mixture travel down in the pot, its temperature increases, thus baking the mixture and converting it to solid carbon.

The second type of reactor, commonly used in modern smelters, uses prebaked carbon anodes. Tabereaux (2000) reported that over 50 types of prebaked pot technology were in used in year 2000. In prebaked technology pots, melted pitch and coke aggregates are mixed together and moulded into blocks called green anodes. These blocks are baked in a

furnace, cooled down and fixed to an aluminum or copper rod. This forms an anode assembly. Prebaked pots are equipped with many anode assemblies, together forming a single operational anode and the lower part of the carbon blocks is dipped in the molten electrolyte. The bottom surface of the anode part, immersed a few centimetres in bath, takes part of the reaction (Eq. [1.1]).

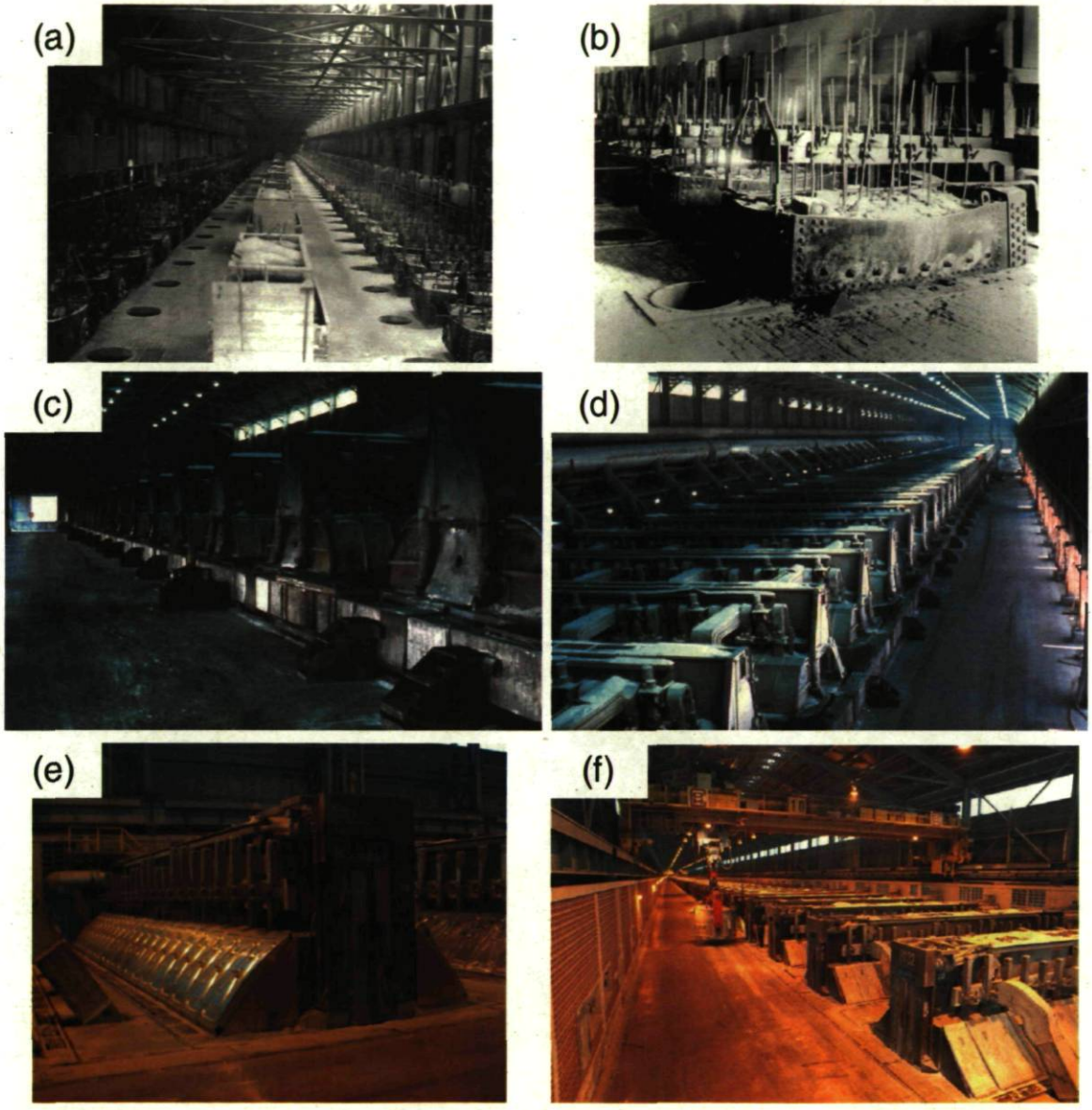


Figure 2.1: Evolution of aluminum reduction cells prebaked technology over the last hundred years. (a,b) at Massena, NY in 1914; (c,d) Alcoa's P-255 at Massena in 1977 and (e,f) Aluminum Pechiney's AP-30 at Deschambault, QC in 2005. Courtesy of Alcoa.

This thesis focuses on prebaked pots, but many of the issues investigated in this thesis are also encountered in Söderberg pots. Most contributions made in this thesis could easily be extended to Söderberg pots. A cross-section view of a Hall-Héroult reactor, using prebaked anodes, is presented in Figure 2.2.

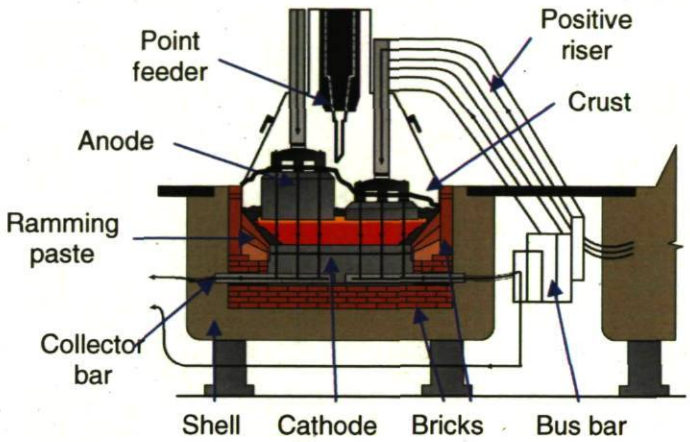


Figure 2.2: Cross-section view of a prebaked Hall-Héroult reactor. Courtesy of Alcoa.

## 2.2 The Electrolyte

Alumina has a melting point of over 2072°C (Patnaik, 2002) and operating the process at this temperature would require a lot of energy. Back in the late 19th century, Hall searched for a solvent for alumina while Héroult was looking for additives to lower the melting point of alumina. This is how they both end up using molten cryolite as a primary bath constituent, due to its capacity to dissolve alumina, but also since this binary system ($Na_3AlF_6$-$Al_2O_3$) has an eutectic point at 965.9°C and 10.07 wt % $Al_2O_3$ (Thonstad et *al.*, 2001). However, by increasing the aluminum fluoride content, it is possible to operate the process in the 940 to 970°C range, at 2-4 weight % $Al_2O_3$. Even if the electrolyte is not consumed by the reaction, some losses occur through vaporisation and hydrolysis (Haupin and Kvande, 1993) or by penetration into the pot lining (Sorlie and Øye, 1989). Different additives like $AlF_3$, $CaF_2$, LiF, $MgF_2$ or KF are also added in order to optimize the

electrolyte physicochemical properties. These additives have an impact on the electrolyte properties such as:

- Liquidus temperature,
- Aluminum solubility,
- Electrical conductivity,
- Density,
- Interfacial tension,
- Vapour pressure,
- Viscosity,
- Etc...

All these additives have the advantage of lowering the electrolyte melting point, which reduces the energy consumption. Unfortunately, they also reduce the alumina solubility and hence, their addition must be carefully controlled through bath chemistry control strategies in order to obtain and maintain the desired physicochemical properties. Typically, bath chemistry is controlled by addition of $AlF_3$ and $Na_2CO_3$ (Entner, 1992; Vanvoren, 2001; Rieck, et *al.*, 2003; Paulino et *al.*, 2006; Kolas and Støre, 2009). $AlF_3$ is added to increase the excess of $AlF_3$, while $Na_2CO_3$ might be added to lower the excess. However, some smelters also control LiF and $MgF_2$ content.

The electrolyte basically plays three roles in the Hall-Héroult cell. First, it is used as a solvent for alumina. Second, it acts as an electrical resistance that makes the pot to be self heated. However, bath electrical resistivity varies with temperature and chemistry. Hence, the amount of heat generated in a pot is controlled through heat balance control strategies manipulating bath chemistry and anode-cathode distance (ACD), which is the distance the electrical current has to flow in the bath. Finally, the electrolyte also acts as a self container. The electrolytic bath, a hot mixture of fluoride salts, has the capacity of dissolving almost any materials suitable for pot construction. However, if heat balance is well controlled (i.e.

chemistry and ACD are in control), it is possible to freeze a layer of bath over the cell's internal walls, preventing molten bath to chemically attack pot materials.

Industrial modern prebaked cells contain between 4 and 7 tons of bath which gives bath levels in the range of 13-20 cm and a frozen layer thickness of a few centimetres on the sidewalls of the pot. However, strategies used to increase production often involve increasing the anode dimensions, leading to a greater anode bottom surface, allowing for nearly constant anode current density. As the reactor dimensions remain constant, this has the negative impact of lowering the volume of molten bath available to dissolve alumina.

## 2.3 The Alumina

Modern pots are equipped with 1 to 5 automatic point feeders (Figure 2.2) used to supply small dumps of 1-2 kg of alumina. Together with heat balance, alumina concentration is an important parameter to control for maintaining pot performance. Unfortunately, no device is yet available to monitor alumina concentration in bath during normal operation. Nevertheless, it is known that bath resistivity changes with alumina concentration. Figure 2.3 presents typical curves of total cell resistance against alumina composition obtained from three industrial pots with different bath chemistries and temperatures. The three curves follow the same shape and their differences are mostly driven by bath properties. Still, independently of the exact location of the curve, it can be used to determine if a pot is running too rich or too lean in alumina. For a defined period of time, the alumina feeders are stopped, the ACD is kept constant and the pot control system tracks the derivative of the pot resistance over time. The resistance variation is hence only associated to the alumina depletion rate in the bath. This procedure computes the slope of the resistance with respect to time ($\frac{dr}{dt}$) and, based on the value and the sign of the slope, the feeders feed frequency are set to a new value. Basically, these feeding frequencies are called *over-feed*, *theoretical-feed* or *under-feed*, meaning that the feeders deliver more, equal or less than the theoretical alumina consumption, depending upon whether the pot is lean, on target or rich in alumina.

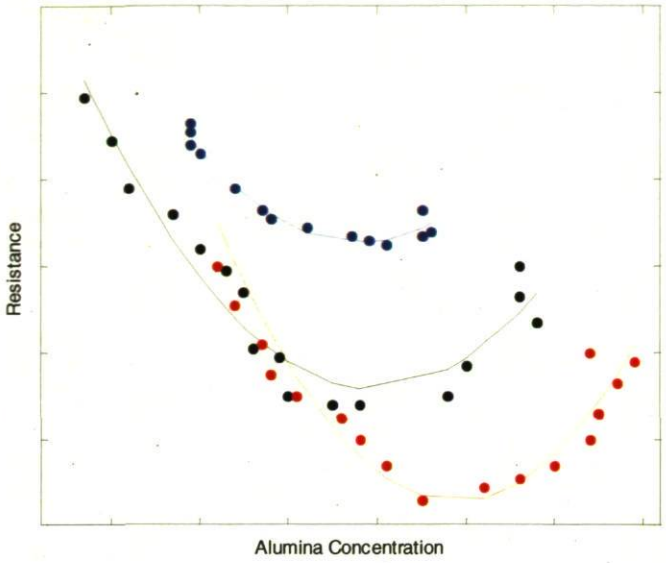


Figure 2.3: Variation of cell resistance with alumina concentration at constant ACD.

In the past, large doses of alumina were added to the pots of older technology every few hour's intervals, creating important upset in pot behaviour induced by large variations in alumina concentration. However, in modern cells, the use of point feeders enable the addition of smaller doses of alumina which increases its mixing and dissolution rates in the bath and also ensure smaller composition variations. Dissolved alumina composition is kept in the range of 1.5-3.0 wt % through complex alumina feeding strategies, which are different for each company. This minimizes the electrical consumption since this range gives the lowest bath resistivity (i.e. the minima of the curves in Figure 2.3) if all other parameters are kept constant.

Fine tuning of the feeding strategies is one of the keys to improve pot performance. *Over-feeding* a pot for a long period of time can generate excessive amount of undissolved alumina that settles at the bottom of the pot. This will further create sludge or muck lowering pot performance through the generation of horizontal magnetic fields inside the pot. On the other hand, *under-feeding* a pot for an extended period of time may lead to an anode effect and, in turn, to a very high cell voltage of up to 30-40 V (Metson et *al.*, 2002; Tabereaux, 2007). Anode effects have a negative impact on pot performance since they

disturb the thermal balance of the pot, but also generate perfluorocarbons compounds (gaseous $CF_4$ and $C_2F_6$) involved in global warming (Dando et *al.*, 2008).

Smelter grade alumina is generally not directly fed to the pot. Since it has the ability to capture fluoride gases, alumina is used in pot gas scrubbing systems, called dry scrubbers, to capture most of fluoride gases coming out of the pots through evaporation and entrainment (Haupin and Kvande, 1993). By capturing fluoride gases emitted from the pots, dry scrubbers charge the smelter grade alumina with fluoride, producing the so-called enriched or secondary alumina used to feed the pots. Therefore, fluoride is reintroduced in the pot, thus lowering the $AlF_3$ consumption and protecting the environment by lowering the amount of fluoride gases escaping aluminum reduction plants. Secondary alumina is generally fed to most of the pots unless a plant has a high purity *potline* where smelter grade alumina is preferred in order to reduce metallic impurities coming from pot gases flowing in the gas treatment systems. In such cases, pot gases can be treated with wet scrubbers.

## 2.4 The Anodes

Prebaked anodes are a mixture of petroleum coke aggregate and coal tar pitch binder. The mixture is moulded in blocks, called green anodes, weighting from 500 to 1000 kg and baked in a furnace at temperatures in the range of 1050-1200°C (Fisher et *al.*, 1995). The final baking temperature is extremely important as it directly affects air and $CO_2$ anode reactivity. An anode assembly is presented in Figure 2.4. This picture presents the different parts of the assembly. An anode rod, made of aluminum or copper, is used to connect the anode to the pot superstructure anode beam and is linked to the steel stubs by a metal clad. The connection between the carbon block and the steel stub is made with cast iron.

Modern prebaked pots have between 16 and 40 anodes. These are consumed in the process (Eq. [1.1]) and must be replaced at regular interval, typically on a 20 to 30 days cycle, before being completely consumed. Hence, by changing some of the anodes on a daily basis, it is possible to change all anodes within the anode cycle. The spent anodes, called butts, are removed from the pots, then air cooled, cleaned from bath particles, dismantled from the anode rod, crushed and reused in the green anode recipe with coke and pitch.


Figure 2.4: Baked carbon anode assembly.

Once a new anode is introduced in the pot, it is covered with a particulate mixture of secondary alumina and/or crushed solid bath, called the anode cover material. This mixture hardens with pot heat losses and forms a crust (Figure 2.2) over the anodes. This crust plays different roles related to pot performance and are discussed in chapter 7.

## 2.5 The Cathode

Typically, a pot is made of an outer steel shell in which different layers of thermal insulating and refractory bricks are placed on its bottom (Figure 2.2). The cathode consists of many prebaked carbon blocks (graphitized, semi-graphitized, semi-graphitic or amorphous), sealed together with a carbonaceous seam mix, placed over the bottom brick layers. Steel collectors bars are embedded in grooves formed at the bottom of the blocks and are fixed by cast iron or a carbon paste (type of glue). The steel shell inner sidewalls are also protected with different layers of thermal insulating and refractory bricks and a carbon-based paste joint, often called ramming paste, is used to fill the gaps between sidewalls and cathode blocks. The refractory bricks layers are used in order to contain the hot electrolytic bath and the molten aluminum. However, no material is known to resist the aggressive conditions inside a pot. Hence thermal insulating bricks layers are designed so

that a defined thickness of protective layer of frozen electrolyte can forms over the sidewalls refractory materials. Pots are thermally designed to insure that the right thickness of frozen bath covers the sidewalls while preventing the bath from freezing over the cathode surface. As it is the case with alumina *over-feeding*, frozen bath over the cathode surface, called *bottom ridge*, would generate horizontal magnetic fields in the pot (Grjotheim and Kvande, 1993) and would also deteriorate the electrical contact between the aluminum pad and the cathode blocks (Thonstad et *al.*, 2001). In fact, even if the carbon blocks are called cathodes, the operational cathode is actually the liquid aluminum pool surface laying on the cathode blocks.

## 2.6 The Potlines

In an aluminum reduction plant, several pots are electrically connected in series to form a *potline*, with the cathode of an upstream pot connected to the anodes of its downstream pot. For example, the Alcoa Deschambault smelter (ADQ) operates 264 AP-30 pots. In order to close the electric circuit, the *potline* is divided in two *potrooms* each containing 132 pots. Figure 2.1(f) presents a picture of ADQ's *potroom* B.

For a single pot, the current enters through the positive risers (Figure 2.2) and flows through the anode beam and the anode assemblies which are connected in parallel to the anode beam using clamps (Figure 2.4). The current leaves the anodes and passes through the electrolytic bath, the aluminum pad and the cathodes blocks. Finally, the current exits the pot through the collector bars and is directed to the next pot through a bus bar system.

Some modern smelters operate in the 350-370 kA electrical current range (Martin et *al.*, 2006; Proulx et *al.*, 2006; Benkahla et *al.*, 2008) and the side-by-side pot arrangement helps reducing the magnetic fields induced by the high electrical current flowing inside the *potline*. The bus bar system is designed in order to compensate magnetic fields imbalance and thus lowering the magnetic stirring of liquid aluminum. However, even with the best magnetic compensation arrangement, pots often experience periods of magnetic fields imbalance called instability or *pot noise*. In general, these periods are characterized by a lower metallurgical output and actions must be quickly taken to bring *noisy* pots back to good operational performance.

Each pot is controlled using one or many levels of pot controllers aiming at rejecting disturbances and stabilising pot operation during various manual operations. The main sub-processes controlled by pot controllers are alumina feeding, bath chemistry, heat balance, noise control, anode effect suppression, metal tapping and anode setting. Due to the proprietary information enclosed in the control logics, few details are given in the open literature and no further details will be given here.

## 2.7 The Pot Life Cycle

The aluminum reduction reaction (Eq. [1.1]) is carried out at high temperature in the presence of different fluoride compounds. Hence, the combined effect yields extremely aggressive conditions deteriorating pot materials. Even if the pot lining is protected by a layer of frozen bath, pot materials have a limited lifespan due to exposure to the aggressive conditions. For example, repeated high temperature excursions can attack the brick layers by degrading their insulating and refractory performance to the point where the outer steel shell can deform, exfoliate or even melt. Cathode blocks can even crack if mechanical stresses are above their mechanical limits. These cracks could enable liquid aluminum or molten bath to penetrate and infiltrate through the brick layers, which is harmful to pot life and performance since it disturbs the heat balance as it may create a heat sinks. Hence, material deterioration from many repeated events, or even from one single, but important event, can eventually end pot service life.

End of a pot life can happen in many ways. A pot can stop operating due to a metal leak, where liquid aluminum penetrates the cathode blocks and attacks the bricks or the collector bars. In the worst case scenario, liquid aluminum reaches and melts the steel collector bars and liquid aluminum can flows out of a pot. A pot life can also end as a result of a side failure which happens when molten bath flows through the sidewalls bricks, and attacks and melts the steel shell sides. In this case, molten bath flows out of the pots. In the event of damage to the upper sidewalls, it may be possible to lower the pot liquids levels (bath and metal level) and operate this pot for an extended period of time. However, if the attack affects the lower part of the sidewalls or is too severe, the pot life ends from the molten bath attack. These two types of failures are highly undesirable, but are encountered quite often. The other way pot life can ends is due to weak metallurgical performance or high

metal contamination, resulting from pot materials deterioration. For example, if the materials deterioration is too advanced to keep the pot in control or if the metallurgical efficiency becomes too low, *potline* operators can decide to stop a pot. It is better to stop a pot before molten bath or liquid aluminum tap out of the pot since both leak types can destroy the bus bar system and break the electrical circuit, jeopardizing plant operation. In general, potlife ranges from 4 to 7 years, depending on pot technologies. However, early failures are an important issue, and Maharaj et *al.*, (1991) reported losing 15% of their pots at an average age of 400 days, which is catastrophic for a smelter economical performance. Unfortunately, such early failures are generally not common in modern smelters. A typical pot life cycle is illustrated in Figure 2.5 and will serve as a basis for discussions.

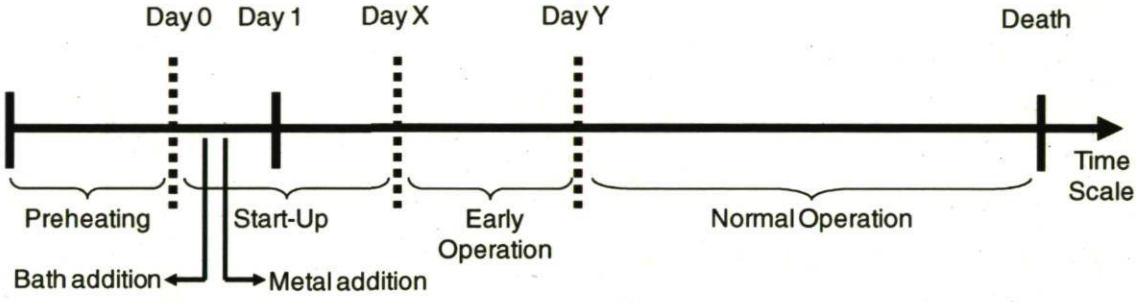


Figure 2.5: Typical pot life cycle.

### 2.7.1 Preheating, start-up and early operation

Following its construction, a new pot must be preheated. The preheating stage slowly raises pot materials from room temperature of 20-30°C to their operating temperature of 800-950°C. This step gives times to the steel shell, cathode blocks and collector bars to expand due to thermal expansion but also to properly bake the different carbonaceous pastes used to seal the cathodes blocks together. Once baked, this paste should mechanically behave like cathode blocks (Richard, 2004). Preheating objectives are discussed later in this thesis (i.e. chapter 4), but the main objectives are (Zangiacomi et *al.*, 2005, 2006):

- To generate a smooth transition to high pot operating temperature,
- To smoothly bake ramming paste and prevent its pyrolysis,

- To obtain cathode final temperature high enough to prevent bath freezing during start-up.

Following the preheating period, a defined quantity of molten bath is added to the new pot. This initiates the start-up period. This bath fills the cracks within cathode blocks and paste voids to prevent metal and bath infiltration in the brick layers during operation. A few hours later, a defined quantity of liquid metal is added to the pot. It is added to stabilize pot operation since it is designed to operate with a certain level of liquid aluminum (i.e. magnetic and heat balance design). Molten bath and liquid metal is coming from nearby pots located inside the *potline*.

From there, the early operation period aims at bringing pot parameters (bath chemistry, temperature, resistance, etc...) to their designed set-point control bands. This has to be performed very smoothly in order to prevent further operational problems or performance issues and obtain a long pot life (Sorlie and Øye, 1989).

### 2.7.2 Normal operation

In modern *potrooms*, the two most important manual operations are metal tapping and anode replacement. As seen in Figure 2.1(f), *potrooms* are equipped with overhead cranes that allow manual operations on the pots. Two types of cranes are typically used; the tapping cranes, as presented in Figure 2.1(f), are used to tap metal out of the pots whereas the pot tending machines (PTM) cranes are used to replace and cover the anodes and perform anode beam raising operation. Pot control systems are designed to reduce disturbances induced by both of these manual operations. The first two operations are generally performed daily or every other day on a pot basis.

Anode beam raising is also performed manually on the pots. As the anodes are consumed by the reaction (Eq. [1.1]), the anode beam is lowered down relative to the superstructure to keep a fairly constant ACD or resistance. After a few days, the beam becomes too close to its bottom stopper and must be raised so it can be moved downward again. The PTM is hence equipped with a special tool, known as the *spider* or the *octopus*, which releases the anodes from the anode beam, by loosening the clamps, while keeping them electrically connected at a constant ACD. Meanwhile, the anode beam is raised close to its higher

stopper. Anodes are then clamped again to the anode beam and the *spider* travels and performs this operation on another pot. This operation is done every 10 to 20 days.

## 2.8 Pot Performance

### 2.8.1 Introduction

Different metrics are used to quantify pot, *potroom*, and *potlines* performance. However, potlife, current efficiency (CE) and energy consumption (EC) are the three mostly used by process engineers and plant managers to describe and compare performance.

### 2.8.2 Potlife

Potlife is used to report how long pots are operated. Basically, potlife refers to the period of time between start-up and shutdown (Figure 2.5) and is generally expressed in days or years. A large amount of potlife variations are explained by pot technology and cathode type (graphitized, semi-graphitized, semi-graphitic or amorphous). However, for the same pot technology and cathode type, potlife can greatly vary within a smelter. These variations are caused by problems occurring during construction, preheating, start-up and/or normal operation or by pot materials properties variations.

### 2.8.3 Current efficiency

Like any other technical process, the Hall-Héroult process experiences production losses. In the aluminum reduction industry, this is measured using current efficiency. That is the ratio of the actual weight of aluminum produced by electrolysis per unit of time, to the theoretical amount computed from Faraday's laws over the same time period.

The flow of current from the carbon anode to a cathode through the electrolytic bath, containing the dissolved $Al_2O_3$, is used to compute theoretical aluminum production by Faraday's laws (Grjotheim and Kvande, 1993):

- The amount of product formed at each electrode (Al at the cathode and $CO_2$ at the anode) is proportional to the number of coulombs passing through the cell.

- The amount of each electrode product is proportional to the equivalent mass of the product.

Using Faraday's laws, it is possible to determine the amount of aluminum that can theoretically settles at the bottom of a reduction cell during a defined period of time:

$$MP = [Mw/(z * F)] * I * t \qquad [2.1]$$

where MP is the theoretical mass of aluminum produced at the cathode, Mw is the molecular weight of aluminum, z is the number of electrons involved in the electrode reaction, F is Faraday's constant, I is the current flowing through the cell and t is the time window associated with the production of MP.

Using aluminum data, it is possible to rearrange Eq. [2.1] to determine the daily current efficiency of a pot using the correct units:

$$CE = M_{Al} / (I * 0.0080538) \qquad [2.2]$$

where $M_{Al}$ is the metal tap from the pot on a 24 hours basis.

Theoretically, a pot operated at 370 kA could produce 2980 kg of aluminum over a 24 hours basis. However, as mentioned before, production losses lead to current efficiencies lower than 100%. The back reaction is the main reason for current efficiency losses (~ 3 to 5 % CE). In this reaction (Eq. [2.3]), aluminum dissolved in the electrolyte, and in close contact with the $CO_2$ gas formed at the anode, is reoxidized very quickly (assumed to be instantaneous) (Grjotheim and Kvande, 1993). It is thus necessary to keep the amount of metal in solution as low as possible by ensuring good and steady pot operations and control.

$$2\ Al_{(diss)} + 3\ CO_{2(diss)} = Al_2O_{3(diss)} + 3\ CO_{(g)} \qquad [2.3]$$

Some factors increasing aluminum solubility in the bath and thus increasing the back reaction rate are discussed in chapter 5.

For normal operating pots, CE should be around 88-92 % for Söderberg pots and up to 95-96% for modern prebaked cells. There is presently no direct way of measuring current efficiency for process monitoring. In practice, this is computed by dividing the metal tapped from a pot by its theoretical production. However, it is possible to determine the current efficiency over a short period of time using a metal tracer with a quantometer or by potential coulometry (Tarcy and DeCapite, 1990; Tarcy and Sorensen, 1991; Thonstad et *al.*, 2001).

### 2.8.4 Energy consumption

The theoretical energy requirement to carry out the reduction reaction is ~ 6.5 kWh/kg of Al. Operational energy consumption is computed as follows:

$$EC = 2.9806 * U/CE \qquad [2.4]$$

Where, U is the pot voltage (volts), CE is the current efficiency (fraction) and EC is the energy consumption (kWh/kg Al).

However, the benchmark energy consumption is around 13 kWh/kg which leads to 50% energy efficiency. Hence, the remaining energy (6.5 kWh/kg) supplied to the cell is dissipated as heat losses distributed all around the cell. Figure 2.6 presents a typical heat loss distribution for a prebaked cell (Haupin, 1991).

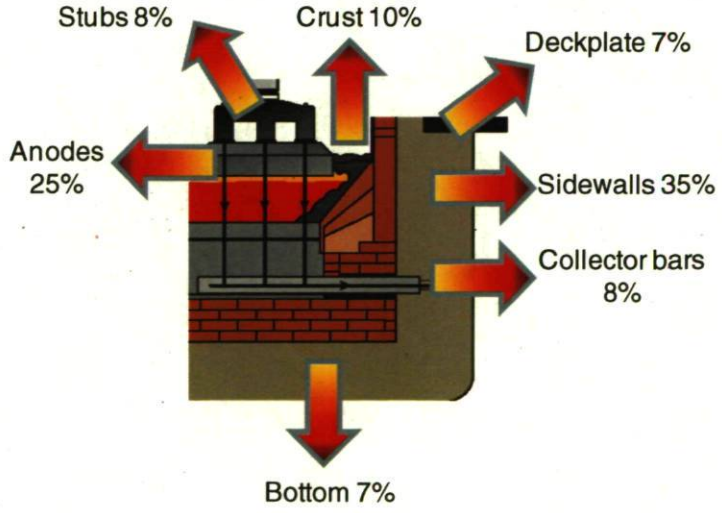


Figure 2.6: Typical prebaked cell heat loss distribution.

## 2.9 Thesis Scope

Pot life cycle can be compared to the human life cycle. The construction and the preheating stages are similar to the foetal development while the start-up period can be seen as a child birth. A child experiencing problems during its foetal development or at birth may have problems during its entire life. Accordingly, a pot experiencing problems during its preheating stage or having trouble during its start-up period may suffers problems leading to low current efficiency, high energy consumption and/or short potlife. The early operation period is similar to the childhood or to the teenage year's period. A young pot needs to mature enough before being operated to its optimal performance, like a child learning how to read and count. During normal operation, a pot is in the productive stage of its life, like most humans during their adult life. Finally, a pot life cycle ends with death just like human life. The performance of mature pots often diminishes slowly before death as many humans physical and mental capacity do.

As mentioned in the Introduction section, the scope of this thesis is to identify sources of variations having an impact on pot performance and to propose efficient monitoring strategies for early detection and, eventually, for implementing appropriate remedial actions. Pot performance is defined jointly by current efficiency, energy consumption and potlife. However, performing such a study is not straightforward since reduction cells are complex multivariate systems. Some of these complex interactions are illustrated in Giuseppe Lazzaro's (formerly at Alcoa Portovesme, Italy) *Pot Flower*, shown in Figure 2.7.

As discussed in the present chapter, reduction cells are a collection of many complex components (i.e. alumina, reactor, electrolyte, etc...) and each of them plays a role with respect to performance. In order to investigate factors having an impact on it, one has to take each of these parts together and cannot study them independently. However, most of the studies performed in the past were carried out in such a way, studying each part, and sometimes just few variables within each part, one at a time.

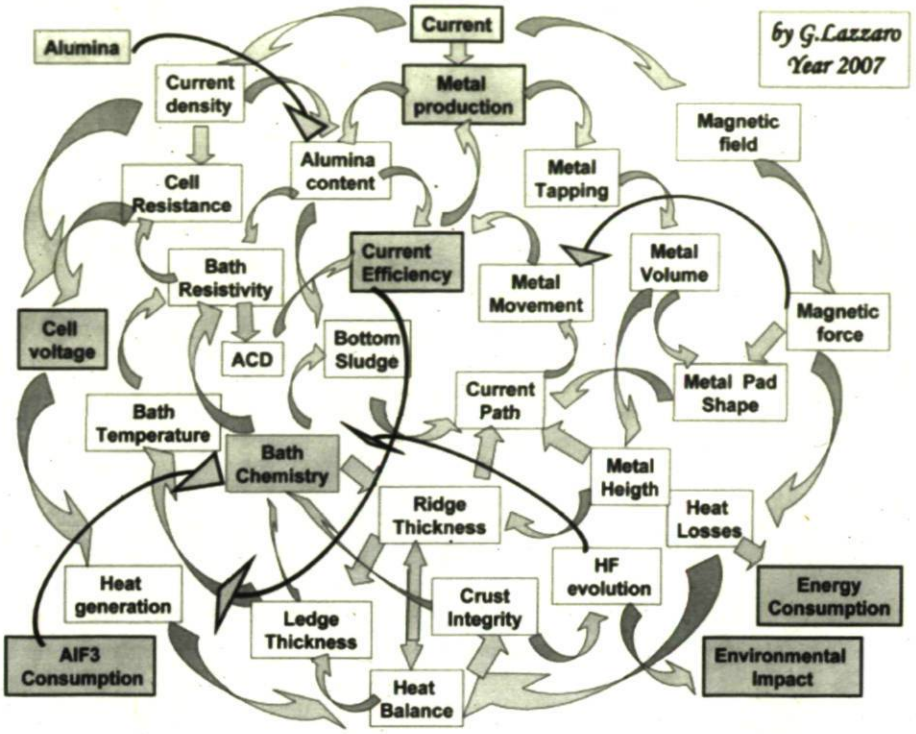


Figure 2.7: Variables interactions within the aluminum reduction process. Courtesy Giuseppe Lazzaro (formerly Alcoa Portovesme, Italy).

The contribution of this thesis is twofold. First, the investigation of factors having an impact on pot performance is presented: (1) the impact of pot preheating, start-up and early operation on potlife variations (Chapter 4), (2) the impact of alumina and anode quality, pot manipulated and state variables and pot preaheating, start-up and early operation on current efficiency and energy consumption throughout a complete pot life cycle (Chapter 5). These studies are performed using multivariate statistical analysis techniques. How to monitor and diagnose performance upsets in a multivariate fashion, as opposed to the traditional univariate methods widely used in the aluminum reduction industry, is also presented. The third study leads to the conclusion that bath level is an important variable in pot performance and hence, factors leading to bath level variations discussed in Chapter 6. Finally, in chapter 7, a new method for estimating anode cover material composition is proposed in order to better monitor and eventually control this leading indicator for bath level variations.

# 3 Background on Multivariate Statistical Methods

Statistics is a mathematical science pertaining to the collection, analysis, interpretation or explanation and presentation of data. It arose, no later than the 17th century, from the need of states to collect data on their people and economies, in order to better administer them (Encyclopoedia Britannica (b)). Its meaning broadened in the early 19th century to include the collection and analysis of data in general.

In the present thesis, statistical methods are used in order to gain a better understanding of process behaviour, or more precisely, for investigating the causes of pot performance variations. Multivariate statistical techniques are used because aluminum reduction is a complex process in which many correlated variables need to be investigated simultaneously. These techniques originate from a particular field of statistics known as chemometrics. This discipline emerged in the 1970's with the better availability and power of computers, although principal component analysis was formulated in 1901 by Karl Pearson (1857-1936), an English mathematician (Wold et *al.*, 1987). Since then, chemometrics methods have been used in different scientific and engineering fields from psychology to chemistry, to process monitoring and control, to image analysis, and in many other areas.

In order to better understand the work presented in following chapters, the basic Chemometrics methods, namely Principal Component Analysis (PCA) and Partial Least Squares (PLS), also known as Projection to Latent Structures, are presented together with additional references for the interested reader. This chapter also discusses the data pre-processing strategies typically used in the field as well as the criteria for selecting the number of principal components in latent variable models. Various extensions to PCA and PLS are also used in this thesis, such as multi-way and multi-block methods, which usage is adapted for specific data structures. These will be presented in sections 4.6, 4.8, 4.9 and 5.5.

Throughout the thesis, vectors are shown using bold lowercase characters (**lowercase**), bold capital characters are used for matrices (**CAPITAL**) and three-dimensional arrays are

similar to matrices but are underlined (**UNDERLINED CAPITAL**). The transpose operator is denoted using uppercase capital T ($\mathbf{X}^T$ or $\mathbf{t}^T$).

Results presented here were obtained using custom codes developed with Matlab® R2006A (The Mathworks Inc., Natick, MA) and the associated Statistics Toolbox V5.3. Moreover, the PLS Toolbox (Eigenvector Research Inc, Wenatchee, WA) was also used in codes development. It is understood here that these codes were developed for the particular problems investigated here and that some modifications may need to be done if one wants to use it for other applications.

## 3.1 Principal Component Analysis (PCA)

Principal Component Analysis is a method used for exploring and modeling multivariate datasets. Detailed mathematical descriptions and tutorials are provided by Wold et *al.* (1987) and Kourti (2002, 2005). Consider **X**, a data table consisting of $I$ observations obtained from $J$ process variables. If *happenstance* data is collected in this matrix (i.e. not gathered under orthogonal designs of experiments) and both $I$ and $J$ are very large (i.e. hundreds to thousands), as it is the case with most datasets obtained from industrial processes, then **X** is not full rank (i.e. **X** is highly collinear). PCA can be used to study the relationships between the variables and to visualise the information contained in **X** (i.e. clusters and patterns) through projecting the data onto a lower dimensional space defined by a small number of principal components or latent variables. In fact, it makes a decomposition of **X**, of rank $R$, as a sum of $R$ matrices of rank 1 which are orthogonal to each other (Geladi and Kowalski, 1986). These matrices ($\mathbf{M}_1$ to $\mathbf{M}_r$) can also be expressed as the outer product of two vectors:

$$\mathbf{X} = \mathbf{M}_1 + \mathbf{M}_2 + \mathbf{M}_3 + \cdots + \mathbf{M}_R + \mathbf{E} \qquad [3.1]$$

$$\mathbf{X} = \mathbf{t}_1\mathbf{p}_1^T + \mathbf{t}_2\mathbf{p}_2^T + \mathbf{t}_3\mathbf{p}_3^T + \cdots + \mathbf{t}_R\mathbf{p}_R^T + \mathbf{E} \qquad [3.2]$$

$$\mathbf{X} = \mathbf{T}\mathbf{P}^T + \mathbf{E} \qquad [3.3]$$

where the $\mathbf{M}_r$ ($r$=1,2,...R) are the rank 1 matrices, the $\mathbf{t}_r$ ($I$x1) are called the score vectors, and the $\mathbf{p}_r$ ($J$x1) are known as the loading vectors. The score and loading vectors are all orthogonal vectors and are collected in the following matrices **T** ($I$x$R$) and **P** ($J$x$R$). The

residuals of this decomposition are stored in matrix **E** (*I*x*J*). The scores are just the projection of each sample or observation onto the lower dimensional space which orientation in $\Re^J$ is given by the loading vectors $\mathbf{p}_r$. The latter also provide information about how variables are correlated to each other. Through the interpretation of different plots like the score plots or loading plots (Geladi et *al.*, 2003), it is possible to visualise and interpret the information contained in the very large process dataset **X**. For example, plotting $\mathbf{t}_2$ vs. $\mathbf{t}_1$ gives the projection of the *I* observations on the plane formed by $\mathbf{p}_2$ and $\mathbf{p}_1$. Therefore, observations having similar variables patterns, would lie close to each other in the plot of $\mathbf{t}_2$ vs. $\mathbf{t}_1$.

Geometrically, PCA is equivalent to finding a vector, a plane or a hyperplane (i.e. a lower dimensional space) explaining the greatest amount of variance, or the best fit, of the high dimensional dataset **X**. To allow visual interpretation, consider that **X** as three columns or variables (*J*=3) $\mathbf{x}_1$, $\mathbf{x}_2$ and $\mathbf{x}_3$, as illustrated in Figure 3.1. It can be seen that the observations (light blue dots) do not fill the entire $\Re^3$ space but, due to collinearity, rather follow a smaller number of specific directions. The direction of the first principal component ($\mathbf{p}_1$) is that explaining the greatest amount of variance in the data **X** (i.e. least squares fit through the swarm of points). The projection of **X** along this first principal direction yields the first score vector $\mathbf{t}_1$. The direction of the second component $\mathbf{p}_2$ is that explaining the greatest amount of residual variance unexplained by the first component. That is, $\mathbf{p}_2$ is orthogonal to $\mathbf{p}_1$. The second score vector $\mathbf{t}_2$ is again obtained by projecting **X** along $\mathbf{p}_2$. Taken together, the first two components form a plane on which the data is projected. The loading vectors $\mathbf{p}_1$ and $\mathbf{p}_2$ define the orientation of that plane in $\Re^3$ space whereas the score vectors $\mathbf{t}_1$ and $\mathbf{t}_2$ provide the new coordinates of each observation on the plane. Finally, a third direction ($\mathbf{p}_3$) could be computed but it would only capture the smallest amount of variance in **X**, perhaps associated with noise, and could be left as residuals **E** (i.e. perpendicular distance of each observation off the plane). Also note that when the number of components equals the number of variables, no dimensional reduction is obtained (i.e. **E**=0) and the set of principal directions correspond to a rotation of the original set of axes. How to decide on the number of components to use will be discussed later in section 3.3.2.

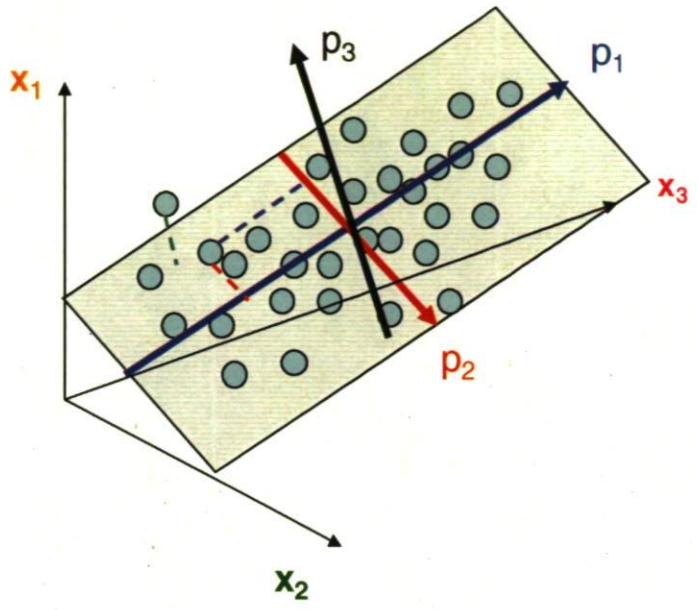


Figure 3.1: Geometrical interpretation of PCA.

Mathematically, the objective function of the first PCA component can be described as follows:

$$\max_{\mathbf{p}_1}\{\mathbf{p}_1^T \mathbf{X}^T \mathbf{X}\, \mathbf{p}_1\} \qquad \text{subject to} \qquad \mathbf{p}_1^T \mathbf{p}_1 = 1 \qquad [3.4]$$

This direction, labelled $\mathbf{p}_1$, is in fact a linear combination of the $J$ process variables in $\mathbf{X}$, each variable having its specific weight. This direction is shown in Figure 3.1. Projecting $\mathbf{X}$ in the direction of $\mathbf{p}_1$ yields the latent variable $\mathbf{t}_1$ capturing the greatest amount of variability in $\mathbf{X}$:

$$\mathbf{t}_1 = \mathbf{X}\, \mathbf{p}_1 \qquad [3.5]$$

Projection residuals $\mathbf{E}_1$, contain the variance of $\mathbf{X}$ unexplained by the first component:

$$\mathbf{E}_1 = \mathbf{X} - \mathbf{t}_1 \mathbf{p}_1^T \qquad [3.6]$$

The model construction continues with the computation of $\mathbf{p}_2$, using Eq. [3.4], explaining the highest amount of unexplained variance in $\mathbf{X}$. This direction is also depicted in Figure 3.1. This is achieved by substituting $\mathbf{p}_1$ by $\mathbf{p}_2$ and $\mathbf{X}$ by $\mathbf{E}_1$ in Eq. [3.4]. However, an

orthogonality constraint is also imposed on Eq. [3.4], to force $\mathbf{p}_2$ to be orthogonal or uncorrelated to $\mathbf{p}_1$:

$$\mathbf{p}_1^T\mathbf{p}_2 = 0 \qquad [3.7]$$

This procedure is repeated until the desired number of directions ($A$) is computed. The PCA model could then be written using matrices product:

$$\mathbf{X} = \mathbf{TP}^T + \mathbf{E}_A \qquad [3.8]$$

PCA is in fact nothing more than the eigenvector decomposition of **X**, where the **p** vectors are the eigenvectors of $\mathbf{X}^T\mathbf{X}$ and the **t** vectors are the eigenvectors of $\mathbf{XX}^T$.

An approach for computing the **p** and **t** vectors sequentially was proposed by Wold et *al.*, (1987) and is referred to as the Nonlinear Iterative Partial Least Squares (NIPALS) algorithm This algorithm is detailed in Figure 3.2.

1: Set **t** to any column of **X**

2: Start convergence loop

- 2.1: $\mathbf{p} = \mathbf{X}^T\mathbf{t}/(\mathbf{t}^T\mathbf{t})$
- 2.2: $\mathbf{p} = \mathbf{p}/(\mathbf{p}^T\mathbf{p})$
- 2.3: $\mathbf{t} = \mathbf{Xp}/(\mathbf{p}^T\mathbf{p})$
- 2.4: Check convergence of **t** and **p**. Go to step 3 if converged.

3: $\mathbf{E} = \mathbf{X} - \mathbf{tp}^T$

4: Store **p** and **t** as new columns in **P** and **T**, respectively

5: Return to step 1 and compute the next direction, replacing **X** by **E**

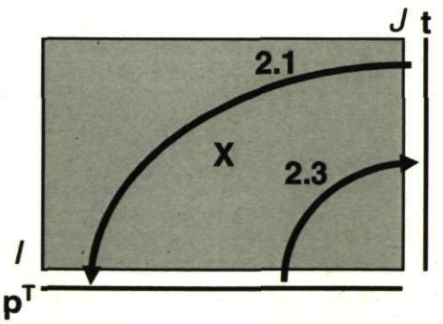


Figure 3.2: NIPALS algorithm for PCA and its arrow scheme.

This approach is advantageous when $J$ is large since eigenvector decomposition (or Singular Value Decomposition-SVD) computes all $J$ components simultaneously when, very often in practice, 3-5 components are sufficient to capture the relevant information in **X**.

## 3.2 Partial Least Squares Regression (PLS)

When a second data matrix **Y** (*IxH*) is available, perhaps containing *H* quality or productivity data for *I* samples or observations, one may wish to explore the information contained in both **X** and **Y** and build a relationship between them. This is accomplished using PLS regression, which can be seen as an extension of PCA for the case of two data matrices. Let **X** contain process data and **Y** some quality or productivity data or whatever data depending on the problem at hand. The basic assumption behind PLS is that variations in **X** and **Y** are both driven by a common set of *A* latent variables **T** (*IxA*). It essentially performs the decomposition of the covariance structure between **X** and **Y**. The reader is referred to Burnham et *al.* (1996), Wold et *al.* (2001), Martens (2001) and Kourti (2002, 2005) for more detailed mathematical descriptions of PLS and for tutorials.

Mathematically, this is achieved by computing the directions in the **X** space that maximize the covariance between **X** and **Y**. These directions, called the weight vectors $\mathbf{w}_a$ ($a = 1,...,A$) are linear combination of the **X** variables and are the solution of the following problem:

$$\max_{\mathbf{w}_i}\{\mathbf{w}_i\,\mathbf{X}^T\mathbf{Y}\mathbf{Y}^T\mathbf{X}\,\mathbf{w}_i^T\} \qquad \text{subject to} \quad \mathbf{w}_i^T\mathbf{w}_i = 1 \qquad [3.9]$$

$$\text{subject to} \quad \mathbf{w}_i^T\mathbf{w}_j = 0 \quad \text{for } i \neq j$$

The structure of the PLS model is given below:

$$\mathbf{X} = \mathbf{T}\,\mathbf{P}^T + \mathbf{E} \qquad [3.10]$$

$$\mathbf{Y} = \mathbf{T}\,\mathbf{Q}^T + \mathbf{F} \qquad [3.11]$$

$$\mathbf{T} = \mathbf{X}\,\mathbf{W}^* \qquad \mathbf{W}^* = \mathbf{W}(\mathbf{P}^T\mathbf{W})^{-1} \qquad [3.12]$$

where **T** (*I*×*A*) is the common latent variable space defined by the weight matrix **W*** (*J*×*A*) and capturing the information in **X** that is the most highly correlated with **Y**. The **P** (*J*×*A*) and **Q** (*H*×*A*) matrices contain the orthogonal loading vectors mapping the common latent variable space in the space of **X** and **Y** (models of these blocks). The PLS model residuals for both blocks are stored in **E** (*I*×*J*) and **F** (*I*×*H*). Since PLS is a regression technique, it is possible, for prediction purposes, to reorganize the model structure (Eqs. [3.10 - 3.12]) and

express it in a simpler form $\mathbf{Y} = \mathbf{X}\,\mathbf{B}+\mathbf{F}$, where $\mathbf{B}$ ($J \times H$) is a set of pseudo regression coefficients:

$$\mathbf{B} = \mathbf{W}^{*}\,\mathbf{Q}^{T} \qquad [3.13]$$

A NIPALS iterative algorithm was also proposed for PLS as described below (Wold et *al.*, 2001), leading to sequential computation of the **w**, **q**, **t** and **u** vectors (Figure 3.3). Alternatively, these vectors could be extracted simultaneously for all dimensions by an eigenvalue-eigenvector decomposition since it was shown by Höskuldsson (1998) that **w**, **q**, **t** and **u** are eigenvectors of $\mathbf{X}^{T}\mathbf{Y}\mathbf{Y}^{T}\mathbf{X}$, $\mathbf{Y}^{T}\mathbf{X}\mathbf{X}^{T}\mathbf{Y}$, $\mathbf{X}\mathbf{X}^{T}\mathbf{Y}\mathbf{Y}^{T}$ and $\mathbf{Y}\mathbf{Y}^{T}\mathbf{X}\mathbf{X}^{T}$, respectively.

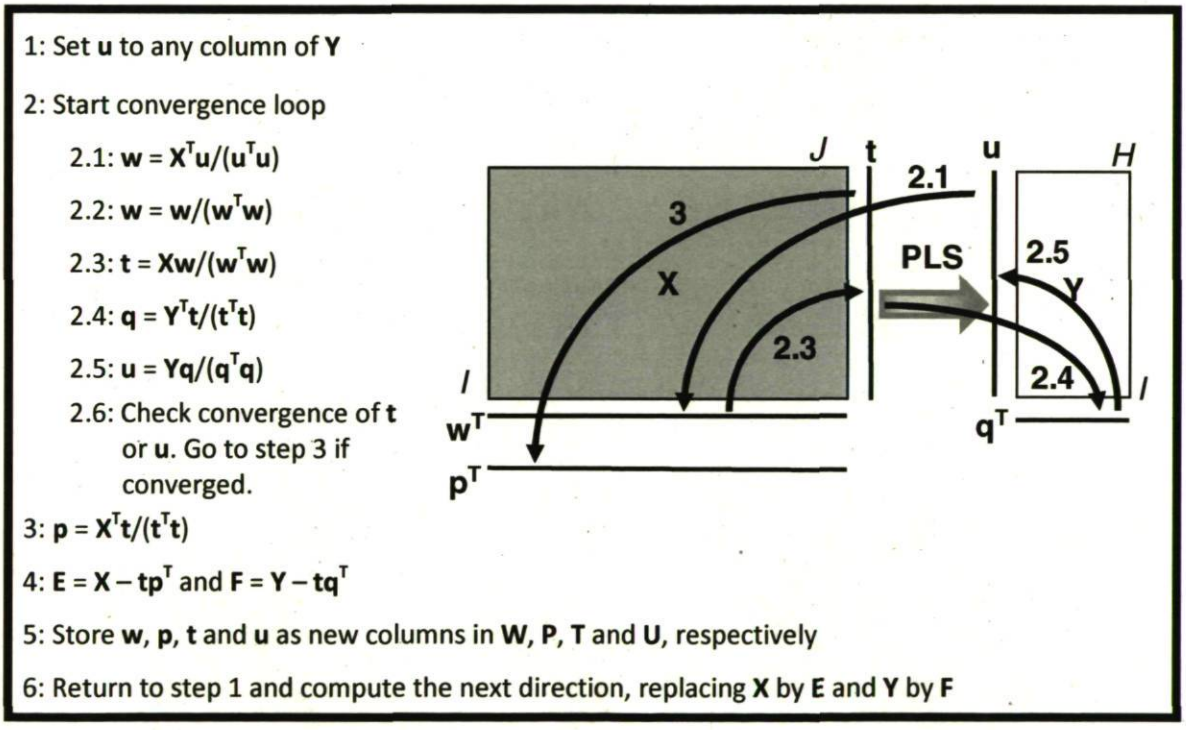


Figure 3.3: NIPALS for PLS regression and its arrow scheme.

## 3.3 Data Scaling and Selection of the Number of Latent Variables

### 3.3.1 Data scaling

Like other projection methods, the results obtained from PCA and PLS decompositions are scale dependent. It is therefore necessary to scale the data (i.e. **X** and **Y**) appropriately before model building. When no prior information is available on the relative importance of the variables in a given problem, a common practice is to mean-center and autoscaling the variables (i.e. columns of **X** and **Y**) to unit variance. This approach was used in the thesis unless otherwise stated.

Mean-centering allow PCA and PLS to capture variations about the mean of the variables whereas scaling to unit variance gives equal importance to each variable in the analysis. This is important, for example, when variables in a dataset are measured in different engineering units (i.e. ppm, %, kg), as it is the case for aluminum reduction process variables. The pre-processing procedure is schematically shown in Figure 3.4 for nine variables (Geladi and Kowalski, 1986).

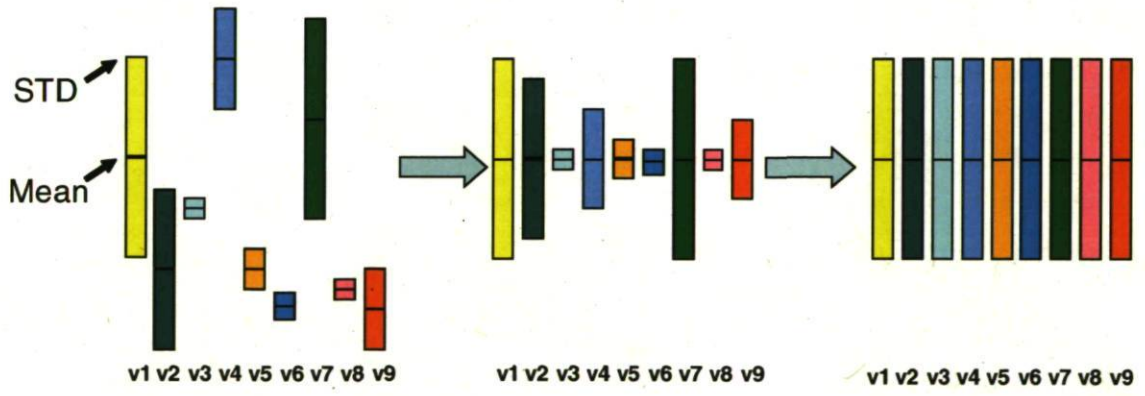


Figure 3.4: Effect of mean-centering and autoscaling. Left, original data; middle, mean-centered data and right, auto-scaled data.

Assuming a row vector of different variables (**x**) and row vectors of variables mean values ($\mathbf{x}_m$) and standard deviations ($\mathbf{x}_{std}$), the autoscaled version of **x** (**x***) is obtained by

substracting the mean from **x** and by dividing each of its element by its corresponding standard deviation, as follows:

$$\mathbf{x}^* = \frac{(\mathbf{x}-\mathbf{x}_m)}{\mathbf{x}_{std}} \qquad [3.14]$$

On the other hand, when process knowledge suggests that the variables can be grouped into conceptually meaningful blocks, with a different number of variables in each block, then it is possible to perform block scaling instead of autoscaling. This will give equal importance (i.e. variance) to each block in PCA or PLS models. For example, if 15 temperature and 3 pressure measurements are available in **X**, and PCA is applied to **X** after autoscaling, the PCA model might extract more information from temperatures simply because the are in greater number (i.e. more variance in that block). Block scaling will remove difference owing to differences in the number of variable within each block. Block scaling is schematically shown in Figure 3.5, again for nine variables grouped in 4 blocks of 3, 4, 1 and 1 variables, respectively.

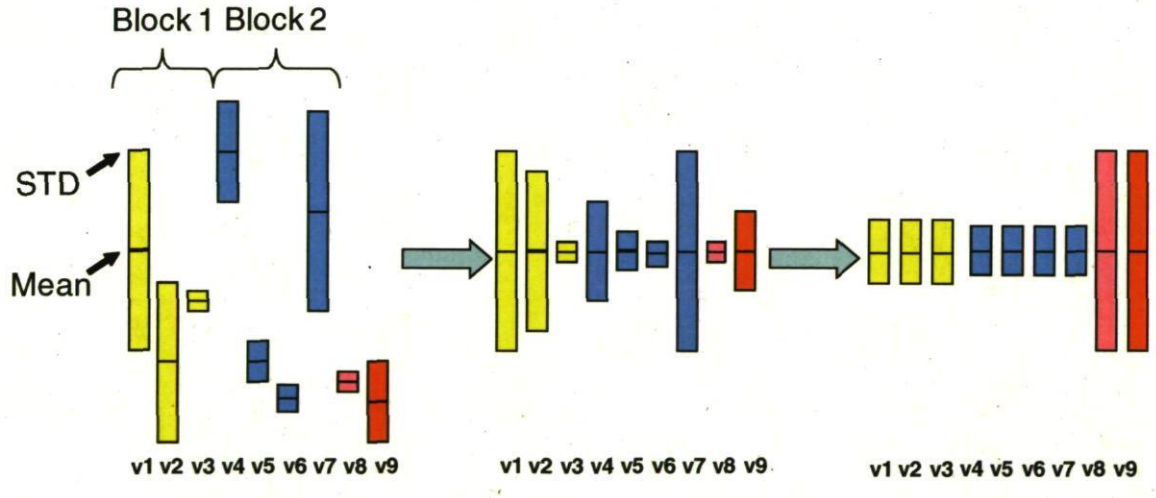


Figure 3.5: Effect of block scaling. Left, original data; middle, mean-centered data and right, block scaled data.

Block scaling is performed by dividing each columns of **x*** (i.e. autoscaled **x**) by the corresponding element of a vector containing the information on the number of variables in each block (Westerhuis et *al.*, 1998):

$$\mathbf{x}_j^+ = \frac{\mathbf{x}_j^*}{\mathbf{x}_{sqrt,j}} \qquad [3.15]$$

In the case of Figure 3.5, $\mathbf{x}_{sqrt}$ is [ $3^{½}$ $3^{½}$ $3^{½}$ $4^{½}$ $4^{½}$ $4^{½}$ $4^{½}$ $1^{½}$ $1^{½}$].

### 3.3.2 Selecting the number of components

Using PCA and PLS, it is possible to compute as many principal components as there are variables in **X** or **Y**, whichever has most. However, doing so only rearranges the information contained in the matrices since the resulting latent variable model is a rotation of the original variable space. Still, process variables are generally driven by a much fewer number of underlying events, or latent variables. These latent variables generally cause some of the measured variables to move together in a correlated way, depending on the event, and thus are hidden in the original dataset. Nevertheless, the number of latent variables is generally much lesser than the number of measured variables, which suggests that studying only the first few latent variables is enough to capture most of the variations enclosed in **X** and/or **Y**. Moreover, as it is often the case with industrial data, **X** and/or **Y** are corrupted by noise and one is interested in studying only the systematic part of the information and leaving the irrelevant information out of the analysis. This is achieved by carefully selecting the number of principal components ($A$). Hence, the systematic variations, captured by the loadings vectors (**P**, **W** and **Q**) are kept in the model and irrelevant variations are left in the residuals **E** and/or **F**. Different methods exists for selecting the number of latent variables to keep in a model (Nomikos and MacGregor, 1995), but the most widely used strategy is cross-validation (Wold, 1978). This approach was used in the thesis.

In cross-validation, the $I$ observations in **X** and **Y** are divided into $g$ sub-groups of $q$ observations ($I = gq$). Each sub-group is removed from the data matrices one at a time and a one latent variable ($A = 1$) PCA or PLS model is built on the remaining $g$-1 sub-groups. The model in then used to predict the data from the group left out and the prediction error sum of squares (PRESS) is computed for this sub-group. This is repeated for every other $g$-1 sub-groups and the sum of the PRESS values across all $g$ cross-validation loops is computed. This procedure is then repeated with two latent variables and so on. The number of principal components or latent variables ($A$) to keep in the model is selected as the one

achieving the lowest overall PRESS across all $g$ sub-groups (i.e. best predictive ability). Selecting a lower number of latent variables would leave relevant information out of the model, thus not capturing all systematic variations. Selecting additional components may lead to overfitting and/or incorporation of irrelevant information in the model.

# 4 Increasing Potlife of Hall-Héroult Reduction Cells through Multivariate On-line Monitoring of Preheating, Start-up and Early Operation

## 4.1 Résumé

Cet article présente l'étude de différents facteurs affectant la durée de vie des cuves d'électrolyse. Avant d'entrer en production, les cuves sont préchauffées, démarrées et opérées avec des points d'opération différents des cuves en opération normale. Cependant, différents problèmes d'opération peuvent survenir durant ces étapes et il est démontré que ces derniers ont un impact direct sur la durée de vie des cuves. En effet, en utilisant un modèle de régression de type PLS, il est possible de prédire la durée de vie des cuves, avec une erreur de prédiction inférieur à 90 jours et ce, 60 jours seulement après leur démarrage. Cette erreur de prédiction est satisfaisante compte tenu des critères décisionnels entourant le moment exact de l'arrêt d'une cuve. Finalement, des chartes de contrôle statistique multivariée des procédés sont proposées afin de suivre correctement ces trois étapes, dans le but de minimiser les effets des variations ayant un impact sur la durée de vie des cuves.

Tessier, J., Duchesne, C., Tarcy, G.P., Gauthier, C., Dufour, G., Submitted to *Metallurgical and Materials Transactions B* (Manuscript E-TP-09-195-B, June 23rd, 2009).

## 4.2 Abstract

Aluminum is produced inside metallurgical reactors known as pots that are replaced at the end of their service life. New pots are preheated, started and then enter a period known as early operation where different control strategies are used before entering regular operation. It is known that how preheating, start-up and early operation are performed can damage a well designed pot and lead to shorter service life. However, the impact of these phases with respect to potlife is not well documented quantitatively. In this paper, multivariate statistical analysis techniques are used to investigate the impact of pot-to-pot variations during the three phases. A PLS regression model is first proposed for predicting potlife, within an error of 90 days, using process data gathered until the end of early operation. This model is also used to identify those variables having the greatest influence on potlife. Finally, multivariate statistical process control charts are proposed to efficiently monitor the three steps. These charts have a low false alarm rate and can help find the root cause of abnormal operation occurring during the early phases. A few examples are used to illustrate how operators and engineers could use the charts to maintain consistent early operation and help improve mean potlife.

## 4.3 Introduction

In the Hall-Héroult process, aluminum (Al) is obtained by the electrochemical dissociation of smelter grade alumina powder ($Al_2O_3$) inside metallurgical reactors commonly called reduction cells or pots (Figure 2.2).

This reduction reaction is described using the following overall reaction:

$$2\,Al_2O_{3(diss)} + 3\,C_{(s)} = 4\,Al_{(l)} + 3\,CO_{2(g)} \qquad [4.1]$$

Based on this mechanism, the theoretical dissociation voltage of alumina is approximately 1.2 V (Grjotheim and Kvande, 1993). However, in practice, a much higher voltage in the range of 4.0-4.6 V (Grjotheim and Kvande, 1993) is required to overcome a number of operational issues such as anode and cathode overvoltage and gas bubble resistance. It is also partly driven by the pot heat balance requirement (Grjotheim and Kvande, 1993). The pot production rate approximately follows Faraday's law (Thonstad et *al.*, 2001) with Faradaic efficiency typically between 90 and 96%. To be economically attractive, aluminum smelters typically operate hundreds of pots in the 100 to 500 kA range.

A typical Hall-Héroult cell (Figure 2.2) is made of an outer steel shell container, the internal surface of which (i.e. bottom and sidewalls) are covered with different layers of thermal insulating and refractory materials. Carbon cathode blocks are then placed on the bottom brick layers. Different carbonaceous pastes are finally used to fill the gaps between the carbon cathode blocks and the sidewalls. An electric current flowing from the carbon anodes to the electrolytic bath, a molten mixture of cryolite ($Na_3AlF_6$) and additives, dissociates alumina as described by Eq. [4.1]. Current then flows through the liquid metal pad located between the bath and the carbon cathode blocks, and exits the pot by the carbon cathodes connected to the collector bars. Since the cells are electrically connected in series, the current exiting one pot is directed to the next downstream pot through a busbar network.

Over time during normal production, the integrity and the behaviour of the shell, the cathode blocks, the bottom and the side brick layers deteriorate due to the combined effects

of high temperature, sodium infiltration and aggressive corrosive attacks of the fluoride bath and molten aluminum (Sorlie et Øye, 1989). The materials deterioration is such that reduction cells are either preventively stopped or die in operation and, in either cases, the cells are rebuilt with new materials. In the former case, the cell is typically shutdown due to low production efficiency, metal purity problems or when prolonging operation may lead to safety hazards. In the latter case, the cell dies from a metal or bath tap-out from the side or the bottom of the cell.

Once in place, the new cell must be preheated before start-up. The preheating stage slowly raises pot materials from the 20 to 30°C range to their operating temperature of 800 to 950°C. This step is essential to avoid as much as possible cracks due to thermal stresses, but also to properly bake the carbonaceous pastes used to seal the cathode blocks and the brick sidewalls together. Once baked, the paste materials should behave similarly as the carbon cathode blocks (Richard et *al.*, 2005). The main preheating objectives are (Sorlie and Øye, 1989; Zangiacomi et *al.*, 2005): (1) to generate a smooth transition from room temperature to high pot operating temperature, (2) to smoothly bake the ramming paste and prevent its pyrolysis and (3) to obtain a high enough cathode final temperature to avoid excessive bath freezing during the cell start-up. Different preheating techniques are used throughout the industry and are overviewed in details in the literature (Sorlie and Øye, 1989).

Following the preheating period, a few tons of hot liquid bath and metal, coming from nearby cells, are poured in the newly preheated cell. Once again, different techniques and recipes are used throughout the industry (Sorlie and Øye, 1989) but the main steps are shared by most primary aluminum smelters.

The new cell then enters production or operation. During the first few weeks after start-up, the set points and control strategies used to operate the pot are different than those used in normal operation. This period is referred to as the early operation. This special extra care period helps the new pot reaching its designed set points with minimal detrimental impact on the properties of the various materials. In this period, close monitoring is performed to detect any abnormal deviations or operational issues, and prompt control actions are applied when needed. Tight control of the molten bath chemistry is also required since

sodium (Na), mainly introduced by $Na_2O$ impurity from alumina and $Na_2CO_3$ additions to maintain bath chemistry, migrates in the carbon cathode blocks and brick layers and cause undesired mechanical expansion of these materials. Indeed, expansion due to sodium infiltration can reach up to 10 times the dilation caused by thermal expansion (Sorlie and Øye, 1989). The pot heat balance also has to be well controlled during early operation in order to keep the frozen ledge to a defined thickness. This ledge is in fact a layer of frozen bath and plays a crucial role by protecting the cell materials (i.e. sidewalls) from deterioration (Sorlie and Øye, 1989).

Over the years, research and development efforts have been oriented towards the development of better cells and understanding the thermo-electro-mechanical behaviour of the materials during preheating. The thermo-mechanical behaviour of carbon cathode blocks and that of non-carbonaceous materials during preheating have been investigated by D'Amours et *al.* (2003) and Richard (2004), respectively. Modeling of the behaviour of carbonaceous pastes during preheating was also proposed by Richard et *al.* (2005). These studies contributed to a better understanding of the phenomena occurring during the preheating phase which, in turn, could be used to improve pot design and construction, and to compute optimal preheating policies for heat input and temperature profiles. However, the models developed in these investigations do not account for the pot-to-pot deterministic and stochastic variations encountered in practice in industrial smelters. Indeed, the potential benefits of additional efforts invested in cell design and construction can be significantly reduced or completely lost if abnormal operation occurs during preheating, start-up and early operation. Permanent damage caused to the various materials during these periods may adversely affect pot life and overall production performance.

A few authors have investigated the impact of pot-to-pot preheating variations, but the literature is very scarce since; (1) quantifying the impact of preheating, start-up and early operation on potlife requires a good data infrastructure for collecting measurements from a large number of pots over their lifespan (i.e. many years), (2) such data is not easily reproduced in laboratory, (3) most of these data follow some multivariate dynamic trends which are not straightforward to analyze. Still, some authors have reported different works on industrial pot preheating. For instance, the impact of preheating duration and final

cathode blocks temperature were investigated with respect to thermal gradients across cathode blocks and early pot noise (Zangiacomi et *al.*, 2005, 2006). Dunn and Galadari (1997) have presented results on the electrical resistance evolution of different pot materials during preheating. Nevertheless, the impact of pot-to-pot preheating variations has not been investigated systematically even if these variations could be accountable for some early pot failures or deaths.

This paper presents the analysis of pot-to-pot variations encountered during preheating, start-up and early operation phases with respect to potlife. The objectives are: (1) to identify key variables from the preheating, start-up and early operation that have meaningful statistical effects on potlife (2) to determine how much data (i.e. time since beginning of preheating) are required to obtain a statistically reliable potlife prediction for a new started cell and (3) to propose advanced statistical monitoring charts, based on Multiway Partial Least Squares (MPLS), to help achieve consistent high quality preheating, start-up and early operation and, eventually, longer potlife.

This paper is arranged as follows. First, the nature of the data used in this study is presented. Then, the multivariate statistical methods used throughout this work are briefly described. Potlife prediction results are presented and the key variables having meaningful statistical influence on potlife are identified. Finally, the development of multivariate statistical process control charts (MSPC) to monitor pot behavior during preheating, start-up and operation is presented and illustrated using industrial pot data.

## 4.4 Nature of Preheating, Start-up and Operation Data

The data used throughout this paper were collected from 31 pots started at the Alcoa Deschambault smelter (Quebec, Canada), all of them sharing a similar design. For each of these pots, the data was collected during their preheating, start-up and operation, from the very beginning to the end of their service life. Preheating and start-up data were retrieved from log books. Operation data were extracted from the plant historical database. The data structure available for this study is shown in Figure 4.1. It mainly consists of three blocks of regressor (or input) variables ($\underline{\mathbf{X}}$, $\mathbf{S}$, and $\underline{\mathbf{Z}}$), corresponding to preheating, start-up and

operation, respectively, and one response block **Y** containing potlife data. The nature of the data collected within each of these blocks is described below:

- $\underline{\mathbf{X}}$ ($I \times J \times K$): this block contains the trajectories of $J$ variables measured $K$ times (samples) during the preheating of $I$ pots (i.e. temperature profiles, duration of preheating, etc.). A three-way array structure is therefore obtained similarly as for the data collected from batch processes (Nomikos and MacGregor, 1995). Each horizontal slice ($i$ = 1, 2, ..., $I$) is a ($J \times K$) matrix containing the trajectories of all preheating variables for a given pot. In this work, 10 variables were sampled 18 times during the preheating of the 31 pots (i.e. $I$=31, $J$=10, and $K$=18).
- **S** ($I \times R$): contains snapshot measurements of $R$ start-up conditions for each of the $I$ pots (i.e. bath/metal quantities, anode effect duration etc.). These variables ($R$=9 in this work) characterize the state of the pot after the preheating period, and before entering operation.
- $\underline{\mathbf{Z}}$ ($I \times M \times N$): a second array containing the trajectories of the $M$ variables (i.e. electrical, temperatures, frequency of alumina shots, etc.) measured at $N$ sampling instants for each of the $I$ pots, from the beginning of the early operation to end of service life. In total, $N$=3000 daily averages of $M$=60 variables were available for describing the pots lifespan.
- **Y** ($I \times H$): represents a collection of $H$ response variables measured for each of the $I$ pots. In the present study, a single response is used (i.e. potlife measured in days). Hence, **Y** is a vector. Note that other variables describing the overall pot performance could also be included in this analysis with no change in the approach.

The autoscaled potlife distribution of the 31 pots available in this study is shown in Figure 4.2. It was obtained by subtracting each element of **Y** by the mean potlife and then dividing by potlife variance. An autoscaled potlife value above -0.5 is considered to be a good potlife duration for the cell design considered in this work. Hence, from these 31 pots, 22 were classified as "high potlife" pots and 9 were considered as "low potlife" pots.

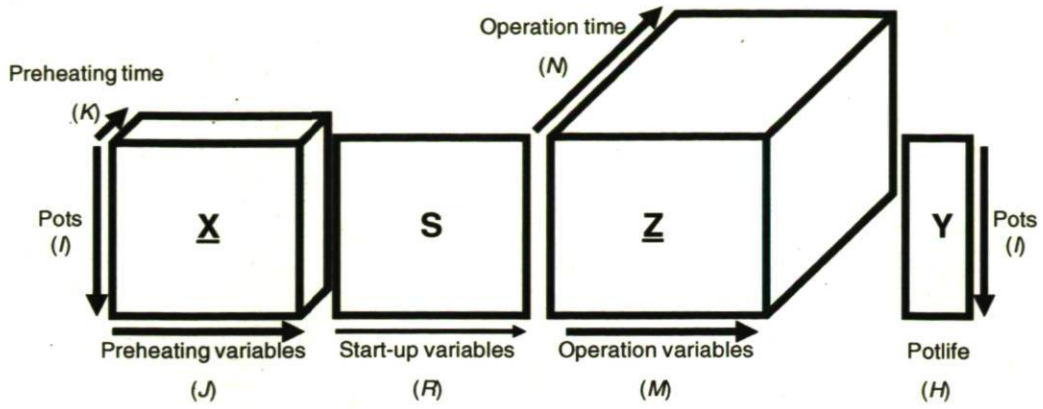


Figure 4.1: Nature of the data available during preheating, start-up and operation of reduction cells.

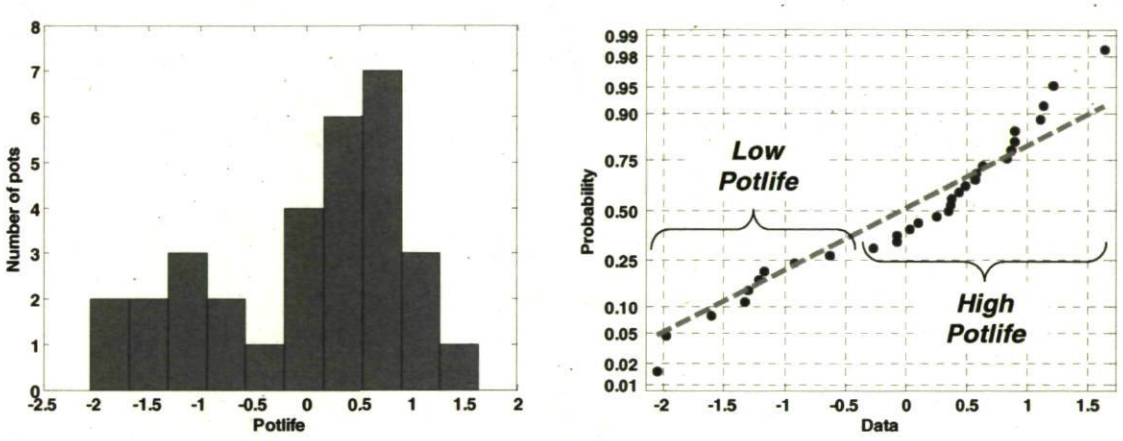


(a) (b)

Figure 4.2: (a) Autoscaled potlife distribution for the 31 pots and (b) Normal probability distribution.

## 4.5 Latent Variable Models

Multivariate statistical methods such as Principal Component Analysis (PCA) and Partial Least Squares (PLS) belong to a family of latent variable modeling techniques which have been shown over the years to be very efficient for analyzing large industrial databases by projection onto a lower dimensional space (i.e. latent variable space). Their ability to cope with the typical difficulties encountered with large amounts of industrial data (i.e. colinearity between variables, low signal/noise ratio, missing data) and their flexibility to

be tailored to various problems and data structures (multi-block, multi-way data) makes them perfect candidates for analyzing the pot early operation data collected in this research. The mathematical foundations of PCA and PLS is described in details in several papers (Geladi and Kowalski, 1986; Wold et *al.*, 1987, 2001; Höskuldsson, 1988; Jackson, 1991). A few good reviews of their applications for solving a number of problems in various industrial areas are also available in the literature (Kourti and MacGregor, 1995; Duchesne et *al.*, 2002; Kourti, 2002, 2005; Miletic et *al.*, 2004, MacGregor et *al.*, 2005). Only a brief overview of PCA and PLS is provided in this section.

Consider a matrix of process data $\mathbf{X}$ ($I \times J$) containing $I$ observations on $J$ process variables. Also assume that both systematic and stochastic variations are present in this data. Systematic process variations are, in general, driven by only a few underlying events (latent variables), which cause most process measurements to vary in a correlated fashion (i.e. in certain directions). Thus, $\mathbf{X}$ is typically not full rank. It is therefore possible to lower the dimensionality of $\mathbf{X}$ by finding the latent variables governing these systematic variations, but leaving noise or irrelevant information as residuals. PCA performs this dimensional reduction by finding a small set of $A$ orthogonal latent variables ($A \ll J$), or the principal components (PC), defined as a linear combinations of the original process variables (i.e. $\mathbf{X}$). The data is then projected onto this latent variable space (i.e. plane or hyperplane) for visual interpretation. The residuals correspond to the distance of each multivariate observation (i.e. row of $\mathbf{X}$) off the plane. Hence, the information explained by the PCA model is that part of $\mathbf{X}$ that lies on the plane after projection. The part of $\mathbf{X}$ orthogonal to the plane is unexplained variance.

Mathematically, the PCA variance-covariance decomposition is expressed as:

$$\mathbf{X} = \sum_{a=1}^{A} \mathbf{t_a} \mathbf{p_a^T} + \mathbf{E} = \mathbf{T}\,\mathbf{P^T} + \mathbf{E} \qquad [4.2]$$

where the orthogonal $\mathbf{t_a}$ ($I \times A$) vectors are those latent variables (also called scores) and provide the coordinates of each observation on the plane after projection. The plane is defined by a set of $A$ orthonormal loading vectors $\mathbf{p_a}$ ($J \times 1$), which are linear combinations of the original variables (i.e. $\mathbf{t_a} = \mathbf{X}\,\mathbf{p_a}$). The projection residuals are collected in the residual matrix $\mathbf{E}$ ($I \times J$). The loading vectors are found in such a way that $\mathbf{t_1}$ explains the

greatest amount of variance in **X**, $\mathbf{t}_2$ the second greatest amount of variance, not explained by the first component, and so on. Mathematically, the solution for the scores and/or loadings is formulated as an eigenproblem. These vectors are computed either using singular value decomposition (SVD) or sequentially using the Nonlinear Iterative Partial Least Squares (NIPALS) algorithm (Geladi and Kowalski, 1986, Kourti and MacGregor, 1995). The number of components *A* is typically selected using a leave-n-out cross-validation procedure (Wold, 1978).

On the other hand, PLS regression performs a decomposition of the covariance between two blocks of data, **X** and **Y**. It finds a common set of latent variables **T** that captures the information in **X** that is the most highly correlated with **Y** (*I*×*H*) while building a model also describing both of these data blocks. The structure of the PLS model is given below:

$$\mathbf{X} = \mathbf{T}\,\mathbf{P}^{\mathbf{T}} + \mathbf{E} \qquad [4.3]$$

$$\mathbf{Y} = \mathbf{T}\,\mathbf{Q}^{\mathbf{T}} + \mathbf{F} \qquad [4.4]$$

$$\mathbf{T} = \mathbf{X}\,\mathbf{W}^{*} \qquad \mathbf{W}^{*} = \mathbf{W}(\mathbf{P}^{\mathbf{T}}\mathbf{W})^{-1} \qquad [4.5]$$

where **T** (*I*×*A*) is the common latent variable space defined by the loading matrix **W*** (*J*×*A*) and capturing the information in **X** that is the most highly correlated with **Y**. The **P** (*J*×*A*) and **Q** (*H*×*A*) matrices contain the orthogonal vectors mapping the common latent variable space in the space of **X** and **Y** (models of these blocks). The PLS model residuals for both blocks are stored in **E** (*I*×*J*) and **F** (*I*×*H*), respectively. Since PLS is a regression technique, it is possible, for prediction purposes, to reorganize the model structure (Eqs. [4.3 - 4.5]) to express it as $\mathbf{Y} = \mathbf{X}\,\mathbf{B}+\mathbf{F}$, where **B** (*J*×*H*) is a set of pseudo regression coefficients:

$$\mathbf{B} = \mathbf{W}^{*}\,\mathbf{Q}^{\mathbf{T}} \qquad [4.6]$$

Once again, cross-validation is used to find the *A* number of PC to use in the model and the NIPALS algorithm can be used.

From these latent variable models, it is possible to interpret the behaviour of the variables relative to each other (i.e. their correlation structure) by means of the loading vectors stored

in **P**, **Q** and **W***. On the other hand, the latent variables **T** can be used to visualize clusters and patterns defined by the observations.

Like many other data analysis methods, PCA and PLS are scale dependent. Therefore, an appropriate scaling is applied prior to perform the analysis. A common practice is to autoscale the data by removing the mean of each variable and dividing by their standard deviation. This gives equal importance to each variable in the model.

The PCA and PLS techniques are suited for decomposition of two-dimensional matrices. However, when the data structure is organized into 3-way arrays, as is the case in this paper (see Figure 4.1), this array $\underline{\mathbf{X}}$ ($I \times J \times K$) can be rearranged into a matrix **X** using a so-called unfolding operation, which can be performed in six different ways (Westerhuis et *al.*, 1999). Throughout this paper, the pot-wise unfolding approach is used for the 3-way arrays ($\underline{\mathbf{X}}$ and $\underline{\mathbf{Z}}$ in Figure 4.1): each $K$ vertical slices ($I \times J$) are juxtaposed from left to right, resulting in a matrix of dimensions **X** ($I \times KJ$) as illustrated in Figure 4.3.

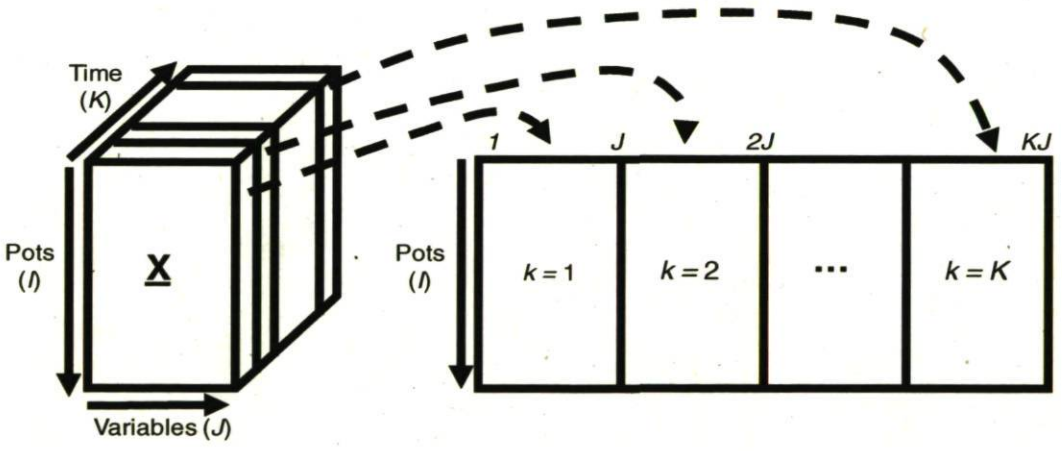


Figure 4.3: Pot-wise unfolding of a three-dimensional array.

This approach is equivalent to the batch-wise unfolding approach used in the analysis of batch process trajectories (Nomikos and MacGregor, 1995). It will be used in this work to investigate the pot-to-pot variability in the preheating and early operation trajectories. Autoscaling is also used for these arrays. This removes the mean trajectory and the

nonlinear behaviour of each variable allowing PCA and PLS to explain variations about the mean trajectories (Nomikos and MacGregor, 1995).

## 4.6 Earliest Potlife Prediction Time and Most Influential Variables

The first objective of this study is to determine how much time since the beginning of the preheating phase is necessary for obtaining reliable potlife prediction. Alternatively, the question to be answered here is how much data is required for making such prediction. As described in section 4.4, the available smelter database consists of 31 pots ($I$ = 31), 5 preheating variables sampled 18 times ($J$ = 5, $K$ = 18), 9 start-up variables ($R$ = 9) and 60 process condition during operation from the start-up until the end of service life ($M$ = 60, $N$ = 3000). If both 3-way arrays $\underline{\mathbf{X}}$ and $\underline{\mathbf{Z}}$ are pot-wise unfolded as described earlier and then combined with $\mathbf{S}$ in a large augmented regressor matrix $[\mathbf{X}\ \mathbf{S}\ \mathbf{Z}]$, this would result in a matrix of dimensions (31×180189) which is difficult to manage, although not impossible with PCA and PLS methods. This motivated the search for the minimal amount of data necessary for obtaining potlife predictions within a desired accuracy.

Two approaches were tested for the earliest potlife prediction as shown in Figure 4.4, each involving modifications to the trajectory data contained in $\underline{\mathbf{X}}$ and $\underline{\mathbf{Z}}$ ($\mathbf{S}$ was used as is):

- Five variables in the original $\underline{\mathbf{X}}$ were computed (i.e. not independently measured) from other measurements. These were left out of this first analysis since they did not bring new information. Furthermore, it was found that keeping the entire trajectories during preheating was not necessary. The trajectories of 3 of the 5 variables were very similar and had a simple shape. These trajectories are represented by the averaged slope and final value, the standard deviation of their final value, and the total duration of the preheating phase. This simpler preheating data matrix $\mathbf{X}$ (31×4) explained the same amount of potlife variance than when using the full pot-wise unfolded trajectories, which would be (31×90) dimensional. The $\mathbf{X}$ (31×4) matrix was used in both approaches shown in Figure 4.4.

- The **Z** array contains the pot operation data from the end of start-up phase to the end of service life. One approach (method 1) for testing how much operation data was needed for predicting potlife was to average the process data from the end of the start-up phase to sometime *t* during the operation phase (Figure 4.4(a)). Different such time windows were tested and used for predicting potlife. In this approach, **Z** is always a (31×60) matrix. In the second approach (method 2) **Z** rather consists of monthly averaged operating conditions juxtaposed from left to right (Figure 4.4(b)). Therefore, the number of months used to predict potlife increases, the dimensions of **Z** increases as (31×*t*·60) where *t* is the number of months used in the analysis.

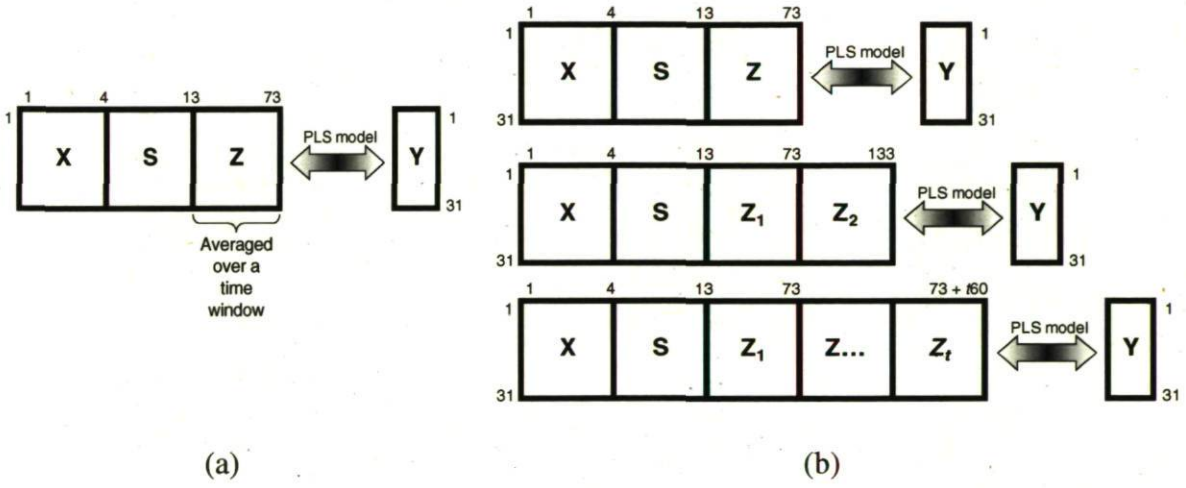


Figure 4.4: Data arrangements studied for the earliest potlife prediction. (a) method 1 and (b) method 2.

### 4.6.1 Earliest meaningful potlife prediction time

The two different data arrangement techniques illustrated in Figure 4.4 are compared in order to find the earliest meaningful potlife prediction time. To be meaningful for the plant operator and engineers, the average potlife prediction error needs to be below 90 days. This value is referred to as the lower bound potlife prediction error limit below which decisions to end a pot life cycle is not based on poor performance (i.e. predictable using process data) but rather based on plant operation logistics. As plant operators aim at having the maximum

number of pots in operation, a pot decommissioning could be postponed or prompt a few days or weeks due to plant operational constraints like job planning. For example a pot supposed to be decommissioned might be delayed to minimize extra hours or because another pot might have to be stopped in emergency following a tap-out. Unfortunately, these slight variations cannot be captured using the data driven modeling approach and could therefore be considered as "noise" (i.e. useless to try improving the model below that limit). Hence, this work aims at finding a PLS model achieving a potlife Root Mean Prediction Squared Error by Cross-Validation (RMSECV) below 90 days. Since **X** and **S** are the same for both data arrangements (Figure 4.4), the objective is to determine how much operation data is required in **Z** to achieve potlife predictions within the 90 days limit. Several PLS models were constructed using data collected during preheating (**X**), start-up (**S**), and increasing number of months of operational data (**Z**) organized using the two methods described in Figure 4.4.

Potlife prediction errors (RMSECV) are presented in Figure 4.5 as a function of months elapsed after start-up, where each point correspond to the prediction ability of one of the PLS models. This figure demonstrates that prediction error increases when data from the first month of operation are added to the preheating and start-up data. The two data arrangements methods exhibit a similar behaviour due to the high data variability over the first month of operation.

Adding data from the second month of operation yields a significant reduction in the prediction error for both data arrangements methods. The prediction error is below 90 days for method 1 after two months, and becomes fairly stable over time beyond 4 months of data. For method 2, prediction errors decrease steadily and until about ten months of operation data are used in the PLS model. However, both arrangements show an increased prediction error when using three months of data. This might be caused by the application of different operational procedures in this particular month as well as variations arising from these procedures. Indeed, it was found that one of the pots contributed largely to this prediction error increase. Nevertheless, this behaviour disappears when more operation data are added. Had a greater number of pots be available for this study, one could have

removed this particular pot from the analysis, although this shows the ability of the method to detect outlier pots having a very different behaviour.

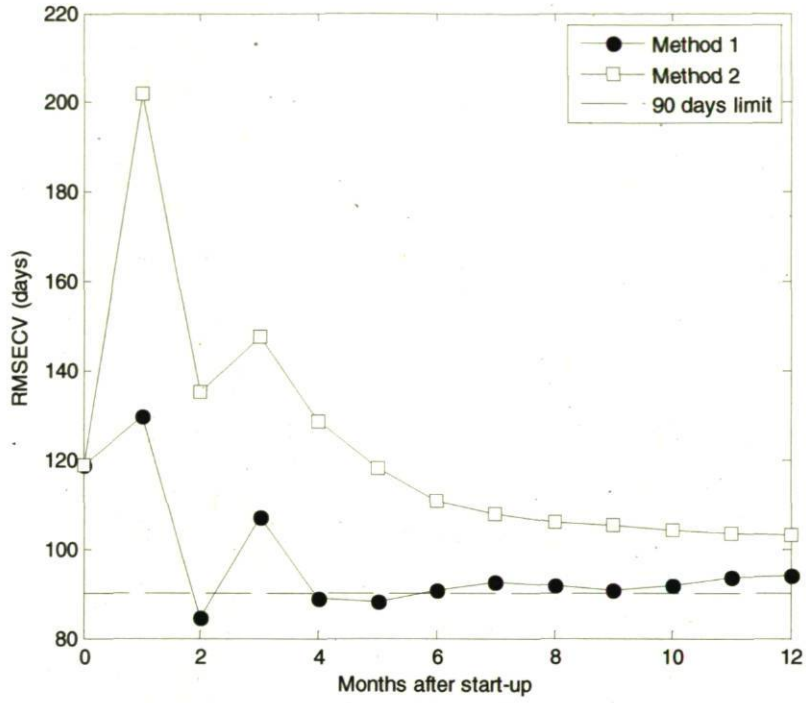


Figure 4.5: Potlife prediction errors as a function of months after start-up for the two data arrangement methods.

The fact that the prediction error goes down early in a pot life demonstrates that preheating, start-up and early operation have a significant impact on aluminum reduction cell life. Indeed, using only data from the pre-heating and start-up yields a potlife prediction error of 117 days (see results at 0 months in Figure 4.5), which is already very close to the 90 days limit. This value is the same for both data arrangement methods since they share the same preheating and start-up data (i.e. **X** and **S**). Using data from the first two months of operation, it is possible to provide potlife predictions within 84 and 135 days, respectively, for method 1 and 2. Hence, using process data averages over the first two months of operation (i.e. method 1) yields the earliest reliable potlife prediction for the data set of 31 pots. Note that using 4 months of data with method 1 would also be a good choice.

The autoscaled cross-validated potlife predictions for the 31 pots are presented in Figure 4.6 as a function of the truly achieved potlife of each reduction cell. These predictions were obtained using the PLS model built using preheating, start-up and two months of operation data and method 1 (Figure 4.4(a)). This model has two ($A$=2) cross-validated latent variables together explaining 73% of the potlife variance and resulting in a RMSECV of 84 days.

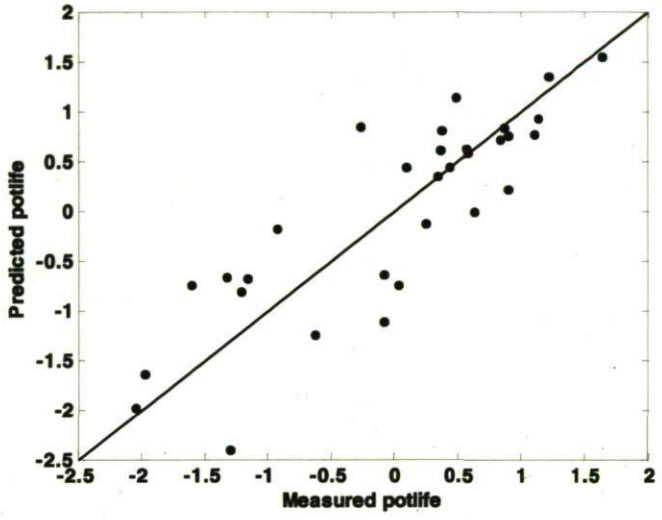


Figure 4.6: Predicted potlife as a function of truly achieved (i.e. measured) potlife.

### 4.6.2 Influence of the variables on potlife

Using the PLS model structure, it is also possible to identify variables having the greatest importance for potlife predictions. A commonly used statistic in the Chemometrics literature, called the variable importance on the projection $VIP_{j,A}$, provides a relative measure of importance of variable $j$ in predicting $\mathbf{Y}$ using a PLS model with $A$ latent variables:

$$VIP_{j,A} = \sqrt{J \sum_{a=1}^{A} w_{aj}^2 (SSY_a / SSY_{tot})} \qquad [4.7]$$

In the above equation, $w_{aj}$ is the loading weight of the $j^{th}$ variable in the $a^{th}$ PLS component, $SSY_a$ is the sum of squares of $\mathbf{Y}$ explained by the $a^{th}$ PLS component and $SSY_{tot}$ is the sum of squares of $\mathbf{Y}$ explained by the model. As a rule of thumb (Chong and Jun, 2005; Ericksson et *al.*, 2006), a variable with a VIP value greater than one is considered to have a

significant impact on the PLS model and thus on potlife predictions. The VIP scores of the best PLS model, using two months of operation data and method 1, are presented in Figure 4.7. This figure also provides the pseudo-regression coefficients (**B**) for that model. Looking at these coefficients complements the information obtained from the VIP since the sign of the coefficient indicate the sign of the correlation between a given variable and **Y** (i.e. potlife).

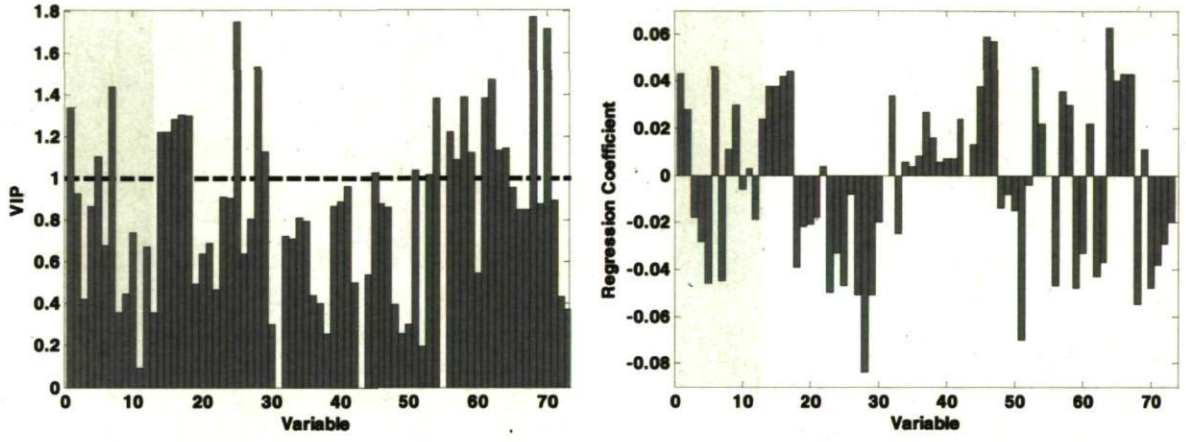


(a) (b)

Figure 4.7: (a) VIP and (b) regression coefficients for the PLS model achieving the earliest potlife prediction. The gray area identifies the preheating and start-up variables.

The gray areas in Figure 4.7 identifies the 13 variables associated with the preheating (4) and the start-up (9) phases. All other variables are associated with the operation phase. In the preheating and start-up phases (i.e. gray region), variables 1, 5, and 7 have the greatest VIP scores and therefore have the strongest correlation with potlife amongst the 13 variables. Plant operators and engineers can combine the information provided by the VIP scores and the regression coefficients for improving potlife. For example, variable 1 is the preheating duration and has a VIP value of 1.35 and its regression coefficient has a positive sign. That is, a longer preheating is positively correlated to potlife. This is consistent with process knowledge since a longer preheating phase gives longer soaking time for pot materials, thus leading to smaller thermal gradients just before start-up.

A similar approach can be used to interpret the impact of the 60 operational variables (numbered 14-73 in Figure 4.7). From these, 22 variables seem to have an important impact on potlife (VIP > 1). Another example is variable 64, which is the bath superheat or temperature over the melting point. This variable has a VIP of 1.15 and a positive regression coefficient. Hence, it has a good impact on the model, with a magnitude close to preheating time and according to the regression coefficient, increasing the bath superheat may help achieving a longer potlife. Again, this result makes sense as supplying enough heat to the pot prevents alumina sludge freezing over the cathode blocks which may lead to horizontal current fields thus degrading side ledge protection and sidewalls materials, leading to a possible shorter potlife. All the other variables having a VIP greater than one were investigated and, for most of them, their contributions in explaining potlife variations were found consistent with process knowledge.

### 4.6.3 Interpretation of the latent variable model

Although VIPs give the relative importance of each variable in the PLS model, one might be interested in understanding how variables interact together with respect to potlife. A way of extracting this information from the model is to plot **X** and **Y** weights, **w*** and **q** together on what is known as a loading bi-plot. An analysis of this plot gives information on the correlation structure among the **X** variables and how they influence potlife.

Figure 4.8 presents the loadings bi-plot of the potlife PLS model. In this case, it is straightforward since the model has only two principal components. Therefore, one only needs to plot **w*q** 2 against **w*q** 1. However, this model includes 73 variables and looking at a graph with so many points could be cumbersome. Therefore, this graph only presents variables having the highest importance on the model, those with a VIP greater than one (i.e. Figure 4.7 (a)). Each dot marks the weight (**w***) of a **X** variable with a VIP greater than one while the red star marks the weight of potlife (**q**). Drawing a line between the potlife weight and the plot origins, the green dotted line, helps to determine how variables interact together to influence potlife variations.

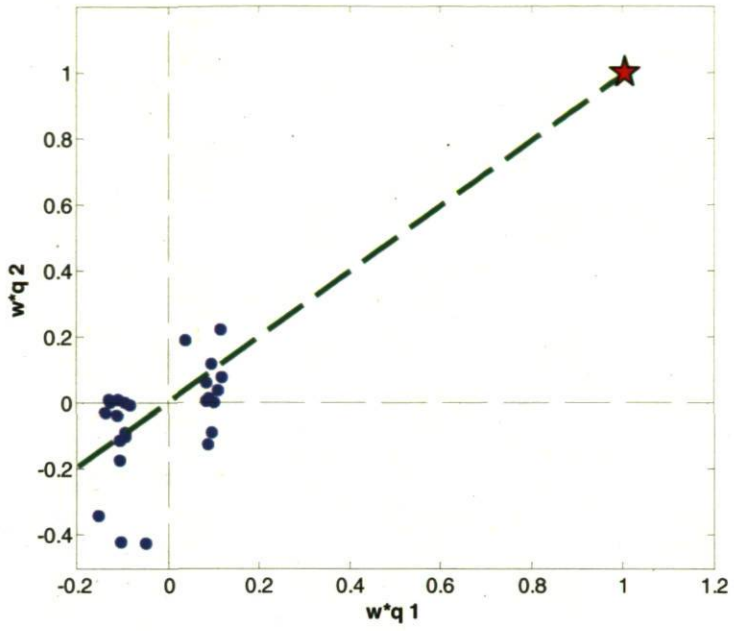


Figure 4.8: Bi-plot of the potlife PLS model.

This plot illustrates mainly two clusters of variables, one on the left hand of the plot origin and the other one on the right hand side. The variables on the right are positively correlated to potlife since their **w*** weights have the same sign as the potlife weight, while those on the left hand side are negatively correlated. To determine the actual influence of variables on potlife, one needs to perpendicularly project each variable on the green dotted line. The farthest a variable is projected from the origin, the greatest is its influence on potlife. A zoomed version of this graph is presented in Figure 4.9 for discussion.

This figure suggests that the first principal component might be driven by power input and thermal balance as many variables related to the pot thermal balance are present far from the plot origin. As mentioned in the discussion around VIPs, preheating time duration is an important variable affecting potlife. This is also seen on the bi-plot as it projects far from the origin on the green dotted line. Moreover, it can be said that performing a shorter preheating may necessitate a higher voltage during (CJ_UMM) early operation at this variable is plotted on the opposite side of the plot. This translates to a higher power input (CJ_Power and CJ_CPower) and a higher energy consumption (CJ_EE). These last

variables are grouped together on the plot, close to CJ_UMM, meaning that they are positively correlated with it and negatively correlated with potlife. This makes sense from process knowledge. Assuming a pot preheating is too short, cathodes core might still be cold and this may generate some bath to freeze during start-up or early operation. Therefore, more power has to be added early during the pot operation and this is achieved by increasing the pot voltage.

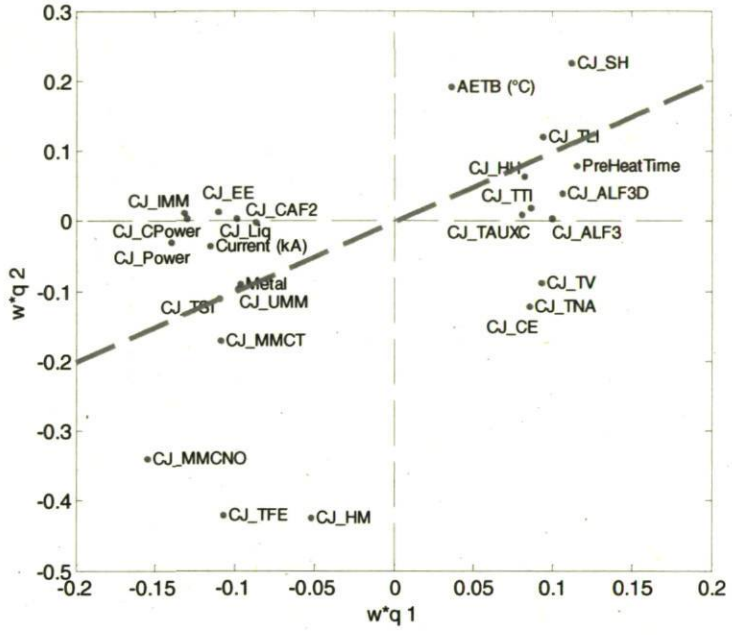


Figure 4.9: Zoomed version of the potlife PLS model bi-plot.

On the other hand, the second principal component seems to be affected by a different factor as metal level (CJ_HM), tap weights (CJ_MMCNO) and the metal iron content (CJ_TFE) are variables with the greatest weight on the second latent variable. This component seems to be related to the metal inventory during the early operation.

## 4.7 On-line Multivariate Statistical Monitoring of Preheating, Start-up and Early Operation

An on-line monitoring scheme is developed in this section for increasing mean service life through reducing the number of shorter potlife pots caused by inappropriate control actions, process drifts and upsets (i.e. abnormal operation) occurring during the preheating, start-up, and early operation phases. As shown previously, the process data collected in these three phases for the 31 pots studied in this paper explain up to 73% of the variations in potlife and yields predictions errors within 90 days of the truly achieved pot service life. Since process variations in the early phases were found highly correlated with potlife, conducting the process more consistently combined with early detection of potential problems may help achieve a higher mean service life.

In the aluminum smelting and in most industries, process operators and engineers typically follow the behavior of a few key variables to determine whether the process is in control or not. This is typically achieved using univariate statistical process control charts developed separately for each of the variables of interest. However, in the process industries, measured variables are almost never independent of one another and important information might be missed by univariate charts since they do not account for correlation structure between the variables (Kourti and MacGregor, 1995; Kourti, 2002, 2005). Hence, the operators might think that a pot is in control based on univariate charts when it is in fact out-of-control due to a change in the correlation structure of the process variables. Multivariate statistical process control charts (MSPC) (Kourti and MacGregor, 1995) will therefore be used in this study.

Multivariate latent variable techniques for monitoring process trajectory data are already available in the literature but, to the author's knowledge, were never used for monitoring early operation in aluminum smelters. A wealth of literature is available on batch process monitoring and fault detection (Nomikos and MacGregor, 1995; Westerhuis et *al.*, 1999, 2000; Kourti, 2002, 2005). Monitoring of start-ups and shutdowns of continuous processes using a similar approach was also investigated (Duchesne et *al.*, 2002). Since the smelter data structure presented in Figure 4.1 is very similar to that of multi-phase batch processes,

the batch MSPC techniques are used in this first attempt at monitoring early operation. The basic idea behind the approach consists of 1) selecting a reference database of pots which had a long service life and for which the early operation went well, 2) building a Multi-Way PLS model (MPLS) on that reference database to capture the correlation structure of the process trajectories associated with longer service life, and 3) after establishing statistical limits, compare the data obtained from new pots against the MPLS model of the reference database in order to detect abnormal operation that could, eventually, be detrimental to potlife. Appropriate corrective actions are then applied when necessary.

## 4.8 Development of MSPC Charts for Early Operation

From the 31 pots, a total of 22 had a scaled potlife value over -0.5 (Figure 4.2) and were confirmed as good early operation by plant operators and engineers. Hence, these pots are used as the reference database required for building the MSPC charts, which now consists of the following data blocks for each of the three phases: preheating $\underline{\mathbf{X}}$ (22×10×18), start-up $\mathbf{S}$ (22×9), and two months of early operation $\underline{\mathbf{Z}}$ (22×50×60). Note that for on-line monitoring, the full trajectory data is used to increase detection sensitivity. It was decided to keep all 10 preheating variables and use the first 60 daily averages in $\underline{\mathbf{Z}}$ (i.e. first two months). However, 10 variables were left out of the $\mathbf{Z}$ block since their variance was very small. After pot-wise unfolding of $\underline{\mathbf{X}}$ and $\underline{\mathbf{Z}}$ followed by concatenation with $\mathbf{S}$, the data structure shown in Figure 4.10 is obtained. This data is used for building the MPLS model describing the natural pot-to-pot variability in the trajectory behavior (i.e. correlation structure of the variables over time) amongst the good pots, those for which early operation is associated with longer potlife. Using again two cross-validated latent variables ($A$=2), the MPLS model explains 88% of the variance of $\mathbf{Y}$ and has a RMSECV of 96 days (i.e. consistent with the best PLS prediction model discussed previously).

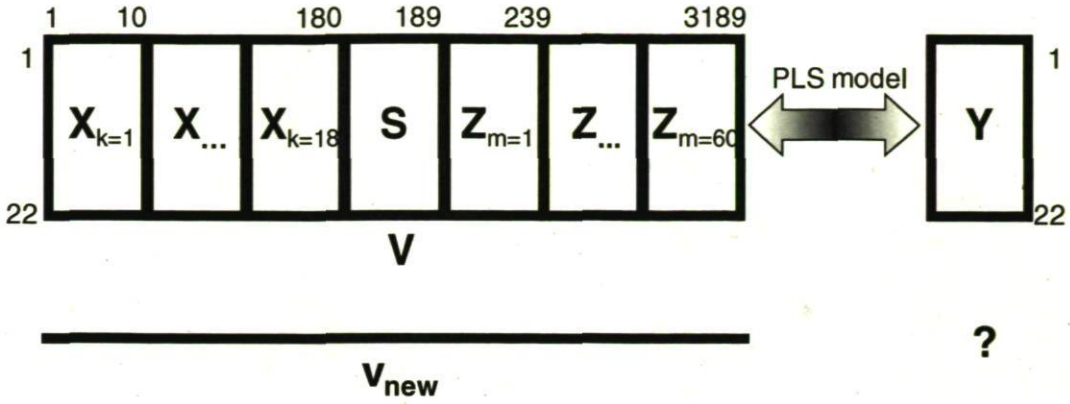


Figure 4.10: Data structure after pot-wise unfolding and concatenation of **X**, **S** and **Z**. Also shown is trajectory data for a newly started pot ($\mathbf{v}_{new}$).

On-line monitoring of a newly built pot involves two multivariate statistics, namely the Hotelling's $T^2$ and the squared prediction error $Q$. The former provides a measure of the distance (i.e. Mahalanobis) of the new pot from the mean trajectories of the reference pot database on the hyperplane defined by the MPLS model. The latter is a measure of how well the correlation structure of the trajectories of the new pot agrees with that of the reference pots (i.e. measure of the distance of the observations off the plane). These two statistics are computed as described below:

$$\mathbf{t}_{new,l} = \mathbf{v}_{new,l}\,\mathbf{W}^{*} \qquad [4.8]$$

$$T^2_{new,l} = \mathbf{t}_{new,l}\,\Sigma_{\mathbf{t}}^{-1}\,\mathbf{t}_{new,l}^{\mathbf{T}} \qquad [4.9]$$

$$Q_{new,l} = \left(\mathbf{v}_{new,l} - \mathbf{t}_{new,l}\mathbf{P}^{\mathrm{T}}\right)^{\mathrm{T}}\left(\mathbf{v}_{new,l} - \mathbf{t}_{new,l}\mathbf{P}^{\mathrm{T}}\right) = \mathbf{e}_{new,l}^{\mathrm{T}}\mathbf{e}_{new,l} \qquad [4.10]$$

where $\mathbf{v}_{new,l}$ corresponds to the trajectory data collected up to time instant $l$ for the new pot, autoscaled using the mean and standard deviations obtained from the reference data (i.e. prior to build the MPLS model). The score vector $\mathbf{t}_{new,l}$ is the projection of these trajectories onto the hyperplane of the MPLS model. The matrices **W*** and **P** contain the MPLS loading vectors (see Eqs. [4.3 - 4.5]), and $\mathbf{\Sigma_t}$, the variance of the score vectors (columns of **T**), which is diagonal due to orthogonality of the score vectors. The **W***, **P**, and $\mathbf{\Sigma_t}$ matrices are obtained from the MPLS model built on the reference trajectories of the good early operation pots. The $T^2_{new,l}$ and $Q_{new,l}$ statistics are computed at each time interval $l$ as the preheating, start-up, and early operation progress towards completion.

It is important to understand here that the complete trajectory data for the new pot (i.e. $\mathbf{v}_{new}$) is only available at the end of the early operation phase (after about 60 days). At the $l^{th}$ time instant, only the measurements collected up to this instant (i.e. $\mathbf{v}_{new,l}$) are available and the rest of the trajectory data need to be filled in order to compute $T^2_{new,l}$ and $Q_{new,l}$. Ways to fill the trajectory vectors have been explored in the batch process literature (Nomikos and MacGregor, 1995). Three of them were tested in this study: 1) assumes that the remaining future observations for each variable correspond to their mean trajectory computed from the reference dataset, 2) assumes that the present deviation from the reference trajectory will remain constant until the early operation is completed, and 3) replacement of missing data using PCA (Nomikos and MacGregor, 1995). A comparison between them will be discussed later.

To discriminate "in-control" from "out-of-control" operation (i.e. detect abnormal operation), statistical limits for $T^2_l$ and $Q_l$ were established based on reference distributions of these statistics computed using the 22 pots that underwent good early operation. That is, for each of the 22 pots, the $T^2_l$ and $Q_l$ were computed for each time instant $l$=1,2,...79 using the reference MPLS model. Hence, 22 replicates of these statistics were available at each instant *l*. The limits were established in such ways that at each instant, 95% of the replicates were within the bounds. Alternatively, one could use F and $\chi^2$ probability distributions to establish these limits (Nomikos and MacGregor, 1995; Kourti, 2005).

The ability of the MPLS model to correctly classify good and bad early operation was then tested. This also motivates the choice of one particular data filling method as well as the way to establish the 95% statistical limits. A summary of the classification results is presented in Table 4.1 for the three data filling approaches identified earlier. The percentage of good alarm is the number of "bad" early operation, among the 9 available in database, that were detected by the MPLS model after violating one or both of the $T^2$ and $Q$ limits, at any time during the preheating, start-up or early operation. A false alarm is when a good early operation violates one or both of the $T^2$ and $Q$ limits at any time during the three phases (i.e. percentage of the 22 good pots in the database). The first data filling approach (i.e. filling with the mean trajectories) was found to be the best suited for the

available data since it provided the lowest false alarm rate (good alarm rates are similar for all three approaches). This approach was therefore used in the rest of this paper.

Table 4.1: Good and false alarm rates for the three data filling methods.

| Data filling method | % of alarms | |
|---|---|---|
| | good | false |
| 1 | 88.9 | 9.1 |
| 2 | 88.9 | 95.5 |
| 3 | 88.9 | 13.6 |

## 4.9 Online Monitoring Results

This section illustrates on-line monitoring of the preheating, start-up and early operation phases of new pots as it would occur in practice. Three pots were selected, namely pots A037 (good), B117 (bad) and A003 (bad). Their corresponding autoscaled potlife were 0.90, -1.22, and -1.34, respectively. Pot A037 was taken from the reference dataset used to build the MPLS model of good early operation. Pots A003 and B117 are considered as bad early operation leading to shorter potlife (i.e. below -0.5) and should be detected as abnormal using the MSPC charts. Had these three pots been monitored on-line, the $T^2_l$ and $Q_l$ charts presented in Figure 4.11 would have been obtained.

From these charts, it is possible to observe different behaviour through the preheating, start-up and early operation of these three pots. The preheating phase corresponds to the time intervals located on the left of the black vertical line, the start-up phase (a snapshot) is on that line, and the early operation trajectories are on the right of the black vertical lines. Pot A037 clearly remains within the $T^2$ and the $Q$ limits at any time during the three phases, indicating that this pot was in control until regular production was reached. On the other hand, pot B117 was barely within limits until time interval 37, or 18 days after start-up, when a special event suddenly occurred and caused the $Q$ statistic to rapidly move outside the limits. This indicates that the correlation structure between the variables was broken compared to normal (good) early operation. Furthermore, at time interval 52 (or 33 days

after start-up) the $Q$ statistic again sharply increased, and this was observed a third time at interval 77 (58 days after start-up). Since the $T^2$ and $Q$ limits are computed from the MPLS model of good early operation, these limits are set to pinpoint on upsets that will likely have an impact on potlife. Hence, it seems that three abnormal events occurred during early operation of B117. Pot A003 also experienced some $Q$ statistic excursions outside the limits. However, as opposed to pot B117, this pot remained in control on the $T^2$ chart, indicating that only the correlation structure was broken at time interval 56, or 37 days after start-up. Hence, a very important event occurred during early operation of pot A003 which might explain shorter potlife.

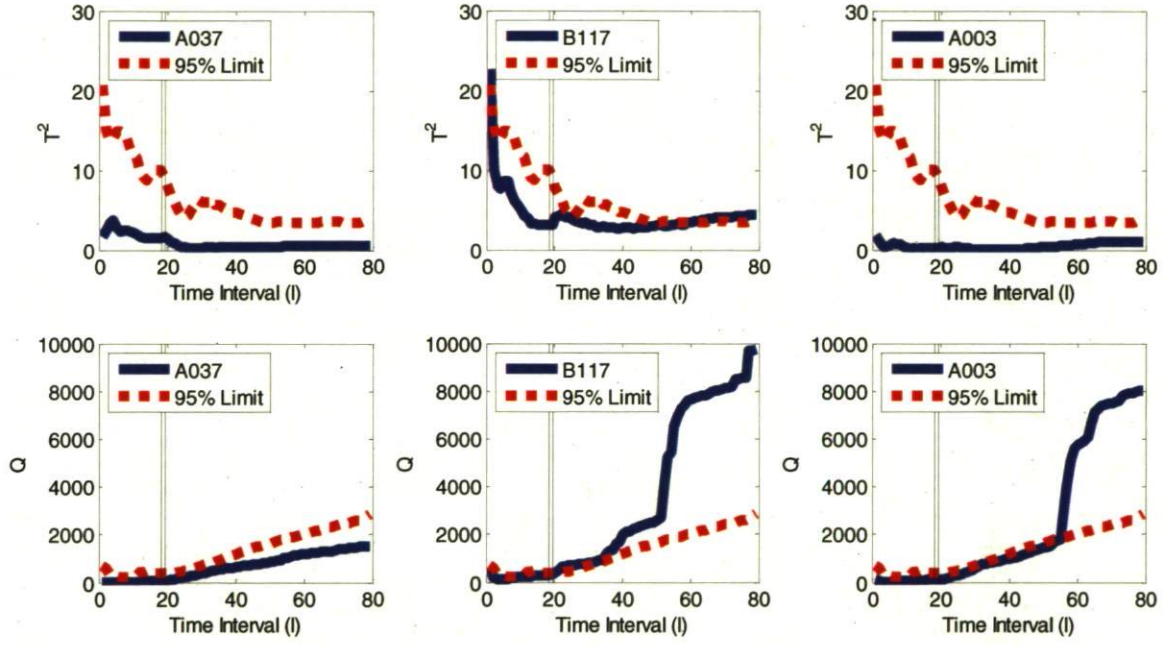


Figure 4.11: MSPC charts showing $T^2$ and $Q$ statistics and their 95% limits for pots A037, B117 and A003.

When the $T^2$ and/or $Q$ limits are violated, an alarm should be issued to get operator's attention and eventually trigger an effort for finding the root causes of the upset. The diagnosis effort is supported by tools such as variable contributions which consists of a bar plot of the relative contribution of each variable to a change in the $T^2$ and $Q$ statistics with respect to the mean trajectories of the reference pots. Assuming a data vector $\mathbf{v}_{new,I}$ ($1 \times JL$),

where $L=K+1+N$, from a newly started pot containing measured data up to the $l$ time instant, and the remainder completed according to a filling approach. The contribution of process variable $j$ at time interval $l$, to the $T^2$ statistic is computed using the following expression (Westerhuis et *al.*, 2000):

$$C_{jl}^{T^2} = \mathbf{t}_{new}^{T} \boldsymbol{\Sigma}_{\mathbf{t}}^{-1} \left[ \mathbf{v}_{new,jl}^{T} \mathbf{W}_{jl}^{T} (\mathbf{W}^{T}\mathbf{W})^{-1} \right]^{T} \quad [4.11]$$

Here, $\boldsymbol{\Sigma}_{\mathbf{t}}$ is variance-covariance of the score matrix ($\mathbf{T}$) obtained from the reference dataset of good pots, and $\mathbf{W}$ is the corresponding weight matrix. It basically accounts for the magnitude of the deviation of variable $j$ at instant $l$ from the reference trajectory as well as the importance of this variable in predicting potlife. The contribution of process variable $j$ at time interval $l$, to the $Q$ statistic is computed according to the following equation (Westerhuis et *al.*, 2000) which provides a measure of how well this particular variable is projected on the plane of the reference MPLS model:

$$C_{jk}^{Q} = (\mathbf{v}_{new,jl} - \hat{\mathbf{v}}_{new,jl})^2 \quad [4.12]$$

The $T^2$ and $Q$ contributions are presented in Figure 4.12 for pots A037, B117 and A003 for each variable $j$ at each time interval $l$. A high contribution means that this variable at this specific time interval contributed significantly to a change in $T^2$ and/or $Q$ and hence, did behave differently compared to the reference dataset. It is clear that early operation trajectories for pot A037 were fairly close to the mean reference trajectories since the contributions of all variables at all times are low for both statistics. In contrast, several of the $T^2$ and $Q$ contributions were high for pot B117 ($jl$ values around 1000 and 2000), but are low at other times, indicating that some variables behaved according to the reference trajectories most of the time, but behaved abnormally at defined periods of time. Similarly, some $Q$ or $T^2$ variables contributions for pot A003 were high at $jl$ values around 2000.

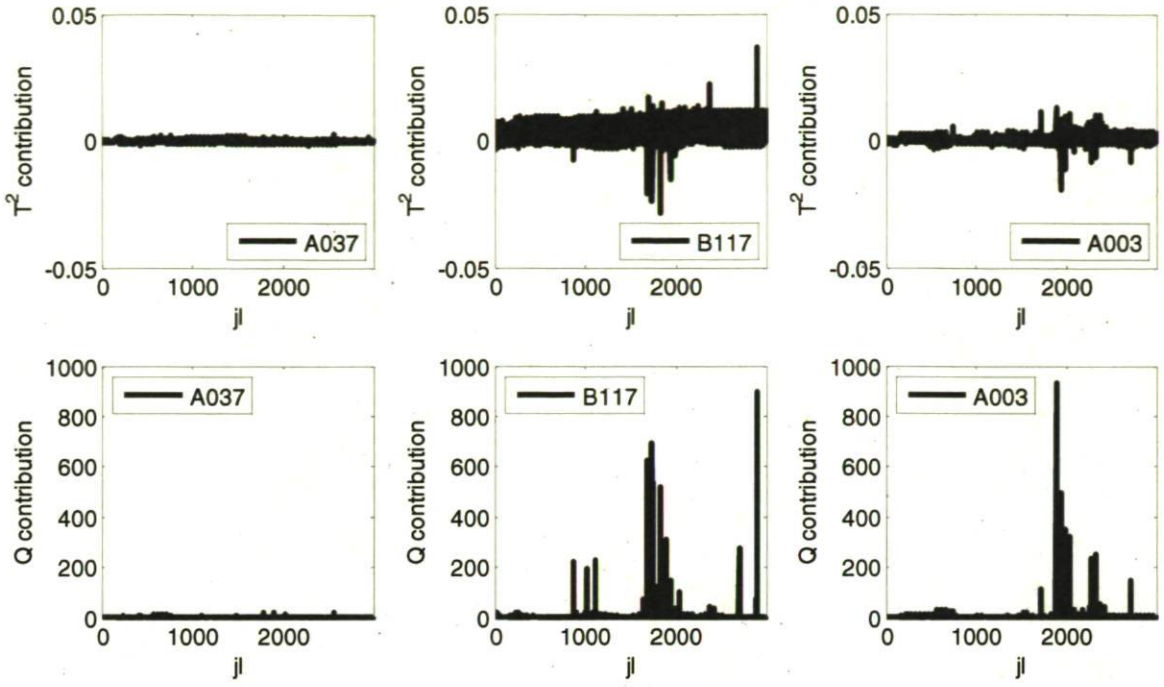


Figure 4.12: $T^2$ and $Q$ contribution plots for pots A037, B117 and A003.

The MSPC charts would draw operator's attention on those pots showing a different behaviour during the preheating, the start-up and the early operation of newly started cells. As shown in Figure 4.11, pot A037 would have been found uneventful. However, pot B117 and A003 went out-of-control at some time instant and would have requested operator's attention. When a special event is detected (i.e. $T^2$ and/or $Q$ outside the limits) the operator could use the contribution plots at this moment to help identify the variables that contributed to this upset. For instance, according to the $Q$ chart in Figure 4.11, pot B117 went out-of-control for the first time at time interval 37. This time interval corresponds to the 18$^{th}$ days of operation. Instead of looking at the complete $Q$ contribution plot, the operator would have looked only at the contributions for all early operation variables but at this specific time interval. Moreover, what happened on the same pot at time interval 52 (day 33) is also of interest. Figure 4.13 presents the $T^2$ and $Q$ contributions for pot B117 at time intervals 37 and 52.

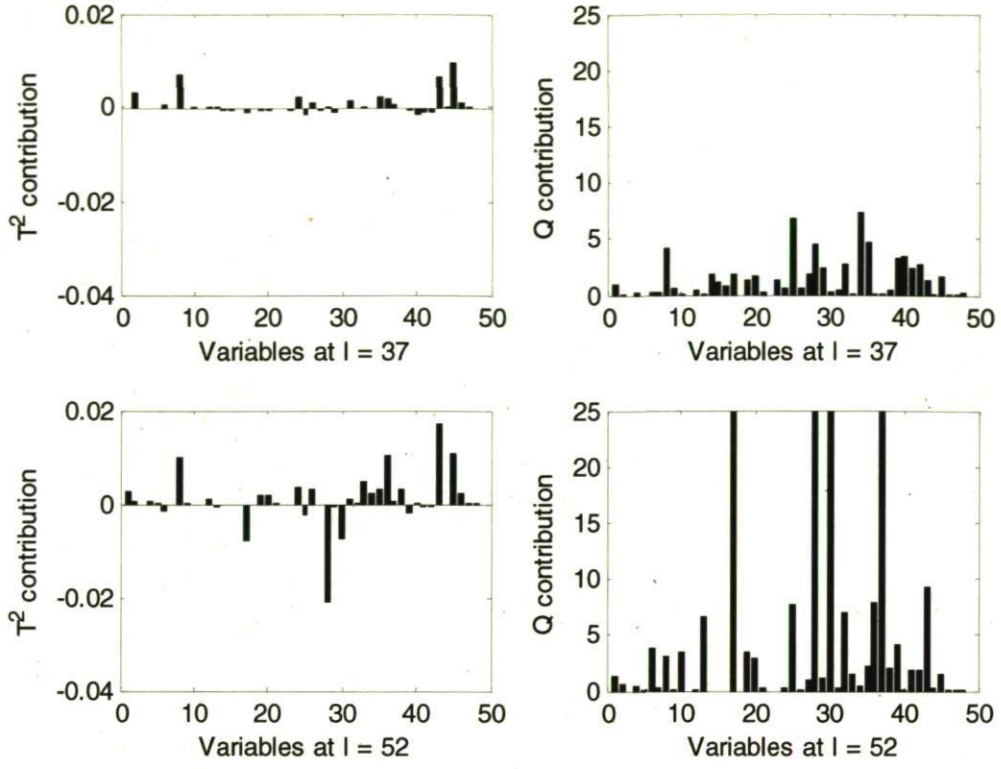


Figure 4.13: Pot B117: Contribution of early operation variables to $T^2$ and $Q$ statistics at time intervals 37 and 52.

These plots indicate that only a few variables contributed to the drift. For example, at time interval 37, $Q$ contributions for variables 8, 28, 34 and 35 are higher compared to the other variables. Violation of the $Q$ limit means that the correlation of these variables is broken compared to the reference dataset of good early operation. At time interval 52, $Q$ contributions for variables 17, 28, 30, 37 and 43 are significantly higher compared to other variables. Also, $T^2$ contributions for variables 8, 28, 30 and 43 highly contributed to the $T^2$ statistic. The combined information led to suspect that something different happened during the early operation phase for this pot and, if possible, corrective action should be taken to avoid affecting potlife. Both of these days happened to be on cold winter days when the smelter had to perform power curtailments to lower the electrical consumption and leave more energy on the Hydro-Quebec network for household heating. When this occurs, the standard policy is to apply the same set of corrective actions to all the pots, regardless of their age, in order to reduce the detrimental impact of lower power input. The drift

observed in the $T^2$ and $Q$ statistics are related to the reduced power input caused by the curtailments as well as the impact of corrective actions. It was found that these actions were not strong enough to bring the operation of this pot any closer to the reference trajectories. This caused a sustained electrical instability (short term voltage fluctuations) at an early age and permanent damage to the pot materials, resulting in shorter service life. Had such a monitoring scheme been in place, additional, but more adapted, corrective actions for this particular pot could have been rapidly taken to reduce material damage and potential impact on potlife.

The last example involves pot A003. Operators or engineers could have looked at the $T^2$ and $Q$ contributions at time interval 56 and 57 (37$^{th}$ and 38$^{th}$ days of operation after start-up), that is when the $Q$ statistics began drifting (see Figure 4.11). These contributions are shown in Figure 4.14.

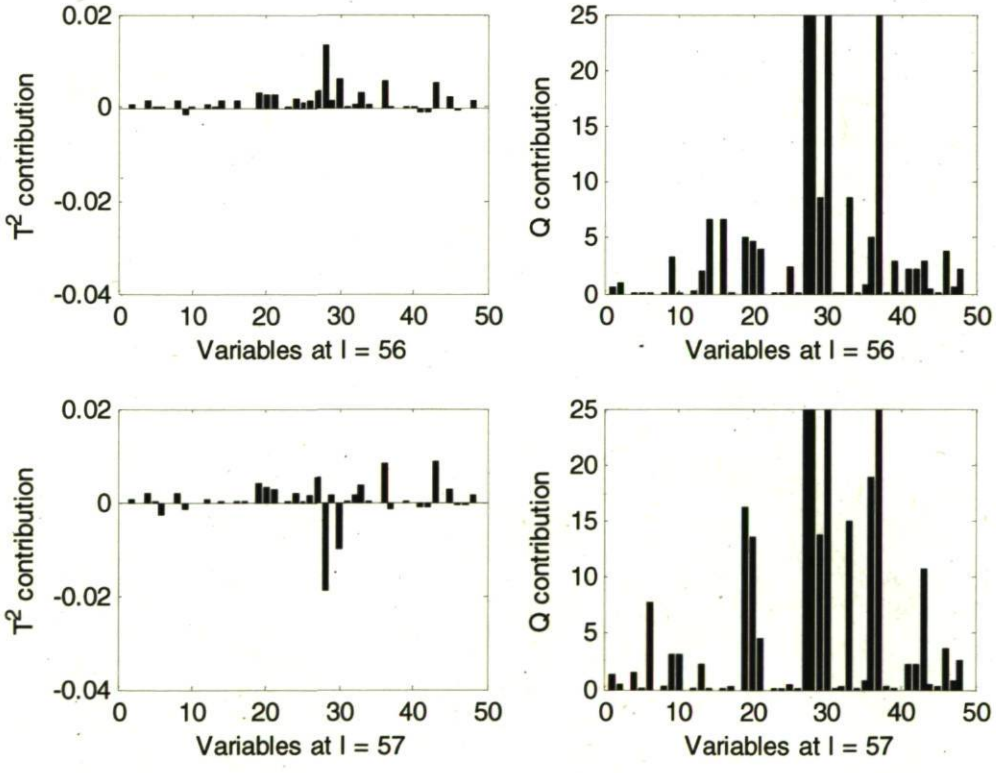


Figure 4.14: Pot A003: contribution of early operation variables on $T^2$ and $Q$ at time intervals 56 and 57.

Variables 14, 16, 28, 30, 33 and 37 mainly contributed to the drift in the $Q$ statistic, which means that the way they behave relative to one another was much different compared to good early operation. The signature left by these variables is associated with both a noisy behavior (short term voltage fluctuations) and a sustained anode effect, both occurring at time interval 56. When an anode effect is detected, the standard troubleshooting policy does not involve an immediate investigation of the anodes, but rather a series of verifications and actions are made by the operators. In the following days (time interval 57 for example) this pot remained very noisy showing that previous actions did not resolve the problem (i.e. detected by the $Q$ statistics which continued to drift in Figure 4.11) requiring further investigation. Several days later, a defective anode suspected to be the cause of the high noise episode, was pulled out of the pot. Operators tried to fix this anode for a few days before finally pulling it out and replacing it with a new one, which seemed to have contributed to a more stable operation. On-line monitoring could have help operators focusing their attention on the anodes at an earlier stage (i.e. after observing that their initial set of actions did not resolve the problem) and therefore, could have reduced detrimental impact on service life.

## 4.10 Conclusion

In this paper, it was demonstrated that preheating, start-up and early operation have an impact on aluminum reduction cells service life. This was demonstrated through the development of a PLS regression model, predicting potlife of newly started pots, using the information available from the preheating, start-up and early operation phases. Hence, 60 days after start-up, the developed regression model is able to predict potlife with a root mean squared error of prediction of 84 days, which is small enough to be useful for plant operators. Moreover, this model sorted the information from the 73 variables included in the model to highlight 25 variables that are highly correlated with potlife. Plant operators can then focus their attention on these variables in order to improve potlife. Also, efficient MSPC charts were proposed to monitor pots during preheating, start-up and early operation, with respect to potlife. Instead of responding to any kind of variations, these charts only highlight variations having an impact on potlife. These charts can rapidly flag

pots that operate abnormally and also enable engineers to drill down the information and utilize the contribution plots to determine variables contributing to the process upset.

Finally, it is understood that the relatively small number of pots studied in this work do not allow an extensive coverage of pot-to-pot variations and of the various events that may happen during early operation. Further data need to be collected, and models periodically updated, in order to refine the monitoring scheme and increase its robustness. For example, there was no very short life pot in this limited dataset. Hence, more data on such pots need to be collected in order to accurately predict such events. This could be done by adding more pots to the already available dataset and updating the model. However, a proof of concept was presented in this paper, and will be further investigated in the future.

## 4.11 Acknowledgements

Part of this research was financed by the Fonds québécois de la recherche sur la nature et les technologies by the intermediary of the Aluminum Research Centre – REGAL and the National Science and Engineering Research Council. The authors would also like to thank Alcoa Inc. for funding and granting permission to publish these results. Special thank also go to Alcoa Deschambault Potroom Technical Staff for their help and support.

# 5 Multivariate Analysis and Monitoring of the Performance of Aluminum Reduction Cells

## 5.1 Résumé

Cet article présente l'étude de l'impact des variations de la qualité des matières premières, des points de consigne et des variables d'état du procédé, ainsi que des conditions de démarrage sur les performances des cuves d'électrolyse. Les alumineries sont opérées au dessus de leur capacité nominale de conception, ce qui limite leur flexibilité à accepter certaines variations. À l'aide d'un modèle de régression PLS (Projection sur les structures latentes) basé sur 31 cuves, il est démontré qu'il est possible d'expliquer 52% de la variation de l'efficacité de courant et de la consommation énergétique. Ce modèle permet d'investiguer les variables contribuant le plus aux variations des performances des cuves. Les effets de ces variables sont discutés et une stratégie de suivi statistique est proposée afin de repérer efficacement et rapidement les problèmes éventuels provenant des différentes sources de variations affectant l'opération des cuves d'électrolyse.

Tessier, J., Duchesne, C., Tarcy, G.P., Gauthier, C., Dufour, G., Submitted to *Metallurgical and Materials Transactions B* (E-TP-09-335-B, November 24th, 2009).

## 5.2 Abstract

Aluminum reduction smelters, as other metallurgical and chemical plants, are now operated well above their nominal capacity through different process improvements. However, in the case of aluminum smelters, the added production often comes at the cost of lower operational window while alumina and coke quality are degrading. Still, smelter operators try to maintain their production performance metrics at the highest level but face once in a while performances variations. This paper investigates, through the use of multivariate multiblock regression tools, how raw materials quality, measured and manipulated variables and reduction cell start-up interact together to affect performances. Based on a pot-to-pot analysis of 31 industrial pots, the developed model explains about 52% of the performance variations, in spite of all uncertainties associated with operational computation of current efficiency and energy consumption. Important variables are presented and discussed and different month-to-month performance variations are analyzed. This will be use in the future for performance monitoring and early detection and diagnosis of abnormal operation.

## 5.3 Introduction

Aluminum (Al) is the third most abundant element on Earth and makes up to 8% of the Earth's solid weight. However, it is naturally strongly bonded to oxygen and needs to be isolated through a sequence of different processes to be converted into metallic aluminum. Industrial aluminum production begins with bauxite which is converted to alumina ($Al_2O_3$) through the Bayer process (Grjotheim and Kvande, 1993). The latter is then reduced to aluminum (Al) using the Hall-Héroult process (Grjotheim and Kvande, 1993; Thonstad et *al.*, 2001).

In this later process, alumina powder is dissolved in a molten mixture of cryolite and fluoride salts and is electrochemically dissociated into aluminum and oxygen. Using carbon anodes, the theoretical dissociation voltage is 1.2 V (Grjotheim and Kvande, 1993) and the global reaction is:

$$2\ Al_2O_{3(diss)} + 3\ C_{(s)} = 4\ Al_{(l)} + 3\ CO_{2(g)} \qquad [5.1]$$

This reaction takes place in metallurgical reactors called reduction cells or pots. Modern aluminum smelters are equipped with hundreds of cells that are operated for a period of 4 to 10 years depending on cell design, operating conditions and control policies. Throughout operation, cell performance is generally quantified using current efficiency (CE) and energy consumption (EC). Current efficiency is the ratio of real to theoretical metal production, obtained from Faraday's law, and is computed over a defined period of time. On the other hand, energy consumption is defined as the amount of electrical energy used to produce one kilogram of aluminum. These two metrics are computed for each pot over a 24 hours period as follows (Grjotheim and Kvande, 1993):

$$CE = M_{Al}/(I * 0.0080538) \qquad [5.2]$$

$$EC = 2.9806 * U/CE \qquad [5.3]$$

where $M_{Al}$ is the real pot production in kg, over 24 hours; I is the current flowing through the pot in ampere and U is the operational pot voltage in volt, including all external voltage drops.

Figure 5.1 presents overall correlations between CE, EC, and potlife for the 31 pots investigated in this study. From these charts, it is clear that CE and EC are correlated to each other (R = -0.77) while these two metrics seem to be relatively decoupled from potlife as shown by the lower correlation coefficients (CE: R = -0.47; EC: R = 0.34).

Even though these metrics are easily computed, many factors will cause CE and EC to vary during the pot service life. Many scientists and plant operators have worked on improving understanding of the root causes of these fluctuations, and it is known that alumina and anode quality (i.e. process raw materials) are two important sources of disturbances introducing variations in pot performance. Moreover, electrolytic bath chemistry, pot operating conditions, pot design and start-up conditions (i.e. preheating, start-up and early operation) also have an effect on CE and EC. The influence of these variables is briefly described below:

- Alumina quality has an impact on alumina dissolution rate in the electrolyte. Unfortunately, as presented by Wang (2009), inconclusive and contradictory findings are presented in the literature and there is still no agreement on which of the alumina properties really affect alumina dissolution rate.

- Jentoftsen et *al.*, (2009) presented the impact of anode quality, mainly $CO_2$ reactivity, on CE at a plant based level. It is known that an increase in anode air and $CO_2$ reactivity may lead to a more severe selective burning of the anode binder mix in the pots, thus resulting in carbon dust. Dust floats on top of the bath and finally in case of severe dusting, is dispersed within the molten bath. This increases bath thermal insulation and contributes to increasing pot temperature. According to Wang et *al.*, (1994), this may increase bath electrical resistivity and, in turn, reduce anode-cathode distance (ACD). Both of these factors are associated with a lower CE through the back reaction (Grjotheim and Kvande, 1993). A lower ACD may also lead to the formation of anode spikes (Rolots and Wai-Poi, 2000), lowering CE further through different mechanisms. Many smelters have encountered different dust episodes and serious cases can reduce CE by up to 3%. In addition, anode

cracking may lead to severe cell disturbances resulting in higher carbon consumption and manpower (Meir et *al.*, 1994).

- Dewing (1991) investigated the impact of bath chemistry on CE in industrial pots, particularly that of aluminum fluoride ($AlF_3$), lithium fluoride (LiF) and superheat (i.e. temperature above the electrolyte eutectic). Tarcy (1995) reported the influence of alumina concentration in the electrolyte on CE based on industrial cell measurements. It was observed that low alumina content increases CE. Sterten et *al.* (1998) have studied the impact of bath impurities in laboratory cells, highlighting the negative impact of polyvalent impurities such as Fe, P, V, S, Zn, Ti, and Ga on current efficiency. These impurities are mainly introduced by alumina and carbon anodes.

- Tarcy and Sorensen (1991) studied variations in CE using many industrial pots and found that bath temperature could decreases CE by 0.25%/°C. In Tarcy (1995) the impact of metal tapping on CE was presented. Clearly, CE drastically drops right after metal tapping (typically performed on a 24 or 36 hours basis) demonstrating that manual operations also have an impact on pot performance.

These investigations have deepened our knowledge of the factors affecting CE and EC. However, instead of studying the process as a whole, published studies in the open literature generally only take into account the effect of a few variables or group of variables at a time, thus independently focusing on some particular aspects. Recently, Tessier et *al.* (2008) used a multivariate approach to analyze a potline CE drop taking into account alumina and anode quality, as well as some potroom parameters. This study highlighted the negative impact of certain combinations of events causing a number of process variables to move together in the wrong direction, leading to a lower CE.

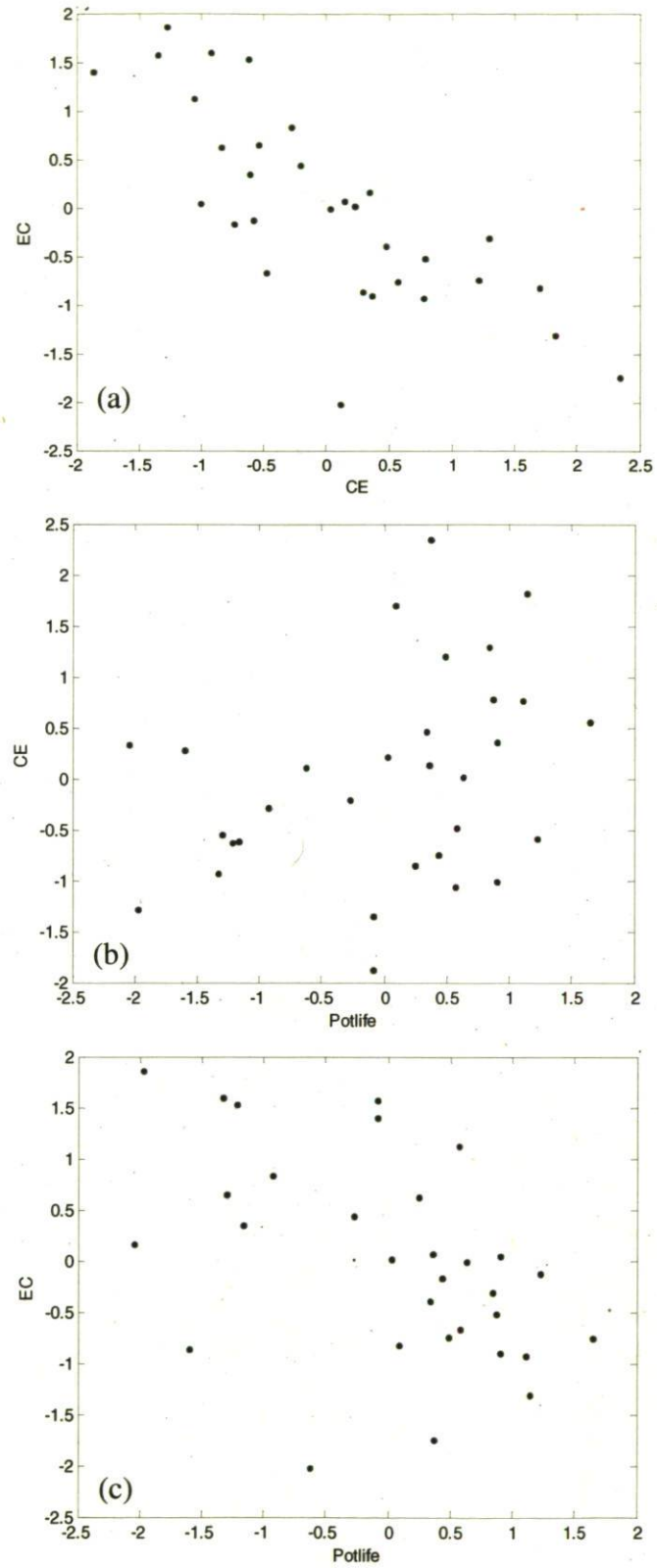


Figure 5.1: Linear relations between (a) CE and EC, (b) CE and potlife and (c) EC and potlife.

A multivariate analysis of the factors influencing reduction cell performance (i.e. CE and EC) over their entire service life is presented in this paper. It uses all available potroom data organized into the following groups: start-up policies, alumina and anode quality properties, pot operation set-points, manipulated and state variables. Studying all these data blocks together should help identify interactions between different groups of variables, or combinations of them, explaining variations in performance over a complete potlife cycle. The approach consists of building a latent variable model, using Multiblock Partial Least Squares model (MBPLS), on a database collected from several pots. The resulting latent variable space is subsequently interpreted to highlight variables statistically contributing to CE and EC variations.

This paper is arranged as follows. First, the nature of the potroom data used in this study is presented, followed by a description of the multivariate latent variable modeling method (i.e. MBPLS). Fluctuations in CE and EC performance metrics are then predicted. Finally, the contribution of each group of variables in explaining CE and EC variations is discussed, and used to investigate and diagnose the possible causes of some short term CE variations on a pot basis.

## 5.4 Dataset

This study was performed using data from the Alcoa Deschambault smelter. This smelter operates 264 AP-30 pots operated beyond their nominal design. Data were gathered from 31 pots started between 2002 and 2004 and by the time this study was performed all 31 pots were stopped and replaced with new ones. For each pot, preheating, start-up and early operation data, as well as alumina and anode quality and pot operating data were retrieved for complete pot life cycles.

### 5.4.1 Alumina quality

Since the Deschambault smelter does not have an alumina refinery on site, alumina is shipped by boat to the smelter from different refineries. For the time period covered by this study, alumina was shipped from six refineries identified as Suppliers A to F. Each shipment comes with a certificate of analysis (COA) reporting chemical impurities, particle

size distribution and physical properties. The analysis included COA variables, some binary variables to indicate alumina supplier and also the % of < 20μm at the outlet of the dust collector systems, representative of the real % of < 20μm alumina particles fed to the pots. These variables are presented in Table 5.1 and are referred to the Al2O3 block throughout this paper.

### 5.4.2 Anode quality

In the same period of time, prebaked carbon anodes used in the cells were produced using blends of seven different cokes identified as Suppliers G to M. In order to minimize anode quality variations and ensure the best possible anode quality, depending on the different cokes used in the recipe, process engineers have used different set points in the green mill and in the baking furnace. Anode quality is assessed on a weekly basis through the analysis of few anodes core sample. These are analyzed for chemical impurities, mechanical and physical properties and air and $CO_2$ reactivity (i.e. Air Rx and $CO_2$ Rx). An overview of anode core samples test methods is presented in Fisher et *al.*, (1995) and Grjotheim and Kvande (1993) and quality variables used in this analysis are presented in Table 5.1 and are referred to the Anode block.

### 5.4.3 Preheating, start-up an early operation data

Before entering production, each new pot has to be preheated for a defined period of time to bring pot materials from ambient temperature to their operating temperature. This is a critical step as uncontrolled variations during this period could be detrimental to potlife (chapter 4; Sorlie and Øye, 1989) and to pot electrical noise (Zangiacomi et *al.*, 2005, 2006). Preheating and start-up data were retrieved from pot start-up log books. Preheating variables are collected at the end of the preheating step. Start-up variables are snapshot values defining start-up conditions. Early operation variables were averaged over the first two months of pot operation as discussed in chapter 4. These variables are presented in Table 5.1 and are referred to the PSE block.

### 5.4.4 Pot manipulated and state variables

To assess and monitor pot state, different variables are routinely sampled on each pot, analyzed by process engineers and stored in the plant database. These variables are either collected by the pot controller, like noise and resistances, or manually by operators, like bath level, temperature and chemistry. Following the analysis of these variables, process engineers and the pot control system will change different set points to improve pot performance. For this particular smelter, this is achieved on a pot-to-pot basis since each pot is equipped with a dedicated local controller. Again, these set-points are stored in the plant database. Pot state and manipulated variables included in this analysis are presented in Table 5.1 and are referred to the SV and MV blocks, respectively.

### 5.4.5 Potroom location variables

Additional variables were selected based on process knowledge in order to take into account pot age and location within the potroom. For example, the average trend of CE and EC computed from the 31 pots suggest that CE decreases with age after the first few months while EC increases. To model these trends, time since start-up was included in the database. Furthermore, it is known that different parts of a potroom perform better or worse than other due to magnetic fields imbalance or differences in the alumina transport or in the dust collection system. Hence, a number of binary variables were used to describe pot location within the potroom. These variables are presented in Table 5.1 and are referred to the PLV block.

# Table 5.1: Blocks of variables included in the analysis.

| Alumina Quality (Al2O3) | |
|---|---|
| Variable | Label |
| 1 | Supplier A |
| 2 | Supplier B |
| 3 | Supplier C |
| 4 | Supplier D |
| 5 | Supplier E |
| 6 | Supplier F |
| 7 | % Al2O3 Dried |
| 8 | % CaO |
| 9 | % Ga2O |
| 10 | % K2O |
| 11 | % Na2O |
| 12 | % P2O5 |
| 13 | % TiO2 |
| 14 | % V2O5 |
| 15 | % ZnO |
| 16 | Ratio CaO/Na2O |
| 17 | % > 150µm |
| 18 | % > 106µm |
| 19 | % > 75µm |
| 20 | % > 53µm |
| 21 | % > 45µm |
| 22 | % < 45µm |
| 23 | % < 20µm |
| 24 | % < 20µm Normalized |
| 25 | % < 45µm Normalized |
| 26 | % α-Al2O3 |
| 27 | Repose Angle |
| 28 | Packed Bulk Density |
| 29 | Loose Bulk Density |
| 30 | % Fe2O3 |
| 31 | Attrition Index |
| 32 | Lost on Ignition 1000 C |
| 33 | % SiO2 |
| 34 | Surface Area (BET) |
| 35 | Flow Funnel Time |
| 36 | % Al2O3 fired |
| 37 | % < 20µm out of DC |

| Anodes Quality (Anode) | |
|---|---|
| Variable | Label |
| 38 | Supplier G |
| 39 | Supplier H |
| 40 | Supplier I |
| 41 | Supplier J |
| 42 | Supplier K |
| 43 | Supplier L |
| 44 | Supplier M |
| 45 | Air Permeability |
| 46 | % Air Rx |
| 47 | % Al |
| 48 | % CO2 Dust |
| 49 | % CO2 Rx |
| 50 | Thermal Expansion Coefficient |
| 51 | Compressive Strength |
| 52 | Thermal Conductivity |
| 53 | % CO2 Lost |
| 54 | Apparent Density |
| 55 | Real Density |
| 56 | Flexural Strength |
| 57 | Fracture Energy |
| 58 | Lc |
| 59 | % Ash |
| 60 | % Ca |
| 61 | % Fe |
| 62 | % Na |
| 63 | % Pb |
| 64 | % Si |
| 65 | % S |

| Anodes Quality (Anode) | |
|---|---|
| Variable | Label |
| 66 | % Air Dust |
| 67 | % Air Lost |
| 68 | % V |
| 69 | Electrical Resistivity |
| 70 | R' |
| 71 | Young's Modulus |
| 72 | Air Permeability std |
| 73 | % Air Rx std |
| 74 | % Al std |
| 75 | % CO2 Dust std |
| 76 | % CO2 Rx std |
| 77 | Thermal Expansion Coeff std |
| 78 | Compressive Strength std |
| 79 | Thermal Conductivity std |
| 80 | % CO2 Lost std |
| 81 | Apprent Density std |
| 82 | Real Density std |
| 83 | Flexural Strength std |
| 84 | Fracture Energy std |
| 85 | Lc std |
| 86 | % Ash std |
| 87 | % Ca std |
| 88 | % Fe std |
| 89 | % Na std |
| 90 | % Si std |
| 91 | % S std |
| 92 | % Air Dust std |
| 93 | % Air Lost std |
| 94 | % V std |
| 95 | Ele Resistivity std |
| 96 | R' std |
| 97 | Young's Modulus std |

| Potroom Location Variables (PLV) | |
|---|---|
| Variable | Label |
| 100 | Time Since Start-up |
| 101 | Pot Position |
| 102 | Pot DC system |
| 103 | Room A |
| 104 | Room B |

| Pot Manipulated Variables (MV) | |
|---|---|
| Variable | Label |
| 98 | Line Amps avg |
| 105 | Set Cycle |
| 106 | Bath Level Target avg |
| 107 | Measuring Pin Height avg |
| 108 | Feed Multiplier Constant avg |
| 109 | Total Resistance Target avg |
| 110 | Base Resistance Target avg. |
| 111 | % AlF3xs Target avg |
| 112 | Bath Temperature Target avg |
| 99 | Line Amps std |
| 113 | Bath Level Target std |
| 114 | Measuring Pin Height std |
| 115 | Feed Multiplier Constant std |
| 116 | Total Resistance Target std |
| 117 | Base Resistance Target std |
| 118 | % AlF3xs Target std |
| 119 | Bath Temperature Target std |

| Preheat, Start-up and Early Operation (PSE) | |
|---|---|
| Variable | Label |
| 120 | Pre-Heating Time |
| 121 | Cathodes Final Temperature avg |
| 122 | Cathodes Final Temperature std |
| 123 | Heat-up Rate |
| 124 | Metal Added During Start-up |
| 125 | Cathodes Curent COV |
| 126 | Line Amps |
| 127 | Lowest Amps |
| 128 | Highest Amps |
| 129 | Anode Effect Duration |
| 130 | Anode Effect Voltage |
| 131 | Anode Effect Bath Level |
| 132 | Anode Effect Bath Temperature |
| 133 | % ALF3xs |
| 134 | % ALF3xs Last Value |
| 135 | % CAF2 |
| 136 | Purge Duration |
| 137 | Bath Level |
| 138 | Bath Level Last Value |
| 139 | Bath Level Target |
| 140 | Metal Pad Level |
| 141 | Measuring Pin Height |
| 142 | Line Amps |
| 143 | Feed Multiplier Constant |
| 144 | Tapped Bath |
| 145 | Normal Metal Tapped |
| 146 | Total Metal Tapped |
| 147 | Number of Al2O3 feeds |
| 148 | Number of AlF3 feeds |
| 149 | Number of Bath feeds |
| 150 | Number of Tracks |
| 151 | Number of Anode Effect |
| 152 | Number of Anode Effect Manual Kill |
| 153 | Number of Anode Effect CPU Kill |
| 154 | Slope Value |
| 155 | Personalized Temporary Resistance |
| 156 | Total Resistance Target |
| 157 | Recorded Resistance |
| 158 | Base Resistance Target |
| 159 | Stable Pot Resistance |
| 160 | Anode Effect Overvoltage |
| 161 | % AlF3xs Target |
| 162 | Bath Temperature |
| 163 | Bath Temperature Last Value |
| 164 | Bath Temperature Target |
| 165 | Cu in metal |
| 166 | % Time Mild Noise |
| 167 | Fe in metal |
| 168 | % Time in Strong Noise |
| 169 | Li in metal |
| 170 | Na in metal |
| 171 | Si in metal |
| 172 | Ti in metal |
| 173 | V in metal |
| 174 | Recorded Voltage |
| 175 | Noise |
| 176 | Current Efficiency |
| 177 | Energy Consumption |
| 178 | Liquidus Temperature |
| 179 | Superheat |
| 180 | Hyperheat |
| 181 | Cumulated Hyperheat |
| 182 | Hyperheat Integral |
| 183 | Power Input |
| 184 | Cumulated Anode Effect |
| 185 | Cumulated Power Input |
| 186 | Cumulated Si |
| 187 | Cumulated CU |
| 188 | Cumulated Noise |

| Pot State Variables (SV) | |
|---|---|
| Variable | Label |
| 189 | Spikes |
| 190 | % AlF3xs avg |
| 191 | % CaF2 avg |
| 192 | Bath Level avg |
| 193 | Number of Bath feeds avg |
| 194 | Number of Anode Effect avg |
| 195 | Anode Effect Overvoltage avg |
| 196 | Bath Temperature avg |
| 197 | Noise avg |
| 198 | Superheat avg |
| 199 | % AlF3xs std |
| 200 | % CaF2 std |
| 201 | Bath Level std |
| 202 | Metal Height std |
| 203 | Number of Bath feeds std |
| 204 | Number of Anode Effect std |
| 205 | Anode Effect Overvoltage std |
| 206 | Bath Temperature std |
| 207 | Noise std |
| 208 | Superheat std |
| 209 | Potroom Dust |

| Preformances | |
|---|---|
| Variable | Label |
| CE | Current Efficiency |
| EC | Energy Consumption |

### 5.4.6 Data treatment and averaging

This study was performed on a pot-to-pot basis to investigate CE and EC variations of each cell. To do so, MV and SV were retrieved from the plant database on a daily basis and CE and EC were computed on accordingly using the daily metal tap weight, pot average voltage and current using Eqs. [5.2 - 5.3]. Unfortunately, some uncertainties are associated with the computed values of CE and EC, since the amount of metal tapped from a pot is driven by a metal height table. One such table is presented in Figure 5.2, and clearly shows that the same amount of metal is tapped for different metal height, until the difference from the metal level target is large enough (D = difference between the measured metal level and its target) to change to a different tapping weight. Hence, different metal heights yield the same operational CE, which certainly does not exactly match the real current efficiency. Moreover, since the bath floats on top of the metal pad, the amount of metal tapped may include some liquid bath, known as bath carryover, which could not be quantified on a pot basis in this study. Hence, if an operator has some problem during a tap, he may generate a higher bath carryover, leaving some metal in the pot as he taps bath instead of metal. Over time, the metal leftover in the pot may increase the metal height in such a way that the next computed metal tap weight will be higher according to the metal height tapping table. If the discrepancy between the metal height target and the measured metal level is large enough, this will artificially increase CE for the day the leftover metal is tapped.

The PLV block variables were also arranged on a daily basis. The PSE block arrangement was presented earlier and provided an indication of the pot initial condition. However, aside from the pot age included in the PLV block these two blocks variables are constant over a pot life cycle.

Unfortunately, raw material properties are difficult to obtain on a daily and a pot-to-pot basis. Alumina certificate of analysis (COA) are available for each shipment and this smelter typically receives 15 to 20 shipments per year. Alumina shipments are stored in a limited number of silos and hence the smelter is generally using a blend from different shipments. Alumina quality properties were estimated using the COA of each shipment and

silo management policies (i.e. blends). Furthermore, anode quality is available on a weekly basis, after lab analysis of anode core samples.

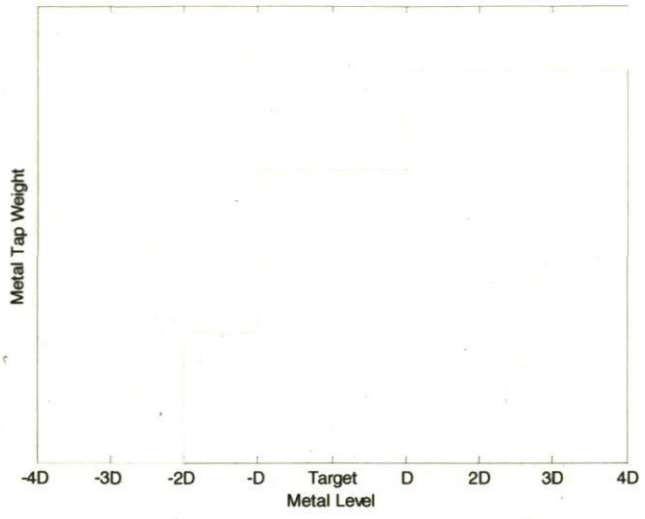


Figure 5.2: A typical metal height tapping table (D = difference between the measured metal level and its target).

This analysis could have been performed on a weekly basis which is the shortest sampling time period imposed by the anode block. However, such an analysis would have been meaningless due to the uncertainties in CE and EC (discussed above) and those associated with the estimation of which alumina blend entered a pot at a given time. Hence, it was decided to average all the data over a four weeks basis (i.e. 28 days). This nearly matches the average anode set cycle used at the plant and hence, averaging the anode properties over a four week window provides a good estimation of anode quality populating a pot during the complete set cycle. Moreover, it also smoothes out some of the uncertainties in the estimation of alumina blends and in computing CE and EC. Finally, CE and EC values are more meaningful to smelter operators on a monthly basis, which is close to the 28 days basis used here. From this point in the paper, the 28 days basis will be referred to months.

## 5.5 Latent Variables Modeling

As presented in Table 5.1, this analysis involves 209 raw material and process variables, available on a monthly basis, to be used for explaining variations in the two key performance indicators, CE and EC. Multivariate Latent Variable methods, such as Principal Component Analysis (PCA) and Partial Least Squares (PLS), can be used for extracting the information contained within the various data blocks taken jointly. These methods have shown their ability to cope with problems typically encountered with industrial data arising from collinearity, noise and missing values. The mathematical foundations of these methods is described in details in several papers (Geladi and Kowalski, 1986; Wold et *al.*, 1987, 2001; Höskuldsson, 1988; Jackson, 1991). A few good reviews of their applications for solving a number of problems in various industrial areas are also available in the literature (Kourti and MacGregor, 1995; Duchesne et *al.*, 2002; Kourti, 2002, 2005; Miletic et *al.*, 2004, MacGregor et *al.*, 2005). Moreover, Tessier et *al.* (2008, 2009) and Majid et *al.* (2009) have also used some of these methods to investigate different aluminum smelting process issues.

### 5.5.1 Partial least squares (PLS)

Consider a matrix of process data **X** ($I \times J$) containing $I$ observations on $J$ process variables and a second matrix, **Y** ($I \times H$), containing $I$ observations on $H$ quality or performance indicators. Assume that both data blocks contain systematic and stochastic variations (i.e. noise) jointly driven by a small number of $A$ underlying events, also called lurking or latent variables (i.e. unmeasured). This is typical of industrial process databases collected during normal or abnormal production (i.e. in the absence of designed experiments), which results in not full rank **X** and **Y** data matrices. Latent Variable Methods consist of a family of multivariate statistical techniques which aim at finding these underlying process events causing both process and quality variables to move together in certain directions. Once this lower dimensional latent variable space **T** ($I \times A$) is identified, the data in **X** and **Y** are projected onto it allowing for easier visualisation and interpretation of large industrial databases. Partial Least Squares (PLS) regression is one such method.

The PLS method performs a decomposition of the covariance structure between **X** and **Y**, by finding a common set of latent variables **T** that captures the information in **X** that is the most highly correlated with **Y** while building a model also describing both of these data blocks. The structure of the PLS model is given below:

$$\mathbf{X} = \mathbf{T}\,\mathbf{P}^{\mathbf{T}} + \mathbf{E} \qquad [5.4]$$

$$\mathbf{Y} = \mathbf{T}\,\mathbf{Q}^{\mathbf{T}} + \mathbf{F} \qquad [5.5]$$

$$\mathbf{T} = \mathbf{X}\,\mathbf{W}^{*} \qquad \mathbf{W}^{*} = \mathbf{W}(\mathbf{P}^{\mathbf{T}}\mathbf{W})^{-1} \qquad [5.6]$$

where **T** ($I \times A$) is the common latent variable space defined by the loading matrix **W*** ($J \times A$) and capturing the information in **X** that is the most highly correlated with **Y**. The **P** ($J \times A$) and **Q** ($H \times A$) matrices contain the orthogonal loading vectors mapping the common latent variable space in the original spaces of **X** and **Y** (models of these blocks). The PLS model residuals for both blocks are stored in **E** ($I \times J$) and **F** ($I \times H$), respectively.

The number of latent variables ($A$) to include in the model can be determined by a leave-n-out cross-validation procedure [Wold, 1978] and the NIPALS (Geladi and Kowalski, 1986, Kourti and MacGregor, 1995) algorithm is often used to iteratively compute **T**, **P**, **Q**, **W** and **W***.

From these latent variable models, it is possible to interpret the behaviour of the variables relative to each other (i.e. their correlation structure) by means of the loading vectors stored in **P**, **Q**, **W** and **W***. On the other hand, the latent variables **T** can be used to visualize clusters and patterns defined by the observations.

Like any projection method, PLS is a scale dependent and an appropriate scaling is required prior to performing the analysis. To give an equal importance to each variable in the model, a common practice is to mean-center and autoscale (i.e. divide by the standard deviation) each variable in the **X** and **Y** blocks.

### 5.5.2 Multi-blocks partial least squares (MBPLS)

In the present study, the **X** data could naturally be divided into six blocks as presented in Table 5.1. This enables the use of multi-block PLS (MPLS) algorithms, which are modified

versions of PLS to enhance interpretability when multiple data blocks are associated with separate equipments or sections within a plant. These methods are well described in the literature (Westerhuis and Coenengracht, 1997; Westerhuis et *al.*, 1998, 1999; Smilde, Westerhuis, de Jong, 2003; Höskuldson and Svinning, 2006) and only a brief description is given here.

Consider the process data **X** presented in Table 5.1, composed of *I* observations and *J* process variables and **Y** (*IxH*), a matrix of performance data related to **X**. Here, *H*=2 since CE and EC are used as performance metrics. A regular PLS model could be built to relate **X** (i.e. all variables in a single block, see Figure 5.4(a)) and **Y.** Then, as shown by Westerhuis et *al.*, (1998), the MBPLS results could be obtained from that model after applying block scaling to the **X** matrix. That is (1) autoscale **X**, then (2) divide each variable by the square root of the number of variables within its corresponding block (i.e. $\sqrt{J_{AL2O3}}$, $\sqrt{J_{Anodes}}$, …, $\sqrt{J_{SV}}$), thus giving equal importance to each block in the model. As shown in Figure 5.4(b), MBPLS yields a hierachical model made of a super level and a block level. The scores obtained using PLS and block scaling (**t** and **u**'s) are equal to the MBPLS super scores ($\mathbf{t_x}$ and **u**'s). The block scores ($\mathbf{t}_{Al2O3}$, $\mathbf{t}_{anodes}$, …, $\mathbf{t}_{SV}$), block variable weights ($\mathbf{w}_{Al2O3}$, $\mathbf{w}_{anodes}$, …, $\mathbf{w}_{SV}$) and super weight $\mathbf{w_x}$ of the MBPLS method for each block and each latent variable dimension can be calculated as follows:

$$\mathbf{w}_{Al2O3} = \mathbf{X}_{Al2O3}^{T}\,\mathbf{u}/\mathbf{u}^{T}\mathbf{u} \qquad [5.7]$$

$$\mathbf{t}_{Al2O3} = \mathbf{X}_{Al2O3}\mathbf{w}_{Al2O3}^{T} \qquad [5.8]$$

$$\mathbf{X_T} = [\mathbf{t}_{Al2O3}\,\mathbf{t}_{Anodes}\cdots\,\mathbf{t}_{SV}] \qquad [5.9]$$

$$\mathbf{w_x} = \mathbf{X_T^T}\,\mathbf{u}/\mathbf{u}^{T}\mathbf{u} \qquad [5.10]$$

The main advantage of MBPLS is to allow process monitoring at two levels: 1) the super level where the information within all the blocks are jointly related to performance (**Y**) and provide a plantwide monitoring capability, and 2) the block level where individual equipments, raw materials or sub-processes can monitored. Breaking down the information using such hierachy may help better understand and diagnose process variations leading to poorer performance.

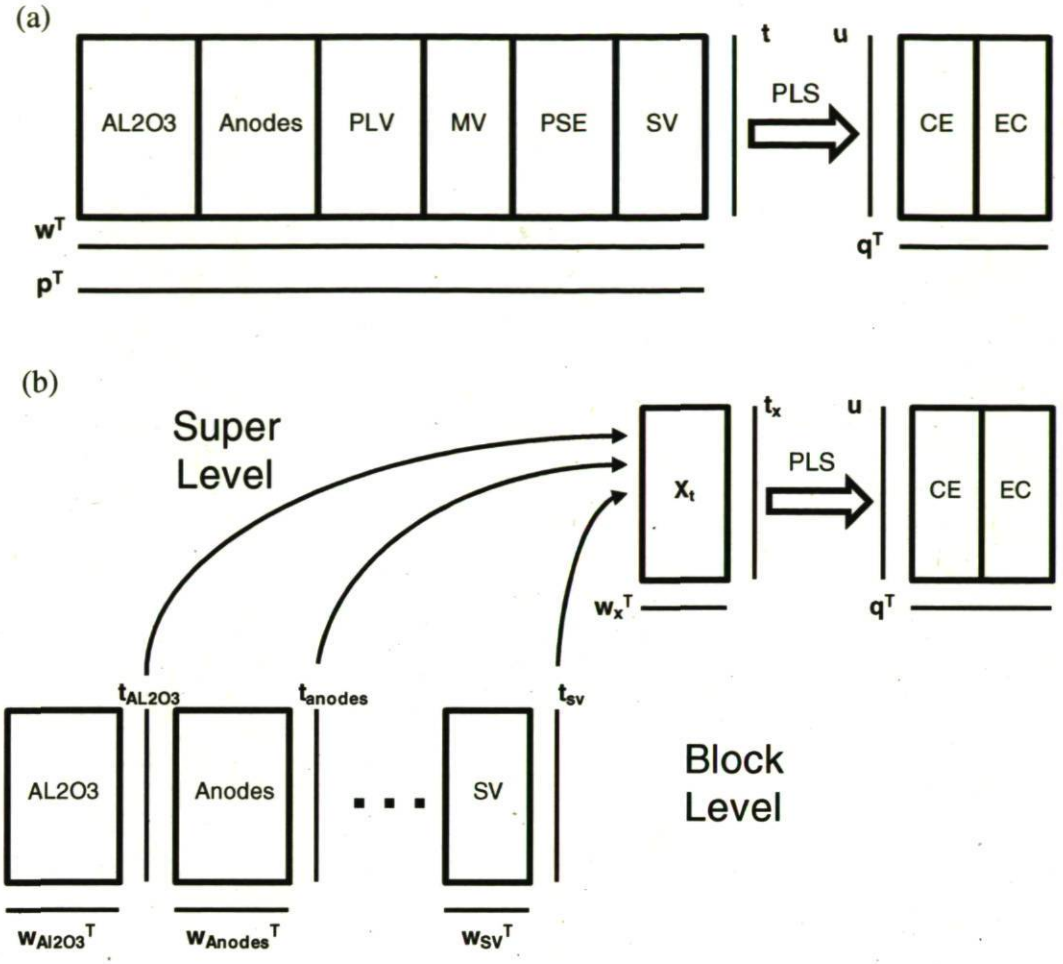


Figure 5.3: Data arrangement for (a) the regular PLS and (b) the MBPLS methods. All vectors are shown for a single component.

## 5.6 Performance Prediction Results

To account for pot dynamics, it was found that using a data history of about 12 weeks (or 3 months) for certain data blocks improved prediction results for CE and EC. This was implemented by the use of moving window averages. Consider $\mathbf{X}_{i,t}$ the $i^{th}$ regressor data block averaged over a 28 days period as discussed in section 5.4.6, that is, the data were averaged over the past 28 days from current time. Also denote $\mathbf{X}_{i,t-1}$ and $\mathbf{X}_{i,t-2}$ the same data block (i.e. variables) but averaged over the past two periods of 28 days, that is from days -

29 to -56 and days -57 to -84 from current time, respectively. Such a moving window structure was implemented for all the blocks except for the PSE and PLV blocks for which dynamics do not apply. This data structure is presented in Figure 5.4, where $\mathbf{Y}_t$ corresponds to CE and EC data averaged over the past 28 days from current time. Using this data structure, performance data for the latest 28 days period ($\mathbf{Y}_t$) will be regressed on a history of about 12 weeks of process data. Accounting for dynamics increases the total number of variables, from the 209 original variables listed in Table 5.1 to 479 variables since the alumina, the anode, the manipulated variables and the state variables are included three times (but averaged over different periods) to account for the 3 months moving window. Since the averaging windows move forward each 28 days period, from pot start-up until the end of service life, a large number of observations are also obtained. This dynamic model structure, for each 28 days period and each pot, was stored row-wise in a large data matrix **X** (see Figure 5.4) Using such a data arrangement, **X** includes 2271 observations and 479 variables ($I$ = 2271 and $J$ = 479) and is used to built a MBPLS model between **X** and **Y** matrices, as described in section 5.5.2.

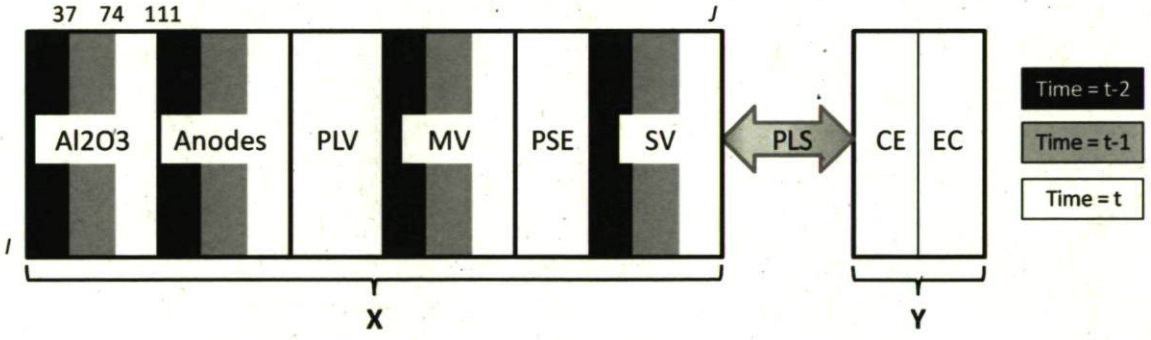


Figure 5.4: Data structure used in the analysis.

A total of 5 components were selected through cross-validation. This model captures 23.52% and 52.54% of the variance (i.e. information) of **X** and **Y**, respectively, and achieves root mean squared prediction errors in cross-validation (RMSECV) of 2.26% for CE and 0.399 kWh/kg for EC. Autoscaled values of predicted CE and EC, obtained in cross validation, are presented in Figure 5.5 against the measured CE and EC values. Moreover, the explained variance and RMSECV are presented in Figure 5.6 for each pot included in the analysis.

Variations in the performance of some pots are better explained than others (ranges from 25-65% for CE and 10-65% for EC), but the precision of the predictions (i.e. RMSECV) seems more consistent among the 31 pots. This might be due to lower systematic variations in CE and EC for some pots but with similar level of noise in the data. Overall, the model explains 54.21% and 50.87% of the variance of CE and EC, respectively. A considerable amount of efforts were made to improve predictive ability using other ways to pre-process the data, but with no significant gain. Data quality may help explain some of the difficulties in capturing a greater percentage of variations in CE and EC. Alumina and anode quality variables are not measured on a pot-to-pot basis. Alumina properties are rather estimated from suppliers COA and blending data, and weekly population averages are used to describe anode quality based on a limited number of analyzed core samples. A better traceability of these raw materials would certainly help explain additional variance. Furthermore, the uncertainties involved in computing the CE and EC values due to the tapping tables and errors may very well limit the theoretically explainable performance fluctuations.

Measured and predicted autoscaled CE values are presented for four pots in Figure 5.7. Pot A003, A096, B102 and A023 correspond to observations 1, 3, 4 and 26 in Figure 5.6, respectively. Predicted CE follow the general trend of measured CE, as shown in Figure 5.7, demonstrating again the relatively good predictive power of the model on a pot basis. However, CE exhibits other higher frequency variations. For example, pot A096 displays a sharp increase from observations 35 to 38 and then a sudden drop from observations 39 to 42. The model captured several of these CE peaks and, even it does not predict them perfectly, the results indicate that the raw material and process data included in **X** carry relevant information for explaining some of these CE fluctuations. Similar observations can be made for the three other pots in Figure 5.7, and of many of the other pots included in this analysis (not shown).

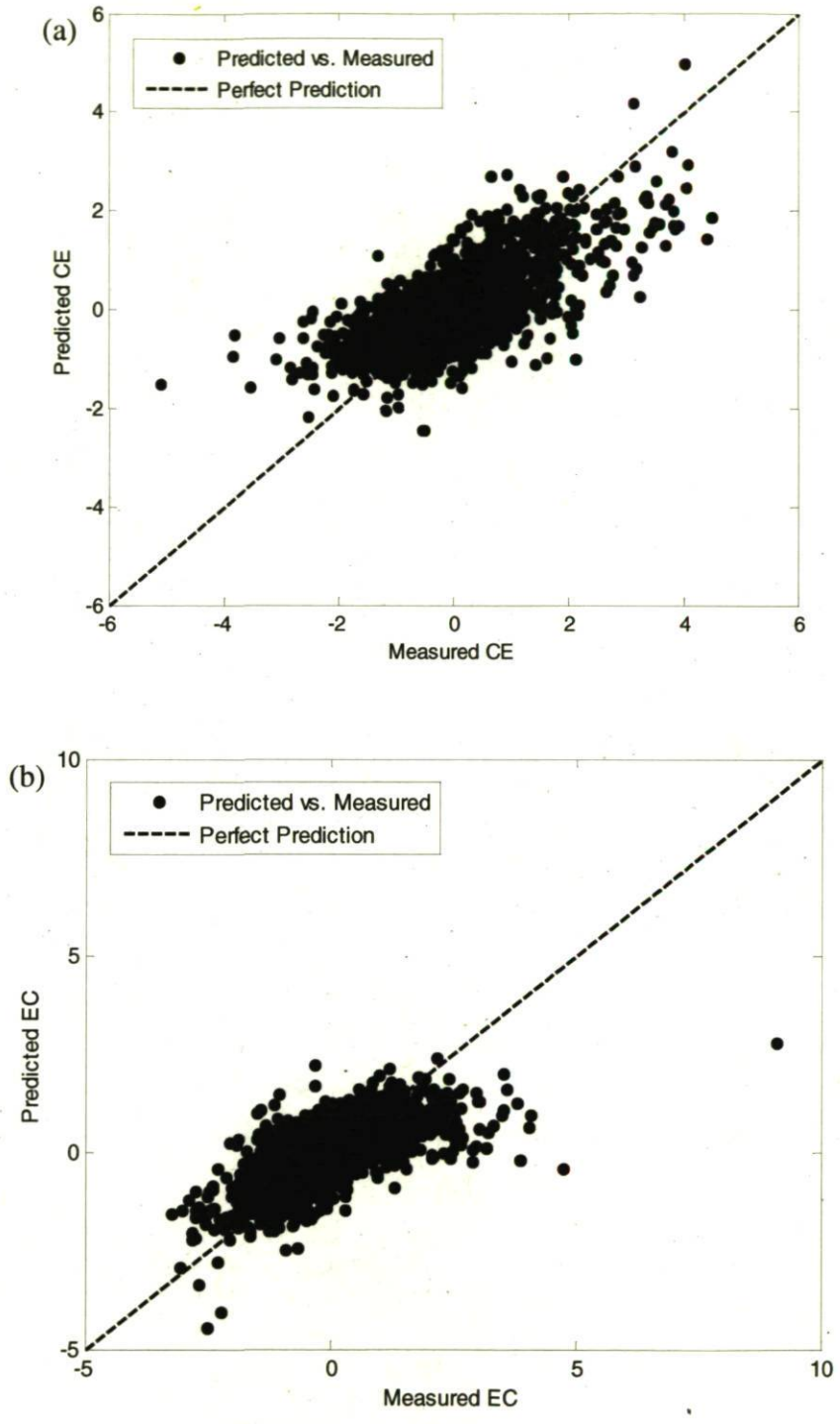


Figure 5.5: Predicted against measured values for (a) CE and (b) EC. Explained variance is 54.21% for CE and 50.87% for EC.

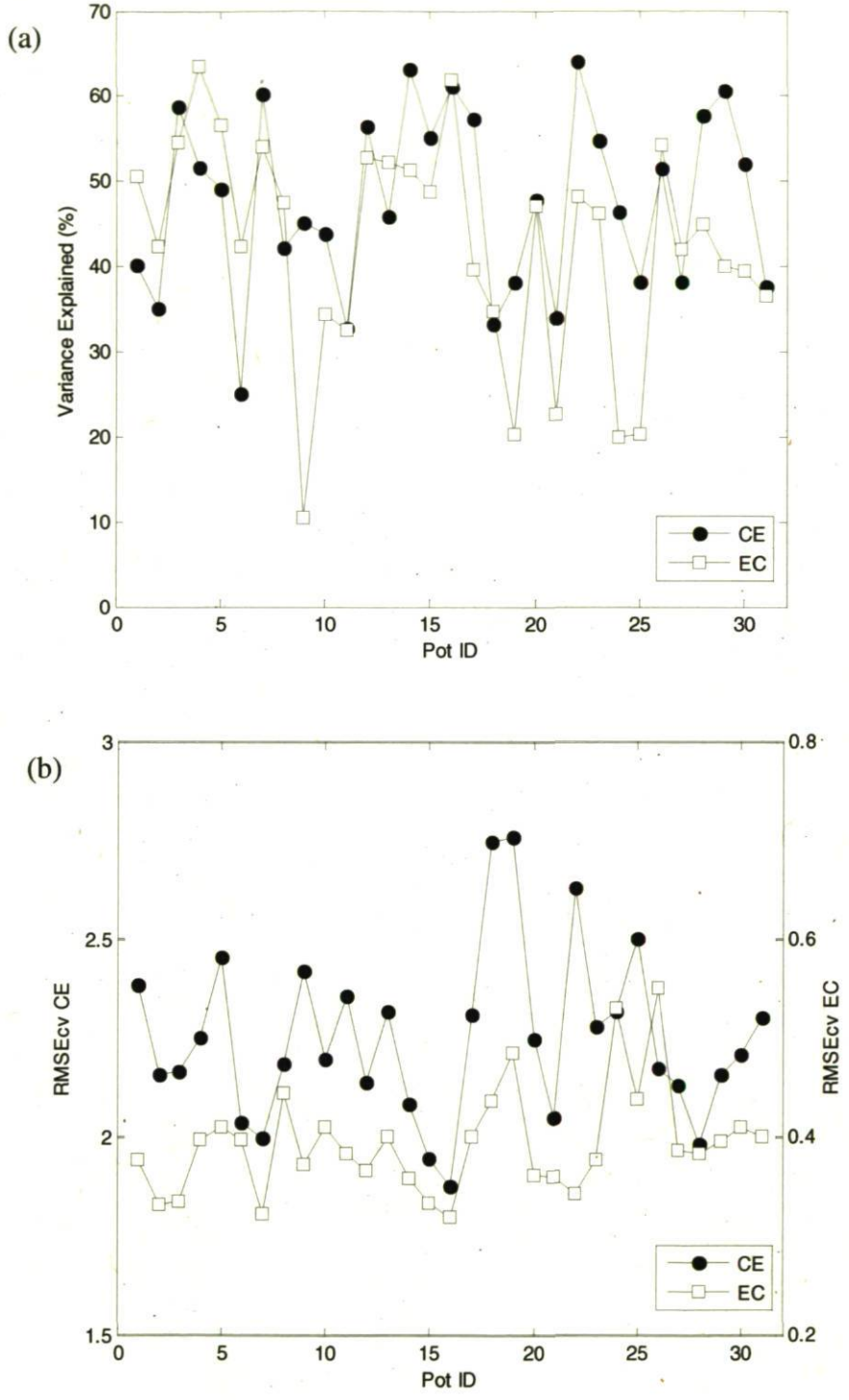


Figure 5.6: Breakdown of the MBPLS model predictive ability for each of the 31 pots used in the analysis. Explained variance in cross-validation (a) for CE and for EC and RMSECV (b) for CE and EC.

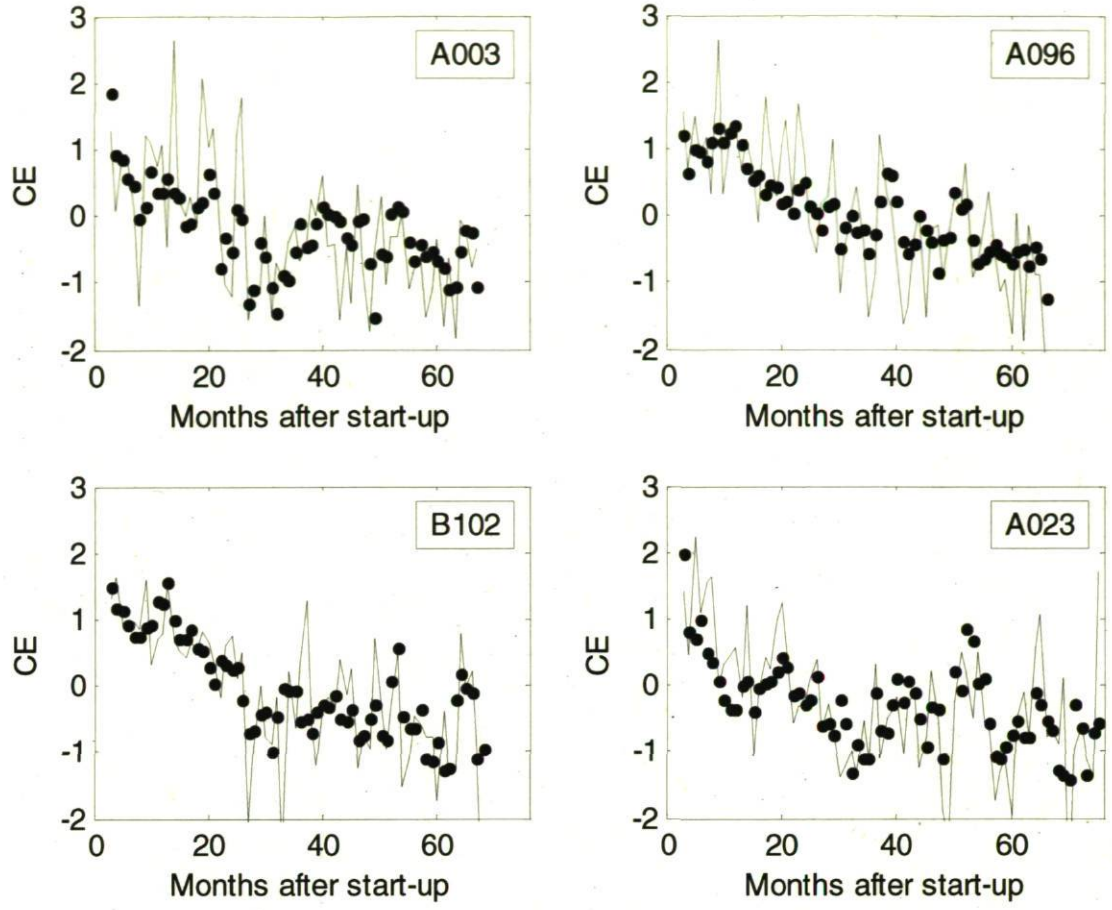


Figure 5.7: Autoscaled CE values for pots A003, A096, B102 and A023. Solid lines are for real measured CE and dots for predicted CE.

From these plots, it is possible to conclude that the model can follow or describe most of the CE variations over the four pots life cycles. For example, the model almost perfectly matches some CE peaks for pot B102 at months 13, 50 to 53 and 63 to 66, demonstrating good predictive performance, but also indicating that the model structure (**P**, **W**, **W*** and **Q**) reproduces typical pot behaviour. However, the model does not capture all peaks as seen for pot A003 at months 6, 12, 17 to 19 and 25, for example. This indicates that either not enough information was included in the data to capture these peaks and that they are driven by different behaviour not accounted using the analyzed variables or they are arising from noise (i.e. tapping tables or measurement errors).

Studying the model's loadings and weights, **P**, **W** and **W***, allow interpreting the correlation structure within **X** and **Y** through the lower dimensional latent variable space **T**.

However, it this case, since many variables ($J$ = 479) and principal components ($A$ = 5) are involved in the model, studying the relationships between these variables using the loadings and weights might not be straightforward. Nevertheless, the importance of each X-variable in explaining variations in **Y** can be computed from the weights (**W**) and the fraction of variance explained by each principal component relative to the total variance explained by the model. The variable importance metric (VIP) for each variable is computed as follows:

$$\mathrm{VIP}_{j,A} = \sqrt{\mathrm{J}\sum_{a=1}^{A} \mathrm{w}_{\mathrm{aj}}^2 \left(\mathrm{SSY}_a/\mathrm{SSY}_{\mathrm{tot}}\right)} \qquad [5.11]$$

In the above equation, $\mathrm{VIP}_{j,A}$, provides a relative measure of importance of variable $j$ in predicting **Y** using the developed PLS or MBPLS model with $A$ latent variables. This statistic adjusts the loading weight ($w_{aj}$) of the $j^{th}$ variable in the $a^{th}$ PLS component, by multiplying its value by the ratio of the sum of squares of **Y** explained by the $a^{th}$ PLS component ($SSY_a$) over the sum of squares of **Y** explained by the model ($SSY_{tot}$). Some rules of thumb were proposed by Eriksson et *al.* (2006) for describing the importance of the variables based on their VIP values: VIP > 1.0 most influential variables, 0.8 ≤ VIP ≤ 1.0 moderate influence, and VIP < 0.8 less influential variables. The overall importance of each data block can also be computed using Eq. [5.7], but replacing $w_{aj}$ by the super weights.

The importance of each data block in the MBPLS model (i.e. VIP) is provided in Table 5.2. To the author's knowledge, this is the first time that the VIP metric is used for quantifying the relative importance of data blocks. As expected, the SV and MV block are the most important for predicting CE and EC, alumina, anodes and location blocks are moderately important, and early operation (PSE) is less important. The fact that the PSE block is less important does not mean that no attention from smelter operators should be put on preheating, start-up and early operations. These are performed very consistently at Deschambault such that little variations in the PSE block are related to CE and EC. However, in older smelters where process control and equipments are older, preheating, start-up and early operation may have more impact of CE and EC and could even be a bottleneck for performance improvement. On the other hand, the VIP presented in Table 5.2 indicates that the variations in the remaining five blocks are more highly correlated to performance variations. It was expected that both the MV and SV blocks would have a

greater importance in the model compared to the alumina and anodes blocks, since the MV and SV data are available on a pot-to-pot basis. This is not the case for alumina and anodes quality, available as bulk or population estimates. Moreover, the SV block also caries all process upsets from raw materials variations and variables in the MV block are adjusted to respond to SV variations. This also explains why these blocks have higher VIP with respect to pot performance. In spite of this, the alumina and anode cannot be removed from the model without significantly degrading the model predictive ability.

Table 5.2: Importance of each data block in the MBPLS model.

| Model | Blocks VIP | | | | | |
|---|---|---|---|---|---|---|
| | Al2O3 | Anodes | PLV | MV | PSE | SV |
| Global | 0.950 | 0.876 | 0.927 | 1.278 | 0.605 | 1.213 |
| CE alone | 0.937 | 0.898 | 1.005 | 1.310 | 0.529 | 1.144 |
| EC alone | 0.963 | 0.852 | 0.843 | 1.246 | 0.673 | 1.277 |

The importance of each individual variable are also computed using Eq. [5.7]. The highest VIPs from each block are presented in Table 5.3. This table also presents the signs of the regression coefficients, obtained using Eq. [3.13], which indicate the sign of the correlation of the most relevant variables with CE. Only one variable is shown in the PLV block since it the VIP of this block is below 1.0. The VIP results for the variables in the other blocks indicate that lagged values (t-1 and t-2) of many variables have an impact on pot performance. For example, in the alumina block, the % of < 20μm out of the dust collection system has an impact on pot performance at time t, t-1 and t-2 (i.e. Figure 5.4), which demonstrates the importance of this variable, and of considering its dynamic impact on performance.

Based on process knowledge, variables presented in Table 5.3 make sense. As discussed earlier, many authors have highlighted the impact of alumina. This is also supported by the present study as particles size distribution, flow funnel times, attrition index, repose angle and some impurities are ranked high in the VIP list. Basically, these variables are believed to have an impact on alumina dissolution. This analysis suggests a negative impact on CE when the fines content of alumina increases, in accordance with Jain et *al.*, (1983) and Kvande (1998). On the other hand, Maeda (1985) reported that no correlation exist between particle size and dissolution times. Furthermore, Johnson (1981) came to the same

conclusions and even proposed an increase in dissolution time beyond a certain particle size. Hence, the impact of alumina fines on alumina dissolution needs to be verified.

Table 5.3: Highest variables VIP, for CE, from each block computed through the MBPLS model.

| Alumina Quality (Al2O3) | | | Anodes Quality (Anode) | | | Potroom Location Variables (PLV) | | |
|---|---|---|---|---|---|---|---|---|
| Lag | Label | Correlation | Lag | Label | Correlation | Lag | Label | Correlation |
| t-2, t-1, t | % < 20µm out of DC | - | t-2, t-1, t | Supplier G | + | --- | Time Since Start-up | - |
| t-2, t-1, t | % < 45µm Normalized | - | t-2, t-1, t | Supplier H | + | | | |
| t-2, t-1, t | Attrition Index | - | t-2, t-1, t | Compressive Strength | - | | | |
| t-2, t-1, t | Flow Funnel Time | - | t-2, t-1, t | Fracture Energy | + | | | |
| t-2, t-1 | % < 20µm Normalized | - | t-2, t-1, t | Electrical Resistivity | - | | | |
| t-2 | Repose Angle | + | t-2, t-1, t | R' | + | | | |
| t-2 | % K2O | - | t-2, t-1, t | % V | + | | | |
| t-2 | % V2O5 | - | t-2, t-1, t | Supplier K | - | | | |
| | | | t | Supplier I | + | | | |
| | | | t-2 | Flexural Strength | + | | | |
| Pot Manipulated Variables (MV) | | | Preheat, Start-up and Early Operation (PSE) | | | Pot State Variables (SV) | | |
| Lag | Label | Correlation | Lag | Label | Correlation | Lag | Label | Correlation |
| t-2, t-1, t | Line Amps avg | - | --- | Anode Effect Bath Level | + | t-2, t-1, t | Noise avg | - |
| t-2, t-1, t | Bath Level Target avg | + | --- | Bath Level Target | - | t-2, t-1, t | Noise std | - |
| t-2, t-1, t | Total Resistance Target avg | - | --- | Slope Value | + | t-1, t | Bath Temperature avg | + |
| t-2, t-1, t | Base Resistance Target avg | + | --- | % Time Mild Noise | - | t-1, t | Bath Level avg | - |
| t-1,t | Feed Multiplier Constant avg | - | --- | Na in metal | - | t-1, t | % AlF3xs avg | + |
| t | % AlF3xs Target avg | - | --- | Noise | + | t-1, t | % CaF2 avg | + |
| t | Bath Temperature Target avg | + | --- | Current Efficiency | - | t | Anode Effect Overvoltage avg | + |
| t | Measuring Pin Height avg | - | --- | Power Input | + | t | Potroom Dust | - |
| | | | --- | Cumulated Power Input | + | | | |
| | | | --- | Number of Al2O3 feeds | - | | | |

As mentioned by Meir et *al.*, (1994), thermally cracked anodes may lead to a decrease in pot performance. Compressive strength and fracture energy are key indicators of anode cracking, and are present in Table 5.3. Moreover, coke suppliers also appear among the variables that are the most highly correlated to performance. It is known that different cokes will lead to different anode properties, even if the best efforts are put in place to smooth out the transition between two different cokes. On the other hand, one would have expected Air Rx and $CO_2$ Rx to be listed in Table 5.3. However, % V, a catalyst for anode air reactivity, is positively correlated with CE. On the other hand, Schmidt-Hatting et *al.* (1986) reported a CE decrease as vanadium increased in the anodes. This opens the door for investigation.

As expected from the fact that CE decreases over time, the variable indicating the time since start-up is also important in predicting performance, as it helps the algorithm to capture the average trend decrease of CE and the increase of EC over time.

Pot manipulated and state variables can be interpreted together since they are strongly linked through feedforward/feedback control loops (i.e. the manipulated variables are adjusted to compensate for pot state variations). As expected from the results of Tarcy and Sorensen (1991) and Tarcy (1995), bath temperature and its target value are listed in the VIP table. It is known that the back reaction rate, re-oxidizing dissolved aluminum in bath, is favoured by higher bath temperature (Grjotheim and Kvande, 1993) and higher contact surface area between bath and metal pad (Grjotheim and Kvande, 1993). Besides increasing the surface area, metal waves characterizing the molten metal pad surface may lead to direct electrical shorting between anodes and metal pad when anode-cathode distance (ACD) is low. This phenomenon creates short term pot voltage variations, increasing the so-called noise variable and directly reducing CE. One way to lower this negative contribution to CE is to increase the ACD, which is directly related to increasing both the base and the total resistance targets. Noise and both resistances are listed in Table 5.3 and hence, are in agreement with process knowledge. Bath level and its target were also found in the list shown in Table 5.3. Stabilising bath level improves alumina feeding strategies, heat balance control, bath chemistry control, and also helps achieving better metal purity. For instance, operating a pot with a low bath level may produce alumina muck beneath the metal pad and may increase the anode effect rate since less alumina is dissolved within the bath. On the opposite, an excessive bath level may increase the iron content in the metal and hence reducing its market value, as dictated by LME premiums, while it also increases noise since the $CO_2$ gas bubbles (i.e. Eq. [5.1]) travel for a longer period of time to escape the molten bath pad. A few bath chemistry variables (% $AlF_3$xs, its target and % $CaF_2$) as well as alumina feed modifier constant, measuring pin height, anode effect overvoltage and dust were also found important for explaining performance variations. A good review of bath chemistry effects on pot performances is provided by Thonstad et *al.* (2001). Feed modifier is manipulated by process operators to force a pot to perform within a specific range of alumina *overfeed-underfeed* cycles (Grjotheim and Kvande, 1993). The measuring pin height is correlated to the real metal pad height and it is known that generally, increasing the metal height lowers the metal pad waving as it helps balancing magnetic fields, but also may help keeping a lower bath temperature as it increases the surface area available for heat losses to the environment. The effect of dusting has been discussed

earlier in this paper and anode effect overvoltage can be detrimental to process performance in two ways. It increases the overall average pot voltage, and hence EC (i.e. Eq. [5.2]), but also since high anode effect voltage contribute to increase the bath temperature (Tabereaux, 2007) and, in turn, increases the back reaction rate.

On the other hand linking variables from the PSE block to pot performance using process knowledge is not straightforward. However, these results may indicate that keeping a pot under control during the early operation is helpful to increase pot performance through the whole pot life cycle. For example, insufficient or excessive bath levels should be avoided and pot electrical power should be kept under control, which is equivalent to carefully controlling pot voltage or resistance.

Again, the loadings bi-plot can help understanding the variables structure affecting CE and EC. Figure 5.8 presents a loadings bi-plot of the first two latent variables of the CE and EC PLS model and Figure 5.9 presents a zoomed version of the same plot, including only variables at time t having a VIP over one. Since this model has five principal components, any combinations of the five set of **w*q** could be investigated. However, by definition, the first two explain the greatest amount of variance of **Y** and hence might be of greatest interest. This figure clearly demonstrates the negative correlation between CE and EC as they fall on opposite quadrants of the graph. Therefore, based on the data available in this study, improving EC with different operational policies would be at the expense of CE and vice-versa. Again, according to the available dataset, improving both simultaneously would require major changes in operating policies and/or process or technology with respect to what has been performed in the past.

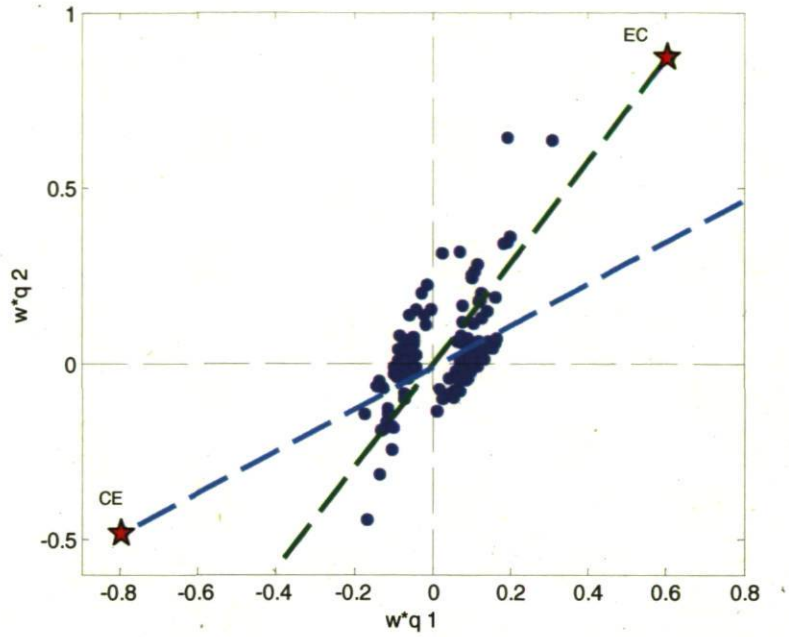


Figure 5.8: Bi-plot of the first two latent variables of the CE and EC PLS model.

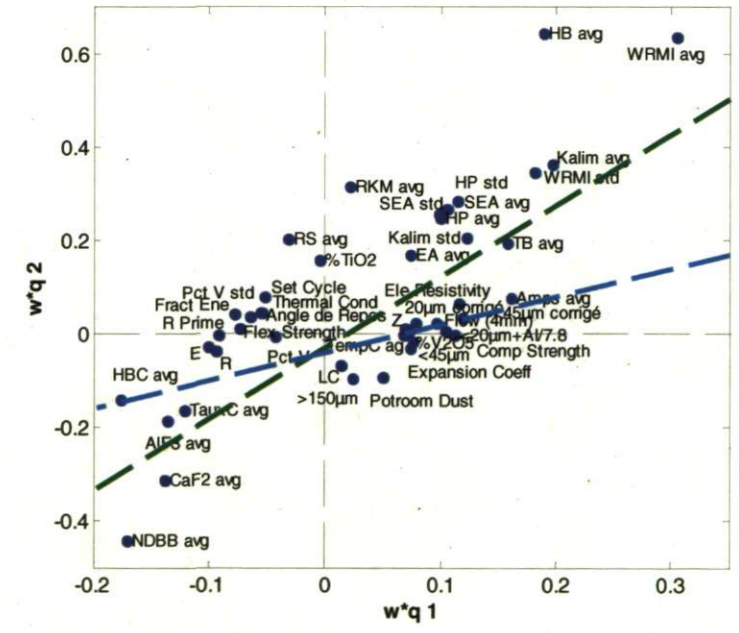


Figure 5.9: Zoomed version of the first two latent variables of the CE and EC PLS model bi-plot.

From this graph, it seems that the first latent variable focuses on raw materials variations as some alumina and coke properties variables are present far from the origin. This demonstrates again the importance of raw materials properties to pot performance. On the other hand, the second principal component is mainly driven by bath level and the pot noise. As seen in this figure, bath level (HB avg) and noise (WRMI avg) are variables with the highest weight on the second principal component.

This should serve as a basis for CE or EC optimisation as it gives the variable structure and interactions within this multivariable system.

## 5.7 Analysis of Month-to-Month Performance Variations

It was shown in the last section that the MBPLS model captures about 50% of the variations in performance indicators. Moreover, the most important raw material and process variables as well as the sign of their correlation to performance were found in agreement with primary smelting knowledge. This section examines how process operators and engineers could use this model in practice to monitor the process as a whole, and to help diagnose drifts and upsets in key performance variables (CE and EC). When an upset is detected, for example when CE sharply increases or decreases within two consecutive months, the MBPLS model could be interrogated in order to find the root causes of the problem. This procedure typically occurs in three steps. First, abnormal operation is usually detected at the super level (or plantwide level) of the MBPLS model. Second, attention is focused on the block level where one could locate the likely source of the drift, which could involve a single block (e.g. sub-section of the plant) or a combination of blocks. Finally, the contribution of each variable, within the blocks of interest, to this drift can be computed using PLS and MBPLS latent variable models. These contribution plots are central tools for narrowing down diagnosis efforts to identify the root cause of abnormal operation.

To illustrate these concepts, consider the analysis of a sudden CE drop shown in Figure 5.10. This figure presents the time series of the five super scores ($\mathbf{t}_{x1}$ to $\mathbf{t}_{x5}$) of the MBPLS model built in the last section as well as that of CE (observed and predicted) for pot A003. The current efficiency drop occurs between observations 26 and 27, marked by vertical dotted lines. Note that the predicted CE also follows this sudden drop, implying that raw

material and/or process variables carry information about this upset. This illustrates the upset detection step at the super level of the MBPLS model. It is also worth observing the signature of the first super scores ($\mathbf{t_{x1}}$), which captures the general CE average trend shown in Figure 5.10(a). Additional components explain variations around this trend.

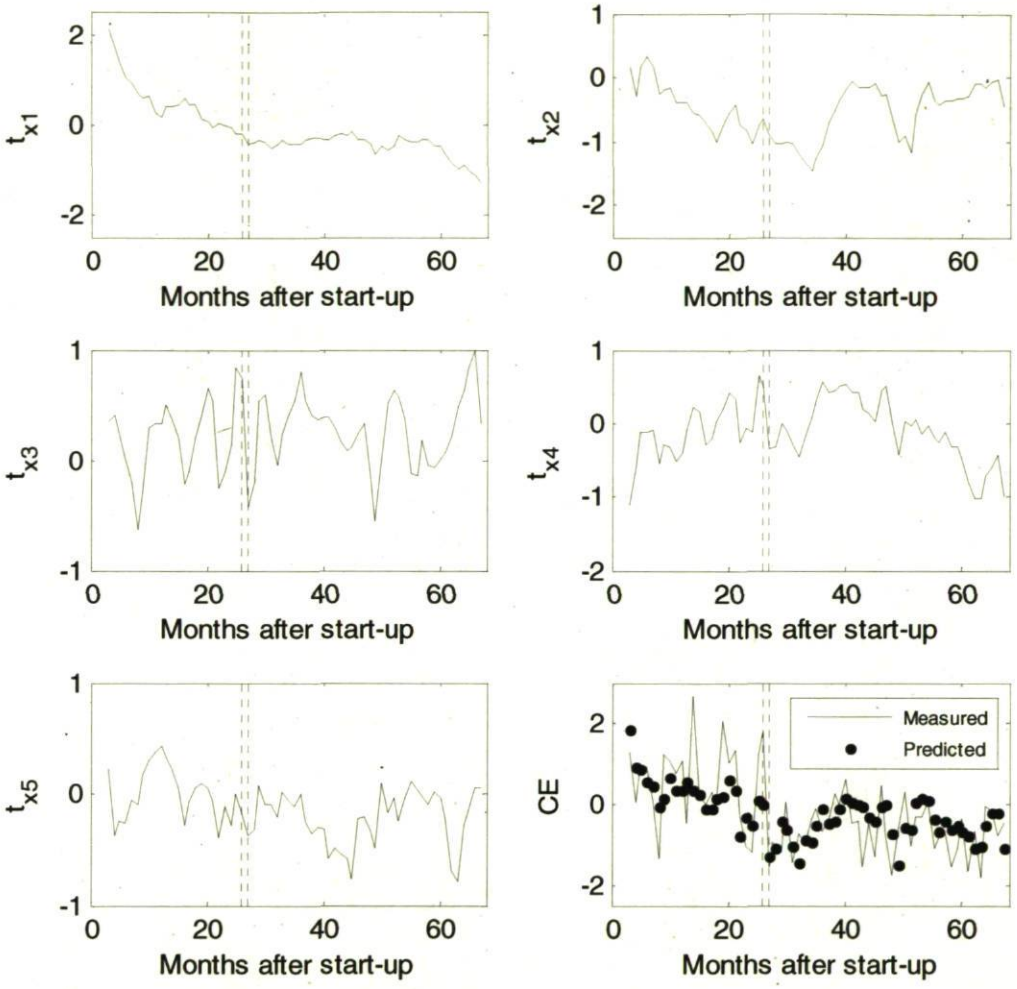


Figure 5.10: Monitoring of CE for pot A003 and detection of an upset (dotted lines) at the super level of the MBPLS model. The time series of the five super scores are shown, as well as the measured and predicted CE.

A closer look at the super scores in Figure 5.10 reveals that the 3rd and 4th principal components (i.e. $\mathbf{t_{x3}}$ and $\mathbf{t_{x4}}$) capture most of the CE drift. To investigate which of the 6 data blocks are associated with this drift, one could look at the super weight vectors for these PCs ($\mathbf{w_{x3}}$ and $\mathbf{w_{x4}}$) and focus on those blocks having the highest weights in absolute value.

Alternatively, one could also plot the block scores ($\mathbf{t}_{Al2O3}$, $\mathbf{t}_{Anodes}$, …, $\mathbf{t}_{SV}$) directly and investigate those blocks which score values show significant deviations. Since the MBPLS model has 5 dimensions (i.e. components) and consists of 6 blocks, it was decided to plot the Hotelling's $T^2$ statistic which summarizes the information carried by all components simultaneously (Kourti and MacGregor, 1995):

$$T_{j,i}^2 = \left(\mathbf{t}_{i,1to5}\right) S_j^{-1} \left(\mathbf{t}_{i,1to5}\right)^T \qquad [5.12]$$

Vector $\mathbf{t}_{i,1to5}$ contains the five scores of observation $i$, within block $j$, and $S_j$ is the variance-covariance matrix estimate of the five scores of block $j$. The Hotelling's $T^2$ statistic provides the Mahalanobis distance of observation $i$ from origin. This information is shown in Figure 5.11 for each block.

From these plots, it is clear that the PLV and PSE blocks are not involved in the drift. This was expected since the variables collected in these two blocks are constant over the entire pot life, except pot age (i.e. number of months after start-up). On the other hand, the $T^2$ values of the Al2O3 and MV blocks exhibit a significant increase between observations 26 and 27, suggesting that some variables within these three blocks should be investigated further. The Anodes and SV blocks also moved but to a lesser extent. These graphs do not provide the exact cause of the upset, but rather help narrowing down the search for possible sources. Another advantage of the block level provided by MBPLS is when the data for one or a few blocks, or sub-sections of the plant, are available earlier than for others, such as when raw material properties are measured before being used in the process. In this situation, operators and engineers could detect events that are potentially detrimental to performance indicators before they occur and affect the process. When possible, proactive actions could be taken at an early stage to alleviate, or at least reduce, the impact of such a disturbance. This would be applicable, for example, to the Al2O3 block as the COA is available before the alumina is fed in the pots. Modification to blending operations may help attenuating variations in alumina properties.

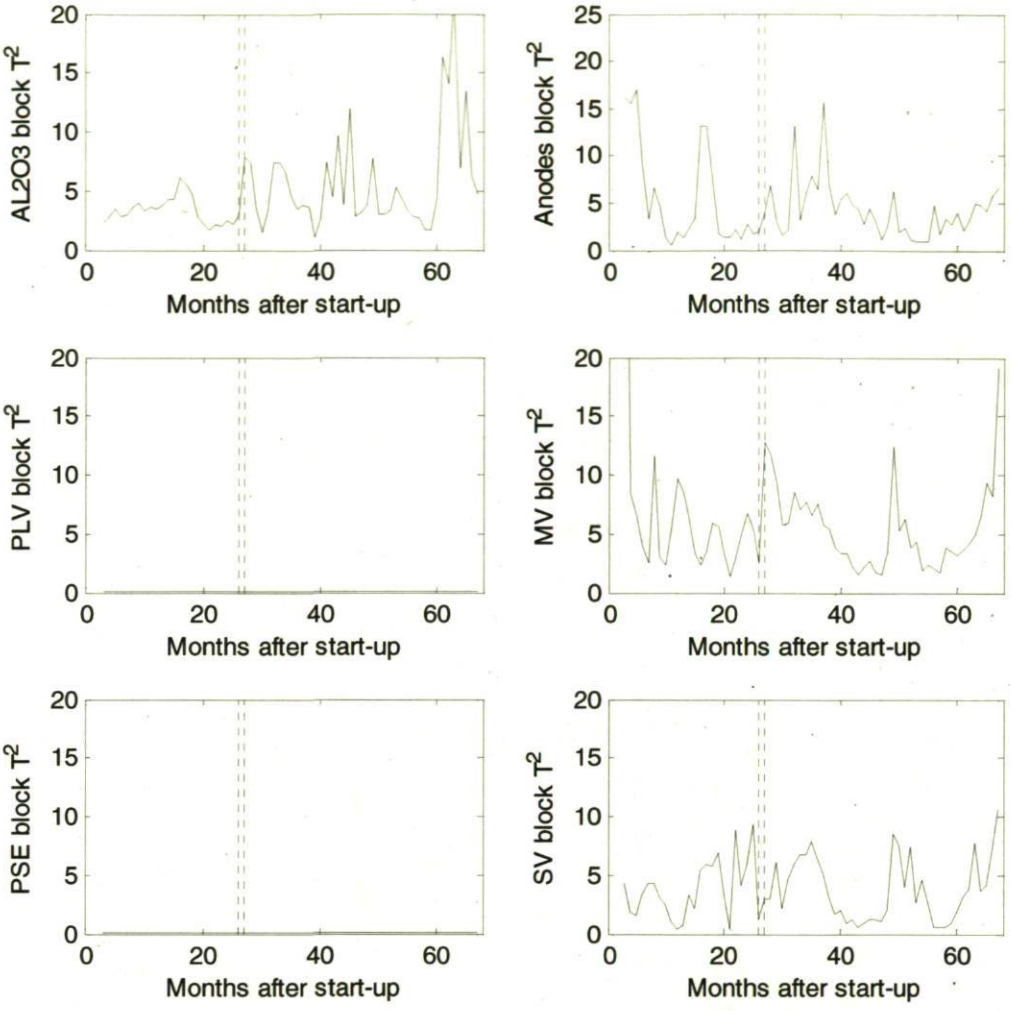


Figure 5.11: Contribution of each block to the CE drift (dotted line) occurring in pot A003. The Hotelling's $T^2$ statistics is shown for each block of the MBPLS model.

The final step in the diagnostic procedure consists of computing the contributions of each variable of the blocks of interest in order to interpret possible root causes for the performance drift. How to compute these contributions based on several components (5 in this case) it described by Kourti (2005). The contribution of variable *j*, to the overall movement between two consecutive observations, *i* and *i-1*, in the five latent space is computed using the expression below.

$$C_{i,j} = \sum_{a=1}^{A} \frac{\left[\left(\mathbf{x}_{i,j} - \mathbf{x}_{i-1,j}\right) * \mathbf{w}_{a,j}^{*}\right]^2}{S_{t_a}^2} \qquad [5.13]$$

where $x_{i,j}$ and $x_{i-1,j}$ are values of the $j^{th}$ variable for observations $i$ and $i-1$; $w^*_{a,j}$ is the weight associated to the $j^{th}$ variable in the $a^{th}$ latent space and $S^2_{ta}$ is the variance of the $a^{th}$ score. It basically consists of the difference between two observations on variable $j$, weighted by its importance in the model (w*). Dividing by the score variance gives equal chance to each latent variable to influence the variable contribution. Note that the weights and variances in the above expression are taken from the regular PLS model with block scaling as discussed in section 5.5.2. To obtain the contribution of the variables in a particular block, one only needs to use the appropriate variables within that block ($x_{i,j}$'s).

The contributions of all variables from all blocks to the performance drift are shown in Figure 5.12(a). Observations 26 and 27 from pot A003 were used to compute the contributions. The plot in Figure 5.12(a) is relatively noisy, especially in the lower range of contributions due to normal (common cause) process variations. To help enhance the diagnostic procedure Westerhuis et *al.* (2000) and Conlin et *al.* (2000) proposed to establish approximate confidence limits around the contributions calculated with Eq. [5.14] and then show only the contributions falling outside these statistical limits. The resulting "filtered" contribution plot is shown in Figure 5.12(b), which provides a clearer picture of those variables that are the most highly associated with the drift.

The approximate confidence intervals for contributions were established as follows. Month-to-month current efficiency variations had a one standard deviation of 3.24% in the available database. This is equivalent to a fluctuation of about 2500 kg in metal production for 28 days at 350 kA. Based on smelter operation knowledge, it was assumed that CE variations (increase or drop) greater than 3.24% are large enough to justify taking corrective actions whereas below that limit, CE variations are likely caused by natural process variations (i.e. errors from different sources). Thus, CE differences between two consecutive months were calculated from all pots and across their respective lifetime. Pairs of consecutive observations for which the CE differences were lower than 3.24% were identified, contributions between them for all variables were computed, and those were used to establish an approximate 95% limit for contributions. A total of 1579 differences were used for that purpose. Many variables in the 425 to 450 range (pot state variables)

were set to zero in Figure 5.12(b) since for this particular drift, the contributions of these variables were smaller than the limit.

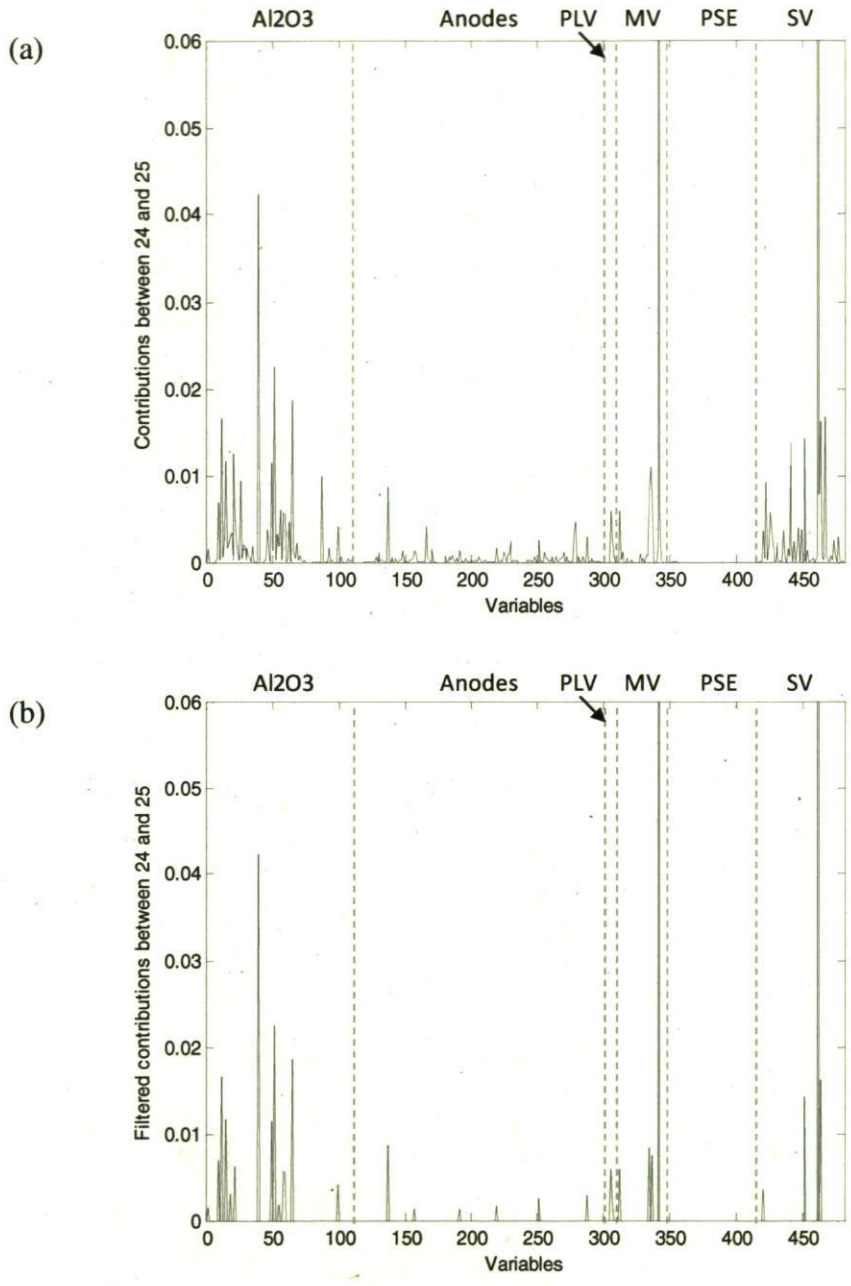


Figure 5.12: Contributions of the variables for all blocks to the CE drift between observations 26 and 27 for pot A003: (a) raw contribution plot and (b) filtered based on approximate confidence limits.

Variables significantly contributing to the CE drop between observations 26 and 27 for pot A003 are shown in (Figure 5.12(b)). Had such a monitoring and diagnostic scheme been in place, smelter operators would have found that various alumina properties and pot state variables were strong contributors to the drift. Some of these variables are the alumina particle size distribution (> 106μm and < 45μm), bath height level and its target as well as the number of anode effects. These correspond to variables 18, 22, 420, 462 and 464, respectively. Basically, the percentage of alumina particles > 106μm was 10% lower than usual, while the percentage of < 45μm was more than 8% higher than usual. This likely affected the alumina dissolution rate. Meanwhile, the bath level dropped by more than 2.2cm, further reducing alumina dissolution capacity due to a smaller bath volume. This also increases the frequency of anode effects since less alumina is dissolved in bath. Hence, it is easier to deplete alumina below the concentration leading to an anode effect. As a matter of fact, the anode effect frequency was three times greater than usual for pot A003 at observation 27 (i.e. monthly average corresponding to observation 27). Finally, the CE drop was most probably the result of a combination of slow dissolving alumina and low bath level. Together, these variables increased anode effect frequency which, in turn, had a negative impact on current efficiency.

Upon reception of the alumina COA, had the MBPLS monitoring scheme been in place, the $T^2$ statistic for the alumina block would have raised the attention of process engineers, who could have computed the contributions for that block. They could have assessed that the fluctuation in alumina size distribution (> 106μm and < 45μm) could possibly reduce the alumina dissolution rate even before feeding it in the cells. Engineers could have taken preventive actions to increase alumina dissolution capacity by increasing (or avoiding to reduce) the bath level target while using this alumina shipment.

An extensive analysis of the contribution of all the raw material and process variables was performed in order to create a Pareto table listing the variables that were the most frequently found highly contributing to significant CE deviations. A total of 167 events were investigated when measured CE drift was greater than 3.24% and the predicted drift was at least 1% and of the same sign. This decision was taken in order to make sure that the investigated variables contributed to a meaningful CE variation, and that the model was

able to capture and predict these CE variations to a certain extent. On average, the model captured 44% of the CE variations in cross-validation for this subset of 167 observations. For each of these 167 events, the contribution of each variable was computed using Eq. [5.9] and filtered using the confidence interval discussed earlier. Table 5.4 presents the Pareto table showing the 15 variables which were the most often found strong contributors to CE fluctuations. The percentage of occurrence is the number of times a variable was involved in a CE variation for two successive months, within the 167 analyzed observations. Most of the variables presented in this table were also listed in Table 5.3 and discussed in section 5.4, and make sense based on process knowledge. However, it is interesting to note that the average bath level is the second most encountered variable with respect to CE variations in the analyzed dataset. This reinforces the premise that bath level control leads to better pot performance as it affects different sub-processes.

Table 5.4: Variables with highest occurrence with respect to CE variations.

| Variable | Block | % of occurrence |
|---|---|---|
| Noise std | SV | 30.9% |
| Bath Level avg | SV | 30.7% |
| Bath Temperature avg | SV | 29.3% |
| Anode Effect Overvoltage avg | SV | 27.5% |
| % AlF3xs avg | SV | 27.3% |
| % CaF2 avg | SV | 27.3% |
| Feed Multiplier Constant avg | MV | 26.9% |
| Number of Anode Effect std | SV | 26.9% |
| % Al2O3 Dried | Alumina | 26.7% |
| Flexural Strength | Anodes | 26.7% |
| Bath Temperature std | SV | 26.7% |
| Surface Area (BET) | Alumina | 26.3% |
| Superheat avg | SV | 26.3% |
| Noise avg | SV | 25.7% |
| Total Resistance Target avg | MV | 25.5% |

## 5.8 Conclusions

In this paper, a multivariate latent variable regression technique known as multiblock PLS was used to investigate how process variables interact with each other to influence current efficiency and energy consumption, the two variables describing pot performance from a production and energy consumption stand-point.

Multivariate methods are advantageous over other methods since the model structure can be used to compute the importance of each variable in the prediction as well as their relative contribution to performance drifts. The developed model generated good current efficiency and energy consumption predictions as about 52% of the variations were covered by the model in cross-validation. Based on variables importance in the prediction it was concluded that performance variations are affected by many variables and as expected, these variables are coming from different blocks of data such as; alumina and anode quality, pot manipulated and state variables or variables related to pre-heating, start-up and early operation. Moreover, important variables highlighted by the model follow known process behaviour. Finally, a subset of observations was used to perform a Pareto type of analysis to study variables contributing the most to significant month-to-month performance variations.

Most smelters are now operated above their nominal capacity through different process improvements, thus, generally reducing the operational window. Meanwhile, alumina and coke quality are degrading, thus requiring more robust pots. Based on this study, smelters operators should, at least, to sustain actual production performance, monitor variables listed as important in the prediction. Moreover, it would be beneficial to monitor and control them using multivariate statistical control charts instead of typical univariate charts as the process would be fully integrated in the monitoring charts. Through the use of MBPLS, it would even be possible to project each block data, as soon as available, onto the model and hence highlight possible solutions to prevent CE and EC fluctuations.

## 5.9 Acknowledgements

Part of this research was financed by the Fonds québécois de la recherche sur la nature et les technologies by the intermediary of the Aluminum Research Centre – REGAL and the National Science and Engineering Research Council. The authors would also like to thank Alcoa Inc. for funding and granting permission to publish these results. Special thank also go to Alcoa Deschambault Potroom Technical Staff for their help and support.

# 6 Investigation of Factors Affecting Bath Level Control

It is well known that bath level control is of great importance to smelter operators. It directly affects different key performance indicators related to current efficiency, energy consumption and metal purity. The impact of bath level on pot performance was demonstrated in chapter 5 where bath level was shown to have high VIP value in the MBPLS model built for predicting CE and EC variations (i.e. Table 5.3). Moreover, bath level variations were often found associated with sudden fluctuations in CE as presented in Table 5.4. Therefore, a tight control of bath level is required to help reduce CE variations. Nevertheless, many factors have an impact on bath level control.

This chapter presents an investigation of the sources of bath level variations, again using multivariate latent variable techniques. In the first part of this chapter, the importance of bath level control is presented and illustrated. The dataset used for this investigation is later presented and the chapter concludes with the results and a discussion.

## 6.1 Importance of Bath Level Control

The electrolytic bath plays different roles in the Hall-Héroult process and affects several process conditions such as the alumina feed control, metal purity, heat balance, pot stability, bath chemistry and environmental emissions. Bath level fluctuations are caused by different mechanisms that can be summarized in two groups. The first group includes mechanisms leading to thermal balance disturbances, while the second consists of all direct contributors to the actual bath quantity in a pot:

- Assume a pot had a strong anode effect or had sustained lower amperage for a while. Compared to the typical pot voltage in the range of 4 to 4.5 V, the anode effect voltage can reach up to 30 to 40 V over the duration of the anode effect. Since the current flowing remains the same, since the pots are connected in series, this additional voltage greatly increases the power input to the pot for that period ($P = V \times I$). On the other hand, a lower current episode would lower the power input to the pot for a certain period of time as the plant electrical switchyard in generally

limited in voltage. However, the pots are designed to dissipate this power as heat as illustrated in Figure 2.6. Nevertheless, these two events disturb the pot thermal balance. As a result, the sideledge will melt or freeze depending on whether the power input is greater or lower than its nominal value according to pot design. The sideledge is made of frozen bath on the brick sidewalls of the cell with a different composition than the bulk molten bath. Hence, under a higher heat input, it partially or completely melts and generates molten bath which, in turn, increase the liquid bath level since molten cryolite takes about 60% more volume than solid cryolite. Conversely, a lower heat input freezes a greater quantity of molten bath into sideledge and this rapidly reduces liquid bath level. However, the sideledge freezing or thawing also create a change in the sideledge profile of the pot and hence changes the volume occupied by the molten bath, introducing additional variations in molten bath level.

- The second group of contributors to bath level fluctuations implies real bath quantity variations. The bath quantity in the pot increases as $Na_2O$ introduced by raw materials reacts with bath fluoride to generate NaF, thus neutralizing or lowering the excess of $AlF_3$ by forming cryolite. This, in turn, requires adding $AlF_3$ to maintain its excess on target, again increasing the quantity of molten bath in the pot. Anode cover material, a mixture of crushed bath and alumina also plays a role in bath level variations since a certain proportion of this material is either spilled in the pot or might later melt and fall in the bath, again increasing its bath quantity.

To overcome these fluctuations, bath level is generally controlled on a pot basis. According to a defined schedule, an operator dips a metal rod in the pot for a few seconds and then pulls it out. As the molten bath and aluminum freeze on the rod, an interface between the two materials becomes clearly visible to the operator, who uses a ruler to measure bath and metal levels. These values are later logged in the plant database. The amount of bath to be tapped is computed based on similar rules as for metal tapping (i.e. section 5.6). However, in this case, if the bath level is too low, operators add molten bath tapped from nearby cells already having a too high bath level. The bath level control frequency varies from a plant to another but greatly affects its control. Overcorrecting bath level may just introduce

additional variations since some of the effects leading to bath level variations almost correct themselves within a few hours (i.e. anode setting, anode effect, etc...). Corrections are thus generally performed daily or every other day.

Operating a pot with high bath level may lead to the following problems:

- *Iron contamination.* As the bath level gets too high, it reaches the top of older anodes, whose top surfaces are closer to the bath surface, and leaches part of the cast iron and iron stubs used in the anode assembly (Figure 2.4). Doiron and Lindsay (2009) reported that by correcting bath levels on a 24 hours basis, compared to a 36 hours basis, resulted in a reduction of 50ppm of iron in the pot metal.

- *Noisy pot.* As the bath level is higher, $CO_2$ gas bubbles have to travel a longer path to reach the surface. These bubbles contribute in the high frequency noise part of the voltage fluctuations within a reduction cell (Banta et *al.*, 2003). As a result, this added noise may lead operators to take corrective actions, such as increasing pot resistance to reduce the noise level and stabilize the pot. However, the negative effect of this corrective action on current efficiency and energy consumption may be more important than the positive effect of reducing the bubbles traveling distance.

On the other hand, operating a pot with a low bath level may lead to the following problems:

- *Lower alumina dissolution capacity.* In chapter 5, it was demonstrated that the contribution of bath level to pot performance variations is important (i.e. listed in Table 5.3 and 5.4). This was also confirmed by Tessier et *al.*, (2008), who suggested that a combination of low bath level and a possibly slow dissolving alumina led to a potroom performance drop. A low bath level reduces the time (or volume) necessary for dissolving alumina. Undissolved alumina settles on the carbon cathode blocks surface and create muck, leading to horizontal current flows. This results in metal pad waves due to vertical magnetic fields, which increase the probability of noise and shorting, and eventually reduce current efficiency.

- *Bath chemistry control.* The freezing and thawing of bath lead to fluctuations in $AlF_3$ concentration since solid sideledge and molten bath do not have the same composition. These variations have an effect on bath properties and are counter balanced by additions of $AlF_3$ or $Na_2CO_3$. This yields a greater bath inventory in the pot as described earlier.

The goal of this study is to identify the variables associated with the variations in bath level and to quantify their impact. It is well known that anode cover material, a mixture of secondary alumina and crushed solid bath, used to cover newly set anodes, has an impact on bath level (Wilkening et *al.*, 2005). A portion of the particulate materials added on top of the new anodes fall in the pot and melts. The alumina within this material dissolves in the bath and contributes to increasing bath inventory. As discussed previously, the power input to a pot plays a role in bath level variations, as well as anode effects and bath temperature as they all affect sideledge thickness and hence, the fraction of bath that is in liquid phase. Weather conditions may also affect the operation since in the Quebec region, temperatures typically vary between -30°C in winter and 25°C in summer. Since the potrooms are not well insulated, seasonal temperature variations change the heat losses from the pots and may affect sideledge thickness (i.e. greater in the winter and smaller in the summer). Finally, the amount of $Na_2O$ present in the alumina also plays a role in bath inventory, since it reacts with the excess of $AlF_3$ to generate NaF and hence increase the amount of bath through the formation of cryolite ($Na_3AlF_6$) (Lindsay, 2005). The variables discussed in this section were all included in the analysis.

## 6.2 Datasets

Data used in this chapter are again from the Alcoa Deschambault smelter. A dataset was gathered on a daily potroom basis. The data were averaged from the 264 pots. The dataset covered the period from January 1$^{st}$ 2006 until July 19$^{th}$ 2009, or 1296 days. During that period, the smelter operated under normal conditions, including short and long term load variations, different alumina sources and through natural weather cycles. In order to account for process dynamics, the data were later averaged on a weekly basis and this also enabled computing weekly standard deviations, which were also used in the analysis.

Following the comments presented above on possible causes of bath level variations, this investigation includes different *potroom* variables, such as CaO and $Na_2O$ impurities from alumina, weather data, *potline* load and anode cover composition, in order to study bath level variations. Variables included in the analysis are presented in Table 6.1. Bath level was pre-processed in a similar way and both average bath level and standard deviation will be studied separately.

Table 6.1: Variables included in the investigation of bath level variations.

| Variable ID | Variable | Variable ID | Variable | Variable ID | Variable |
|---|---|---|---|---|---|
| 1 | Line load | 23 | Number of bath feeds std | 45 | Wind Speed |
| 2 | Noise | 24 | Noise std | 46 | Wind Direction |
| 3 | Bath Temperature | 25 | Bath Temperature std | 47 | Outside Temperature std |
| 4 | Bath Temperature tgt | 26 | Bath Temperature tgt std | 48 | Wind Speed std |
| 5 | Bath level tgt | 27 | Bath level tgt std | 49 | Wind Direction std |
| 6 | Number of Anode Effect | 28 | Number of Anode Effect std | 50 | Line Load Zero Duration |
| 7 | Anode effect overvoltage | 29 | Anode effect overvoltage std | 51 | Low Line Load Duration |
| 8 | Purge Duration | 30 | Purge Duration std | 52 | Power Curtailment Duration |
| 9 | Metal Pad Level | 31 | Metal Pad Level std | 53 | Number of Low Line Load |
| 10 | Number of Tracks | 32 | Number of Tracks std | 54 | Number of Line Load Zero |
| 11 | Personalized Temporary Resistance | 33 | Personalized Temporary Resistance std | 55 | Number of Power Curtailment |
| 12 | Total Resistance Target | 34 | Total Resistance Target std | 56 | Number of Anode Setting |
| 13 | Recorded Resistance | 35 | Recorded Resistance std | 57 | %Na20 in Alumina |
| 14 | Base Resistance Target | 36 | Base Resistance Target std | 58 | %Ca0 in Alumina |
| 15 | Fe in metal | 37 | Fe in metal std | 59 | Ration CaO/Na2O in Alumina |
| 16 | Na in metal | 38 | Na in metal std | 60 | % Al2O3 ACM |
| 17 | Si in metal | 39 | Si in metal std | 61 | % Al2O3 ACM tgt |
| 18 | Number of Al2O3 feeds | 40 | Number of Al2O3 feeds std | 62 | Day-to-day ACM % Al2O3 difference |
| 19 | Number of AlF3 feeds | 41 | Number of AlF3 feeds std | 63 | % Al2O3 ACM std |
| 20 | % ALF3xs | 42 | % ALF3xs std | 64 | % Al2O3 ACM tgt std |
| 21 | % ALF3xs tgt | 43 | % ALF3xs tgt std | 65 | Day-to-day ACM % Al2O3 difference std |
| 22 | Line load std | 44 | Outside Temperature | | |

The weekly average/standard deviation descriptor variables presented in Table 6.1 are collected in $\mathbf{X}$ (185x65). Vector $\mathbf{Y_{BLA}}$ (185x1) contains the weekly bath level averages and $\mathbf{Y_{BLS}}$ (185x1) the weekly bath level standard deviations. These two variables could have been analyzed simultaneously in a single model, as performed for CE and EC in chapter 5. However, the correlation between $\mathbf{Y_{BLA}}$ and $\mathbf{Y_{BLS}}$ is only 0.03, compared to -0.77 between CE and EC in section 5.3, indicating that $\mathbf{Y_{BLA}}$ and $\mathbf{Y_{BLS}}$ are almost perfectly decoupled and hence can be studied independently. Time series of autoscaled bath level averages and standard deviations are presented in Figure 6.1

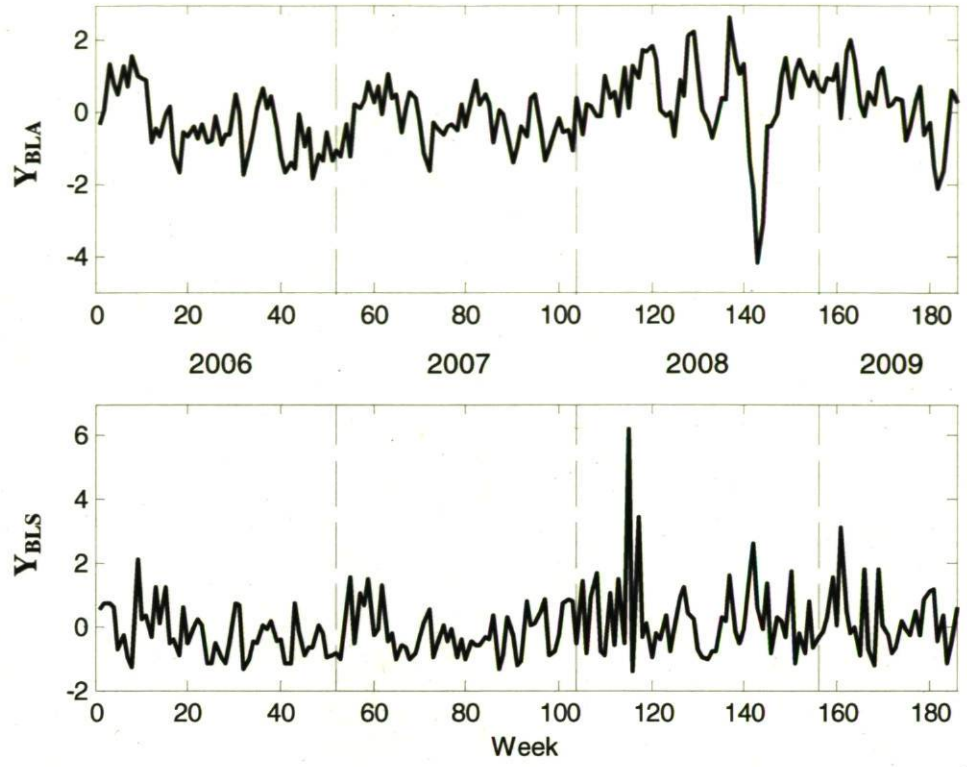


Figure 6.1: Autoscaled bath level averages ($\mathbf{Y}_{BLA}$) and standard deviations ($\mathbf{Y}_{BLS}$) for the 185 weeks investigated in this study.

## 6.3 Investigation of Bath Level Variations

Using the dataset presented in the last section, two PLS regression models were built, one for $\mathbf{Y}_{BLA}$ and one for $\mathbf{Y}_{BLS}$ using the NIPALS algorithm and a leave-one-out cross-validation (see sections 3.2 and 3.3.2). A few statistics describing the predictive ability of these models are presented in Table 6.2, whereas prediction results are shown in Figure 6.2. Table 6.2 presents the number of principal components included in the model (PC), the variance explained for $\mathbf{X}$ and $\mathbf{Y}$ ($R^2X_{fit}$ and $R^2Y_{fit}$) and the root mean squared error of prediction (RMSE).

Table 6.2: PLS model results for $\mathbf{Y_{BLA}}$ and one for $\mathbf{Y_{BLS}}$.

| Model Description | $Y_{BLA}$ | $Y_{BLS}$ |
|---|---|---|
| PC | 8 | 3 |
| $R^2X_{fit}$ | 50.60 | 34.96 |
| $R^2Y_{fit}$ | 69.23 | 66.42 |
| $RMSE_{fit}$ | 0.147 | 0.057 |
| $RMSE_{cv}$ | 0.240 | 0.072 |

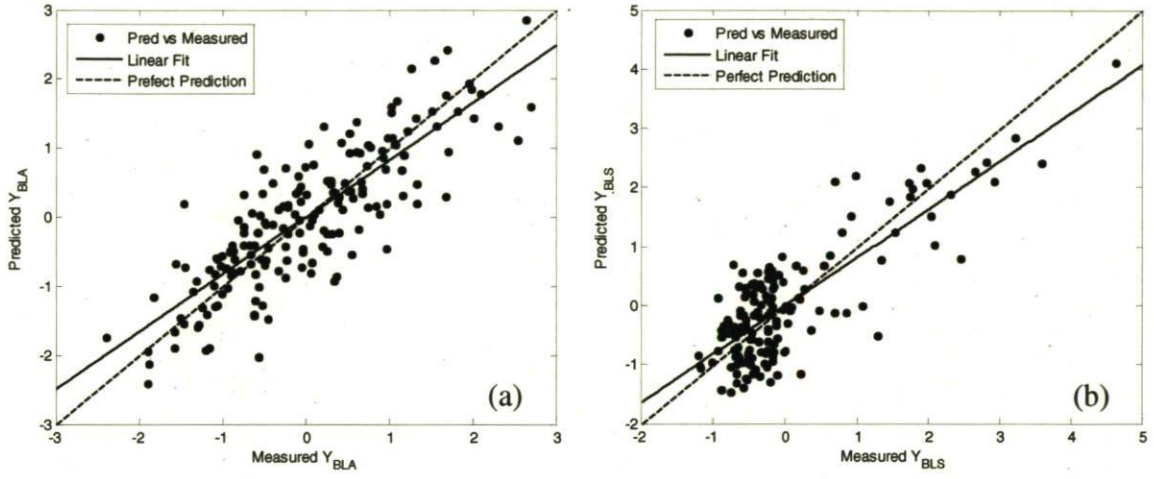


Figure 6.2: Prediction results of the PLS models for (a) average bath level $\mathbf{Y_{BLA}}$ and (b) bath level standard deviation $\mathbf{Y_{BLS}}$.

The objective here is not to accurately predict bath level averages and standard deviations, but to identify the variables that are the most highly correlated with bath level. Hence, Figure 6.2 presents predictions obtained in fit only. The PLS models are interrogated using their variable importance metric (VIP, Eq. [4.7]), which are presented in Figure 6.3 for all the variables included in the analysis. The ten most important variables in each model (i.e. highest VIP's) are also listed in Table 6.3. The sign of their correlation with $\mathbf{Y_{BLA}}$ and $\mathbf{Y_{BLS}}$ is also provided. On the other hand

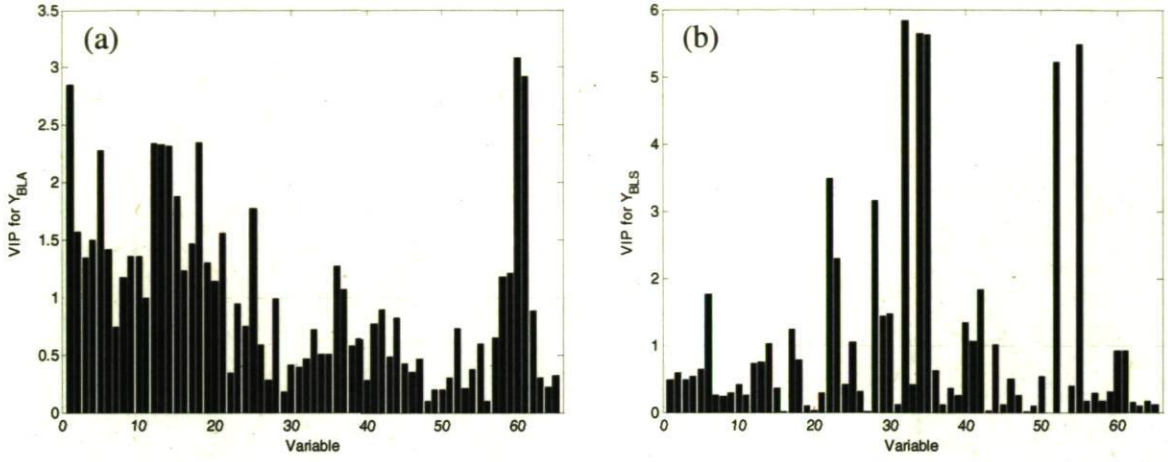


Figure 6.3: Importance of all the variables in the PLS models for (a) $\mathbf{Y_{BLA}}$ and (b) $\mathbf{Y_{BLS}}$.

Table 6.3: The ten most important variables for $\mathbf{Y_{BLA}}$ and $\mathbf{Y_{BLS}}$.

| Variable ID | Variable | Correlation sign with $Y_{BLA}$ | VIP | | Rank | | Variable ID | Variable | Correlation sign with $Y_{BLS}$ | VIP | | Rank | |
|---|---|---|---|---|---|---|---|---|---|---|---|---|---|
| | | | $Y_{BLA}$ | $Y_{BLS}$ | $Y_{BLA}$ | $Y_{BLS}$ | | | | $Y_{BLA}$ | $Y_{BLS}$ | $Y_{BLA}$ | $Y_{BLS}$ |
| 60 | % Al2O3 ACM | - | 3.09 | 0.92 | 1 | 19 | 32 | Number of Tracks std | + | 0.46 | 5.84 | 47 | 1 |
| 61 | % Al2O3 ACM tgt | - | 2.93 | 0.91 | 2 | 20 | 34 | Total Resistance Target std | + | 0.51 | 5.65 | 43 | 2 |
| 1 | Line Load | + | 2.85 | 0.47 | 3 | 31 | 35 | Recorded Resistance std | + | 0.50 | 5.61 | 44 | 3 |
| 18 | Number of Al2O3 feeds | + | 2.35 | 0.77 | 4 | 21 | 55 | Number of Power Curtailment | + | 0.60 | 5.48 | 40 | 4 |
| 12 | Total Resistance Target | + | 2.33 | 0.74 | 5 | 23 | 52 | Power Curtailment Duration | + | 0.73 | 5.22 | 36 | 5 |
| 13 | Recorded Resistance | + | 2.33 | 0.74 | 6 | 22 | 22 | Line Load std | + | 0.34 | 3.49 | 53 | 6 |
| 14 | Base Resistance Target | - | 2.31 | 1.02 | 7 | 17 | 28 | Number of Anode Effect std | + | 0.98 | 3.14 | 28 | 7 |
| 5 | Bath Level tgt | + | 2.28 | 0.64 | 8 | 24 | 23 | Number of Bath feeds std | + | 0.95 | 2.30 | 29 | 8 |
| 15 | Fe in metal | + | 1.88 | 0.35 | 9 | 37 | 41 | Number of AlF3 feeds std | + | 0.90 | 1.84 | 30 | 9 |
| 25 | Bath temperature std | - | 1.78 | 1.04 | 10 | 16 | 6 | Number of Anode Effect | - | 1.42 | 1.77 | 15 | 10 |

As observed in Table 6.3 and Figure 6.3, the most important variables for bath level averages and standard deviations are not the same. For example, the fraction of alumina in anode cover material is the most highly correlated to weekly average bath level variations with a VIP value of 3.09. However, it ranks the 19$^{th}$ out of 65 in the second model (weekly bath level standard deviations), with a VIP of 0.96. This suggests that the actual bath level, averaged over a week ($\mathbf{Y_{BLA}}$), and its variation during the same week ($\mathbf{Y_{BLS}}$) are likely driven by different events.

A closer look at the variables presented in Figure 6.3 and Table 6.3 suggests that bath level variations are correlated with short term effects of process disturbances. Most of the variables listed as the ten most important for bath level weekly variations ($\mathbf{Y_{BLS}}$) are also standard deviations of different process variations. Focusing on $\mathbf{Y_{BLS}}$, its ten highest VIP

make sense based on process knowledge. Moreover, most of these variables are related to power input variations (i.e. resistances std's, power curtailment, line load std and anode effect). These power input variations necessarily had an impact on sideledge thickness for a short period of time (i.e. few days), thus generating variations in the bath level measurements during the weekly basis. However, if bath level was low before the disturbance and high after, its weekly average might have been on target. On the other hand, the number of tracks, bath feeds and $AlF_3$ feeds std's, or number of alumina feed decisions std, are probably more a consequence than a cause of bath level weekly variations. For example, as the inventory of liquid bath varies, its chemistry also varies since sideledge is almost made of pure cryolite and, when it melts, dilutes the $AlF_3$ excess resulting in compensation by the process control system through the addition of $AlF_3$.

Figure 6.4 presents the loading bi-plot of the first two principal components of the bath level PLS model for variable shaving a VIP greater than one. Going back to Table 6.3, it can be seen that the fraction of alumina in anode cover material and its target value are the most important variables to explain bath level weekly variations. A part of this cover material falls and dissolves in the pots. Consequently, anode cover material with less alumina and hence more bath, will generate higher bath levels than anode cover material with more alumina. This is also supported by the loading bi-plot of Figure 6.4, where these two variables fall on the opposite quadrant of bath level and are far from the origin. The next two important variables are line load and number of alumina shots, which are highly correlated together. Increasing the line load creates more aluminum (i.e. Faraday's law) and hence consumes more alumina, thus increasing the number of alumina feeds. These two variables are also dominant and of the same sign as bath level in Figure 6.4. Note that line load and resistances combine together to influence the power input to the pot ($P = R \times I^2$) and hence melt of frozen sideledge. Nevertheless, the bath level target is only ranked $8^{th}$, indicating that all variables ranked higher have a greater correlation with average bath level variations. The projection of this variable on the green dotted line is closer to the origin than the previously discussed variables. Then comes iron in metal, strongly correlated to bath level, as shown in Figure 6.4, a consequence as discussed in section 6.1, since part of its variations is caused by bath level variations.

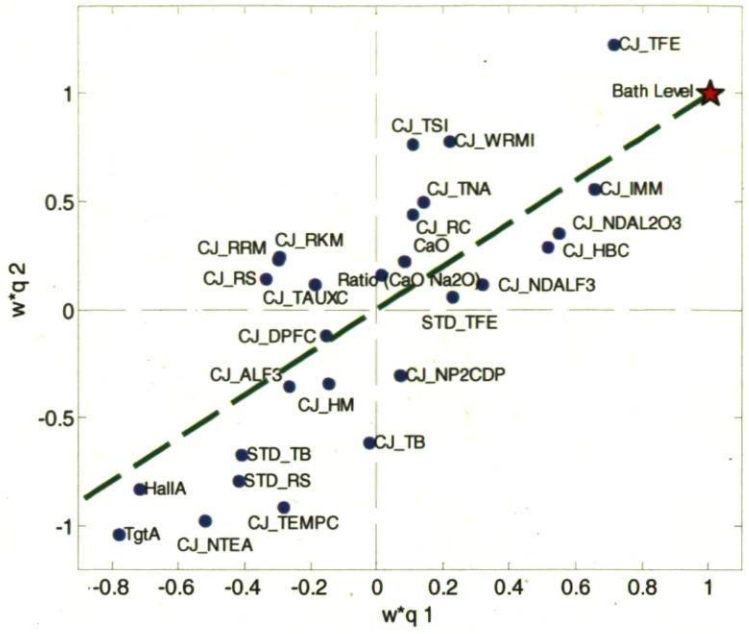


Figure 6.4: Loading bi-plot of the first two principal components of the bath level PLS model.

Following these observations, it can be said that bath level weekly averages and variations are mainly influenced by power input and anode cover material composition. These effects are in fact more important to predict bath levels than the actual bath level target. However, one might have also expected to encounter variables linked to outside temperature somewhere in the list as the smelter experiences great variations in external temperature due to its geographical location. Nevertheless, these variables rank in the 30$^{th}$ to 50$^{th}$ position to explain bath level variations and are thus not a role player in bath level variations which is in accordance with the findings of Haugland et *al.*, (2003).

## 6.4 Issues with Anode Cover Material Composition

It was shown that anode cover material composition, the ratio of alumina and crushed bath, is one of the most important variables to control bath level within reduction cells. Its VIP was much higher compared to all the other variables. Line load is also important, however,

controlling bath level by manipulating it would not be a viable option since it would also create fluctuations in metal production.

To control (i.e. manipulated or stabilize) the composition of the anode cover material, one must ensure that reliable anode cover material composition measurements are available. *If you can't measure it, you can't manage it.* A few smelters perform anode cover composition analysis. In general, a few grabbed samples of anode cover materials are sent to the laboratory for analysis (the control sample). Based on the results, decisions are made to adjust the mixture composition. However, the number of samples analyzed on a daily basis, if not on a weekly or monthly basis is very low, compared to the number of anodes changed on a daily basis and to the variability of anode cover material composition.

The autoscaled daily anode cover material composition from six pots (A028 to A033) is presented in Figure 6.5 for two time periods (90 days and 15 days), together with their respective composition targets and control sample (Ctrl). These graphs clearly demonstrate that new anodes are not always covered with the same material composition. Also note the great variability in anode cover composition with respect to its target value. The variability shown in these graphs is not due to the analytical laboratory analysis which is quite accurate. For example, composition of anode cover material used for the six pots on November 16, was completely different from the monitoring result obtained that day. To give an idea, these pots received anode cover materials containing 13 wt % more alumina compared to the monitoring result. On the other hand, on November 18, the anode cover compositions of five pots were close to the monitoring result. However, anode cover compositions of pots A028 to A031 were close to the monitoring sample. Nevertheless, pot A032 was covered with an anode cover material containing 5% less alumina, while pot A033 anode cover material contained 11% more alumina, when compared to the monitoring sample. Hence, these variations certainly played a role in bath level variations, without being properly measured.

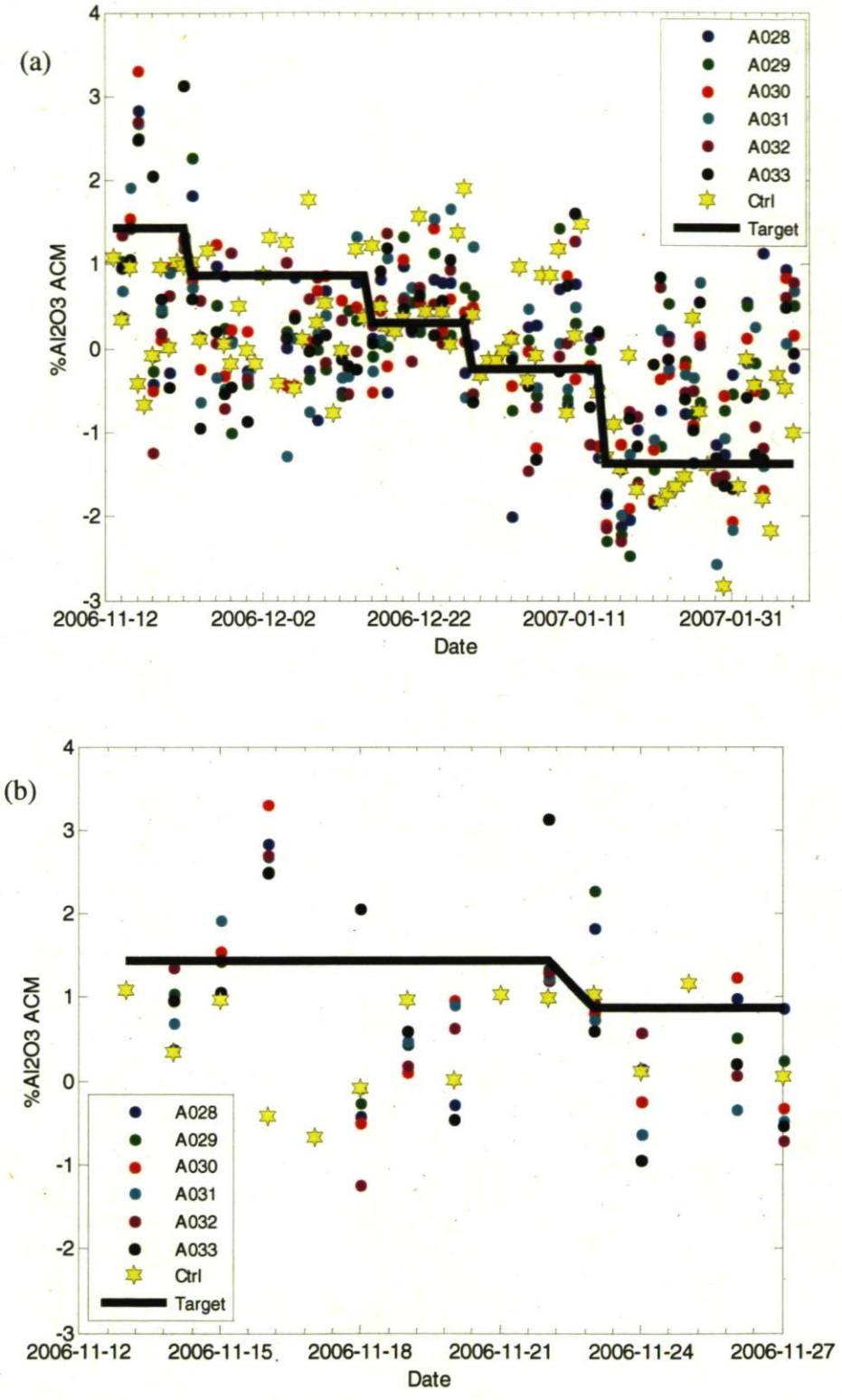


Figure 6.5: Autoscaled daily anode cover material composition for six pots and daily monitoring results (a) over 90 days and (b) over 15 days (zoom-in of figure a).

From the great variability presented in Figure 6.5, it is obvious that control actions on anode cover material composition target cannot be performed efficiently using the actual procedure. Plant operators generally wait a few days before changing the conveyor speed to remain close to the anode cover material composition target. In the end, this is harmful to bath level control, as presented in section 6.3, which finally affects pot performance through different processes as demonstrated in sections 5.6 and 5.7. To efficiently perform anode cover material composition control, smelter operators would have to grab more frequent samples of anode cover materials to increase the confidence on the results. Still, it may generate a reliable result if enough samples are grabbed and analyzed on a *potroom* or *potline* basis.

The next chapter presents a novel method for estimating anode cover composition which would enable the estimation of anode cover material composition used on each pot. This would improve the confidence in this measurement and enhance control decisions on a *potroom* or *potline* basis, while also providing the information on a pot basis since the anode cover material composition could be evaluated for each pots, on a daily basis.

# 7 Estimation of Alumina Content of Anode Cover Materials Using Multivariate Image Analysis Techniques

## 7.1 Résumé

Cet article présente l'étude de différentes techniques d'analyse d'images dans le but de prédire la composition en alumine du mélange de recouvrement des anodes. En utilisant cette approche, il serait possible d'estimer en ligne la composition du mélange de recouvrement et ainsi de prendre des actions en modifiant les valeurs de consigne de certains paramètres des cuves par l'intermédiaire du système de contrôle. Ainsi, des caractéristiques de couleur et de texture sont extraites des images de produit de recouvrement et un modèle de régression (PLS) est développé afin de prédire la composition. La majorité des prédictions se situent entre +/-2 $\sigma$ de l'analyse de laboratoire (fluorescence par rayon-X) bien que les actions des techniciens de procédé soient basés sur des variations d'une plus grande amplitude. Les défis découlant de l'analyse d'image pour cette application sont aussi discutées.

Tessier, J., Duchesne, C., Gauthier, C., Dufour, G., *Chemical Engineering Science,* 63, 1370-1380 (2008)

Tessier, J., Duchesne, C., Gauthier, C., Dufour, G., *Methods, Systems and Apparatus for Determining Composition of Feed Material of Metal Electrolysis Cells*, U.S. Patent Application publication No. 2009/0107840 A1, filed on October 24th, 2008, published on April 30th, 2009.

## 7.2 Abstract

In this paper, the use of different image analysis techniques is investigated for predicting alumina content of anode cover materials used in primary aluminum smelters. This approach is proposed in order to allow on-line estimation of alumina content for feedback control purposes, which is not currently possible due to the long time delays and limited number of samples that can be analyzed in the laboratory. Both color and textural features of various anode cover materials are extracted from digital RGB images, and Partial Least Squares (PLS) regression models are developed for predicting alumina content from these features. Most alumina content prediction errors are within +/-2$\sigma$ of the X-ray fluorescence laboratory measurements, when larger variations are required by operators to make control decisions. Some challenges arising from the use of image analysis techniques for process control are also discussed.

## 7.3 Introduction

Primary aluminum is obtained by electrolysis of alumina through the following reaction, carried out in electrolytic reduction cells, also called Hall-Héroult cells (Figure 2.2):

$$2\,Al_2O_{3,(diss)} + 3\,C_{(s)} \rightarrow 4\,Al_{(l)} + 3\,CO_{2,(g)} \qquad E_0 = 1.2\ V \qquad [7.1]$$

In this process, small quantities of smelter grade alumina powder (typically 1-2 kg) are periodically fed in the reactor. Alumina then dissolves within a high temperature electrolytic bath (i.e. 940 to 970°C), typically made of a molten mixture of cryolite ($Na_3AlF_6$), aluminum fluoride ($AlF_3$) and calcium fluoride ($CaF_2$). Carbon is supplied to the reaction by the pre-baked anode blocks, which are consumed over time. Anodes are typically made of a mixture of coke, pitch and recycled anodes butts. The reduction reaction converting alumina ($Al_2O_3$) to primary aluminum requires the application of a continuous high amperage and low voltage current. Reduction cells continuously operate over a lifetime varying from 4-10 years, after which they need to be rebuild almost completely.

Anodes are consumed by reaction (Eq. [7.1]) and need to be replaced every 20 to 30 days. However, anode replacement is performed almost every day on each and every reduction cell since modern cell designs involve between 20 and 40 anodes per cell. Once replaced, new anodes are covered with a mixture of alumina and crushed electrolytic bath particles. High temperature converts this mixture of particles into a crust called anode cover. This cover plays an important role in keeping a good thermal balance of the reactor, in limiting fluoride emissions, in preventing anode oxidation, and in controlling bath height (Wilkening et *al.*, 2005). The thickness and alumina content are the most important characteristics controlling cover integrity (Taylor et *al.*, 2004). For instance, an inappropriate dosage of alumina in the mixture may increase heat losses through the crust by increasing its thermal conductivity. It may also cause important changes in the mechanical properties of the crust to an extent where collapse can occur around the newly introduced anodes. This would result in even more severe heat losses and fluoride emissions. Maintaining a consistent alumina composition in the anode cover mixture is

therefore very important for primary aluminum smelters to achieve stable operation, high productivity and good environmental performance for each aluminum reduction cells (typical plants can operate up to 1000 cells simultaneously).

In practice, however, achieving consistent cover integrity for each cell and over time is very difficult due to the lack of on-line sensors for measuring alumina content of the anode cover mixture. In several primary aluminum smelters, the crushed electrolytic bath particles and the alumina powder are both conveyed separately and then fed into loading stations located on overhead handling cranes, used to deliver the anode cover mixture to the various electrolytic cells. Therefore, products are poorly mixed and prone to segregation during transportation. Although process operators can modify the composition of this binary mixture by adjusting the relative speed of both conveyors, there is currently no means to verify the mixture composition other than sending a grab sample to the laboratory, and wait about an hour to get the result. A preliminary sampling campaign performed at Alcoa's Deschambault plant showed that important variations occur from cell to cell and over time in the alumina content of the cover mixture, and this might explain poorer performance of some cells. However, to quantify the impact of these variations one needs to be able to reduce this variability and to control mixture composition to desired set-points through feedback control. This requires on-line measurement of alumina content of the anode cover mixture, which can simply not be performed in the laboratory since several tons of cover materials are used every day.

This paper presents a machine vision approach based on RGB color images for estimating alumina content in the anode cover mixture, and to the author's knowledge, this is the very first attempt in the area of primary aluminum production. When installed above conveyors, such a sensor would provide on-line measurements for composition control purposes without physically sampling the powder mixture. Both color and textural features of powder mixture images are extracted in this work using different techniques. Then various combinations of features are tested and compared in order to develop a robust image based predictive model for alumina content. Note that some spectroscopic techniques could also be used to measure $Al_2O_3$ content of the anode cover materials, such as X-ray fluorescence. However, these techniques are difficult to implement on-line for high throughput analyses

since they require sample preparation (i.e. grinding of the materials, etc.). They are also very expansive to buy and maintain.

Machine vision is increasingly used in the process industries for monitoring or process control applications since it generally requires low capital investments, and allow to extract complex information about a process or a product (both deterministic or stochastic) that are difficult to measure otherwise. Some recent examples of machine vision applications include froth health monitoring and grade prediction in flotation froth systems used for mineral separation (Moolman et *al.*, 1994; Duchesne et *al.* 2003; Liu, 2004; Liu et *al.*, 2005; Bartolacci et *al.*; 2006), real-time monitoring and control of combustion flames in boilers and rotary kilns (Yu and MacGregor, 2004; Szatvanyi et *al.*, 2006), automatic grading of steel surfaces (Bharati et *al.*, 2004), and control of seasoning and organoleptic properties of snack food products (Yu et *al.*, 2003). For particulate mixtures more specifically, Chandan et *al.* (2004) applied image analysis techniques to characterize texture, angularity and shape of aggregate particles used in highway construction using Wavelet Texture Analysis (WTA). Bonifazi et *al.* (1999) used both color and textural features extracted from images of mineral sands deposits to classify the material in three different lithotypes. Color features were obtained by computing 16 moments of the pixels intensity distribution whereas textural features were calculated using Gray Levels Co-Occurrences Matrices (GLCM) (Haralick, 1979). Some of these color and textural feature extraction techniques are also used in this work. Imaging techniques for larger rock fragments have also been proposed (Petersen et *al.* 1998; Tessier et *al.*, 2006), however the machine vision problem for large rock fragments is different than for powder mixtures. Finally, Calderon De Anda et *al.* (2005) and Larsen et *al.* (2006) used image segmentation algorithms to extract and compute different features related to crystals morphology for monitoring and control of industrial crystallizers.

## 7.4 Experimental

Anode cover material images were captured using a laboratory setup based on a Hewlett-Packard Photosmart M23 RGB digital camera. A total of eleven mixtures of secondary alumina (i.e. from dry scrubbers) and crushed electrolytic bath have been prepared and

homogenized, covering the range of 19 to 93 wt % $Al_2O_3$ content as shown in Table 7.1. For each of the eleven mixtures, homogenized cover material was dispersed on a tray and many different images (smaller than the tray area) were collected in order to capture the variability in the visual appearance of the solids. Using this procedure, an image data base of 101 pictures of anode cover material was collected. Cover material thickness was about 1 cm which was enough to avoid capturing tray areas in the image. The camera was installed 20 cm above the tray surface and was completely manually operated with constant lightning conditions. In this setup, the resolution of the image was 1792 x1312 pixels and covers an area of 303.56 $cm^2$ on the sample.

Three replicate samples of each of the eleven homogenized cover material mixtures were analyzed using X-ray spectroscopy to determine their alumina content. These analyses were performed by Alcoa Deschambault's personnel using a standard routine procedure. Homogenized cover material samples have been crushed during a defined period of time to obtain the appropriate size distribution and have then been mixed with a ligand compound before X-ray spectroscopy analysis. The results of the laboratory analyses for the eleven mixtures are shown in Table 7.1.

Table 7.1: Mean and standard-deviations from laboratory analyses of the eleven mixtures from the designed experiment.

| Experimental mixtures | $Al_2O_3$ (weight fraction) | |
|---|---|---|
| | Mean | Std |
| 1 | 0.185 | 0.009 |
| 2 | 0.255 | 0.019 |
| 3 | 0.307 | 0.008 |
| 4 | 0.393 | 0.003 |
| 5 | 0.434 | 0.012 |
| 6 | 0.495 | 0.033 |
| 7 | 0.587 | 0.028 |
| 8 | 0.705 | 0.008 |
| 9 | 0.732 | 0.002 |
| 10 | 0.802 | 0.014 |
| 11 | 0.926 | 0.009 |

Images of different alumina mixtures are presented in Figure 7.1. These images show that there exist some differences in color and texture between these sample images. The texture

is coarser in the first image (a) and is smoother in image (c) whereas color goes from brownish (a) to light gray (c). When looking at the entire set of images, it is clear that color and textural features evolve monotonically with alumina content of the cover material mixtures, and therefore justifies the machine vision approach for predicting alumina content of anode cover material.

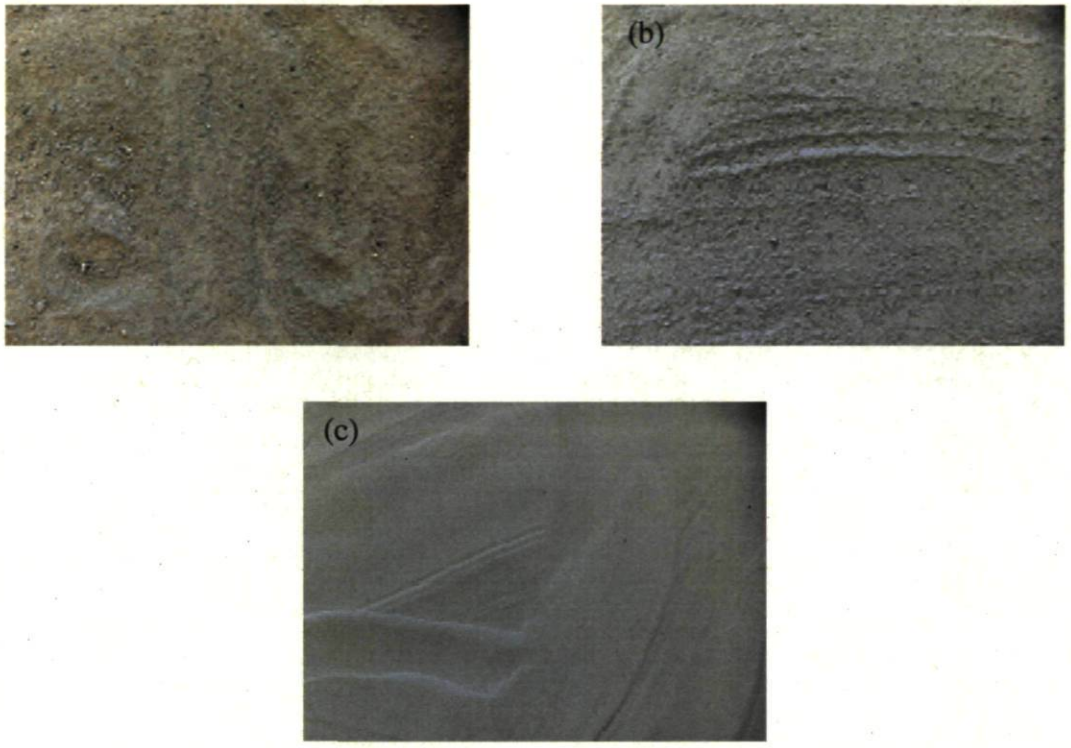


Figure 7.1: Images of cover material for different $Al_2O_3$ weight composition. (a) 19% $Al_2O_3$, (b) 48 % $Al_2O_3$ and (c) 93 % $Al_2O_3$.

## 7.5 Methods for Extraction of Color and Textural Features

Once digitized, an RGB color image consists of a 3-way array of data as shown in Figure 7.2. Each pixel is defined by two spatial coordinates $(x,y)$ whereas the third dimension of the array corresponds to the light intensity recorded by the camera CCD in the red (R), the green (G) and the blue (B) channels. For 8-bits coding cameras, the intensity values of each channel can take discrete values ranging from 0 to 255. Alternatively, the digital color image can be viewed as a stack of three different gray-level images obtained at different

wavelengths of the light spectrum, that is the red, the green and the blue wavelengths (~ 435, 546, and 700 nm, Lepistö et *al.*, 2003). Color and textural features for each image of anode cover material are computed from these 3-way arrays of data.

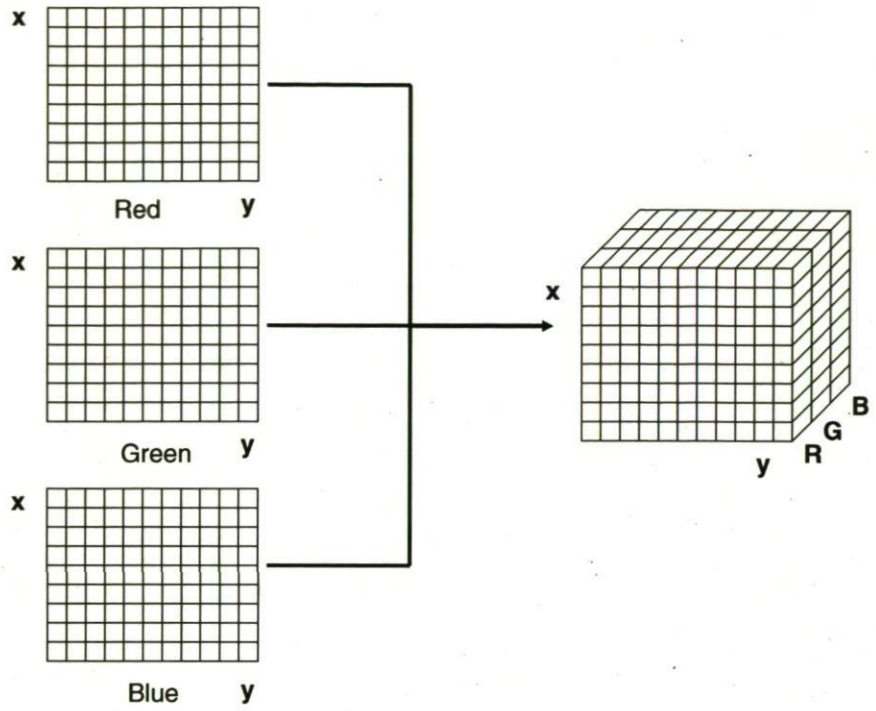


Figure 7.2: Digitized RGB image is a 3-way array of data.

### 7.5.1 Extraction of color features

Color analysis is often used to extract color features related to process performance or to predict product quality in different applications. As shown in Figure 7.1, the overall coloration of the images seems to be related to the alumina content, and suggests using color features might help predict alumina content. In this paper, three alternative methods were used to extract color features from RGB images. The first two are applied directly to the RGB color space whereas the third is rather based on a projection of the RGB color space into a lower dimensional space define by the few dominant contrasts present in the images.

#### 7.5.1.1 Full distribution of the RGB color intensities

As discussed earlier in this paper, the three light intensities (RGB) corresponding to each pixel are coded as discrete numbers from 0 to 255, thus leading to 256 possible light intensities values for each channel. The first method used for extracting color features is to simply use the full RGB color distributions across the images. The distribution of light intensities for each color channel (red, green and blue) is a histogram divided in 256 bins, thus leading to the extraction of 768 color features per image. These features are stored row-wise for each image in a regressor matrix (**X**) that will be used later for regression model building.

#### 7.5.1.2 Mean and standard-deviation of the RGB channels

The second method for extracting color features consists of only using the first two moments of the full RGB color intensity distributions although higher moments could also have been used. This amounts in computing the means and the standard-deviations of the intensities of the red, the green and the blue channels across each image. Hence, 6 color features are extracted from the images and stored row-wise in a regressor matrix (**X**).

#### 7.5.1.3 PCA decomposition of the RGB color space

The third approach consists in applying Multi-Way Principal Component Analysis (MPCA) to the 3-way array of data obtained from each digitized image (Geladi and Grahn, 1996; Bharati, 1997). This procedure is shown schematically in Figure 7.3.

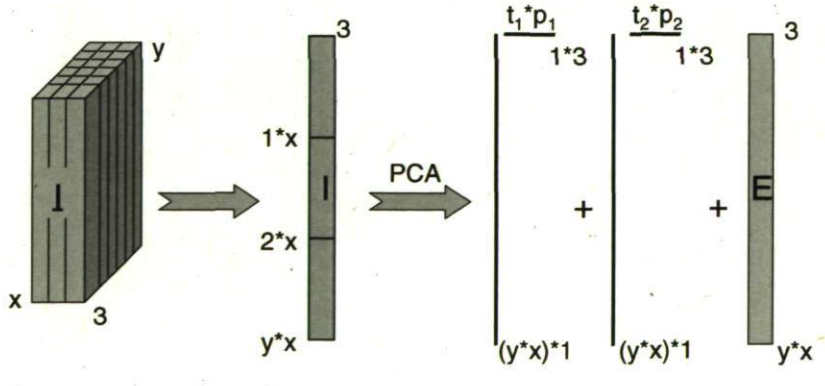


Figure 7.3: A schematic description of the MPCA decomposition.

The digital RGB image $\underline{\mathbf{I}}$ is first unfolded into matrix **I** in such a way that the columns of that matrix correspond to the red (R), green (G), and blue (B) color intensities for each pixel of the image (each row corresponds to a particular pixel of the image). Principal Component Analysis (PCA) is then applied to matrix **I**, and performs an orthogonal decomposition of the covariance matrix of **I** into its *A* principal components (Wold, 1987; Jackson, 1991):

$$\mathbf{I} = \mathbf{T}\,\mathbf{P} + \mathbf{E} = \sum_{a=1}^{A} \mathbf{t_a}\mathbf{p_a} + \mathbf{E} \qquad [7.2]$$

The decomposition of each unfolded image yields a series of *A* loading vectors $\mathbf{p_a}$, which correspond to linear combinations of the RGB intensities explaining most of the variance of **I**, and *A* score vectors $\mathbf{t_a}$, resulting from the projection of each row of matrix **I** onto the loading vectors ($\mathbf{t_a} = \mathbf{I}\,\mathbf{p_a}$). Matrix **E** contains the residuals of this decomposition, and is zero when all principal components are used ($A = 3$ in this case). Since the loading vectors $\mathbf{p_a}$ ($\mathbf{a}$=1,2,3) are linear combinations of the original RGB intensities of each pixel of the image that explain most of the color variations across the image, they can be viewed as representing the various color contrast of the multivariate image, and therefore can be used directly as color features. Each loading vector contains three elements or weights corresponding to the red, green, and blue colors and all three principal components are used in this study. Thus nine features are used to describe color variations using this approach. Hence, 9 color features are extracted from the images and stored row-wise in regressor matrix (**X**).

## 7.5.2 Extraction of textural features

Image texture analysis is now well covered in the literature. In spite of the widespread use of textural information, no official definition exists for image texture. However, it is often defined as a function of the spatial variations in the pixels intensities of a gray-level image (Bharati and MacGregor, 2001). For example, a gray-level image of a plywood board surface is not uniform. Such an image will present different patterns of pixels intensity variations. These different patterns can come from physical defects such as knots, pitch

pockets, fibre orientations or roughness or even from differences in the way light is reflected from the surface. Quantifying the different textures within an image is possible through the computation of several features related to these patterns.

Many approaches have been proposed for image texture analysis. These approaches mainly fall in four different categories: Statistical texture analysis techniques describe image textures by the computation of high-order moments of grayscale histograms. Structural texture analysis techniques can describe regular textures based on the properties and placement rules of defined texture elements. Model-based texture analysis techniques use empirical models of texture and finally, transform-based texture analysis converts images in other coordinates (i.e. frequency) from which different statistical features are computed.

In this paper, two texture analysis methods are presented. Gray Level Co-occurrence Matrix (GLCM) falls in the statistical texture analysis family and Wavelet Texture Analysis (WTA) is part of the transform-based texture analysis group. These methods are presented in the following two sub-sections.

#### 7.5.2.1 Gray Levels Co-occurrence Matrices (GLCM)

The GLCM of an image (**I**) is an estimate of the second order joint probability of the intensity of two pixels (*i,j*), located at *L* pixels and at a specified angle ($\triangleleft$) from each other (Bharati et *al.*, 2004). This joint probability analysis leads to a square matrix whose dimensions are equal to the number of gray-levels of the image (i.e. 256). However, to speed-up the analysis, GLCM are quite often computed on 32 gray-levels versions of images, without losing too much information, consequently leading to 32×32 GLCM matrices.

To illustrate the methodology, four different GLCM are presented in Figure 7.4 for an image containing four gray-levels (Tessier, 2006). Each GLCM has different parameters (distance *L*, and angle $\triangleleft$) thus capturing different textural patterns.

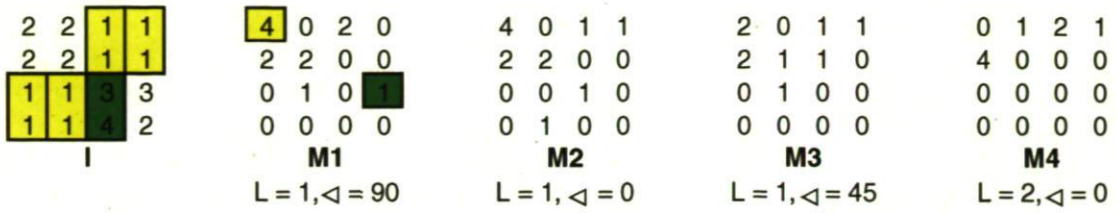


Figure 7.4: Four different GLCM for an image (**I**) of four gray-levels.

From these GLCM matrices, it is possible to compute different statistical descriptors to quantify image textures. Contrast, correlation, energy and homogeneity are the four most frequently used descriptors (Haralick, 1979; Bharati et *al.*, 2004). Contrast is a measure of the intensity contrast between a pixel and its neighbour, correlation measures the correlation between a pixel and its neighbour, energy is the sum of the squared elements of the GLCM and homogeneity is related to the closeness of the elements distribution of the GLCM to the GLCM diagonal.

In some applications, it may be useful to perform the analysis using different distances and angles ($L$ and $\triangleleft$) since strongly oriented textures will manifest themselves in one of the analyzed directions (i.e. horizontal, vertical and diagonal). Moreover, fine textures will be detected with the analysis of small pixels distances compared to coarser textural patterns that will be seen with longer distances. Considering the alumina mixtures shown in Figure 7.1, it is clear that texture patterns do not follow well defined orientations. There are some waves in the images but they are not useful to predict alumina content. Hence, in this paper, GLCM are applied in the horizontal direction of the images ($\triangleleft = 0°$). However, distances between two pixels have to be investigated since particles are of different sizes. In this paper, distances of 1, 2, 5 and 10 pixels have been analyzed. These correspond to actual distances of 114, 228, 570 and 1140 μm on the scene. GLCM was also used in a multi-resolution analysis by combining contrast, correlation, energy and homogeneity from the four studied distances. It is believed that this combination can produce better results since it accounts for the different textures introduced by the differences in the size distribution of the two powders (alumina and crushed bath).

#### 7.5.2.2 Wavelet texture analysis (WTA)

Texture can be defined as a function of the spatial variations in pixels intensities. Since digital images are gray-levels two-way discrete function (Image = f($m$,$n$)), two-dimensional WTA are used to decompose gray-levels images into the space-frequency domain, and converts the textural information of an image into a series of so-called wavelet coefficients. Different textural features (i.e. statistics) are extracted from these coefficients to characterize textures contained within the analyzed image.

Compared to Fourier Transforms, WTA maintains the spatial information from the image signal and this is a clear advantage over other transform-based texture analysis methods (Bartolacci et *al.*, 2006). Another advantage of WTA comes from its ability to analyze textures at different frequencies or resolutions. Therefore, this method is also called multi-resolution since it can be compared to a photographer using a big zoom lens to photograph the fine details of a scene, and then removes it to take a global shot of the complete scene (Tessier et *al.*, 2006). Hence, in terms of signal processing, it analyses fine textures at high frequencies and coarser textures at lower frequencies. To illustrate this, consider the brick wall images of Figure 7.5. In these pictures, WTA would be able to describe different textural patterns depending on the resolution of the analysis. At low resolution or frequency, WTA would be able to describe the mortar-brick pattern of the wall shown in the original image (Figure 7.5(a)). However, from this same image, a WTA of higher resolution would give information about textural patterns within a single brick. For illustration purposes, these patterns are presented in Figure 7.5(b), which correspond to the central brick of the original image zoomed 400%.

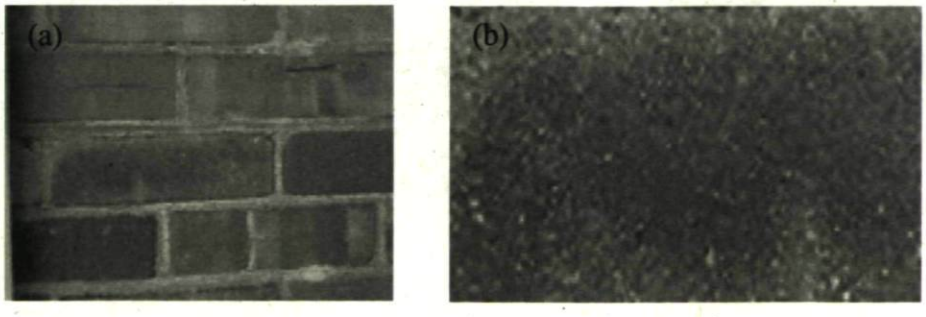


Figure 7.5: Brick wall images: (a) the original image, (b) one brick zoomed 400%.

Consider one wants to decompose a continuous signal, f(x), by the mean of wavelet analysis. This signal is decomposed in different orthonormal bases ($\psi_{m,n}$(x)) obtained through translation and dilatation of a specific mother wavelet $\psi$(x).

$$\psi_{m,n}(x) = 2^{-m/2}\psi(2^{-m}x - n) \quad [7.3]$$

Where $m$ and $n$ are respectively the coefficients of dilatation and translation.

Similarly as Fourier Transforms, different coefficients are computed. They can be computed through the convolution of the signal with the orthonormal bases due to the orthonormal property.

$$C_{m,n} = \int_{\Re} f(x)\psi_{m,n}(x)dx = \langle \psi_{m,n}, f(x) \rangle \quad [7.4]$$

The so-called mother wavelet is linked to the scaling function $\varphi$(x) with a certain sequence of $h[k]$

$$\psi(x) = \sqrt{2}\sum_k h_1[k]\phi(2x - k) \quad [7.5]$$

where

$$\phi(x) = \sqrt{2}\sum_k h_0[k]\phi(2x - k) \quad [7.6]$$

and

$$h_1[k] = -1^k h_0[1 - k] \quad [7.7]$$

The discrete wavelet transform can be applied to a discrete signal with the use of these relations. However, the explicit forms of the scaling function and of the mother wavelet are not required. Hence, for the decomposition at level $j$,

$$\phi_{j,l} = 2^{j/2}h_0^j[k - 2^j l] \quad [7.8]$$

$$\psi_{j,l} = 2^{j/2}h_1^j[k - 2^j l] \quad [7.9]$$

The discrete wavelet coefficients are now computed as

$$a_j[l] = \langle f[k], \phi_{j,l}[k] \rangle \qquad [7.10]$$

and

$$d_j[l] = \langle f[k], \psi_{j,l}[k] \rangle \qquad [7.11]$$

Where $j$ and $l$ are the indices of scale and translation, respectively. The $a_j[l]$'s are called the approximation coefficients and the $d_j[l]$'s are the detail coefficients.

In two-dimensional discrete wavelet analysis, a discrete gray-level image is passed through a series of low-pass and high-pass filters as shown in Figure 7.6. The rows of pixels are first filtered with both low-pass ($H_0$) and high-pass ($H_1$) filters, Eqs. [7.8 - 7.11]. A fit coefficient (i.e. wavelet coefficient) with the wavelet function is computed for every pixel and a column-wise decimation is then performed on both filtered matrices. A column out of two is kept in. These two column-wise decimated matrices of coefficients are again filtered using the same two filters, but this time the filtering step is performed on the columns. This generates four matrices of coefficients which are then decimated one more time. This last decimation is performed row-wise and a row out of two is kept in. The four resulting matrices have half the sizes of the original image matrix.

The coefficient matrix arising from the two low-pass filters is called the approximation matrix ($a_j$). This matrix contains the information of all low frequency textures. Based on the specific order of filtering, the three remaining decimated matrices of coefficients are called details since they contain high frequency textures. One encloses horizontal textural details ($d^h$), another one contains the vertical details ($d^v$) and the last one represents the diagonal details ($d^d$). If one is interested in the extraction of low frequency textural features, it is possible to reintroduce the approximation matrix in the filtering loop. Hence, the first loop will give information about high frequency textures (i.e. fine details) and the second loop of filtering will give information about textures existing at lower frequencies (i.e. coarse details). This can be performed a few times to extract information on coarser textures. Figure 7.6 gives an illustration of the filtering process for single loop (first level) decomposition.

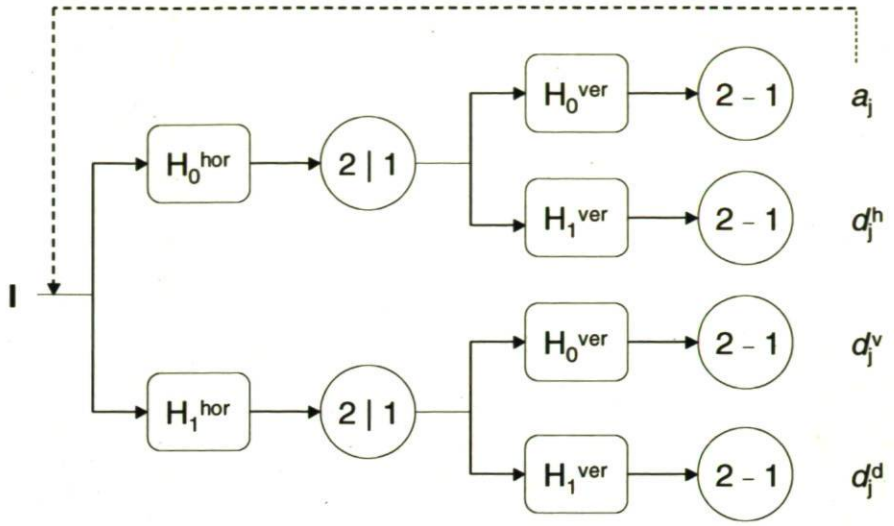


Figure 7.6: Schematic of WTA decomposition.

Once an image has been filtered to the appropriate level of decomposition, statistics are computed based on the elements of the detail matrices ($d_j^h, d_j^v$ and $d_j^d$), the wavelet details coefficients. The Froebenius norm (Bharati et *al.*, 2004; Liu, 2004), often called energy, is one of the most frequently used statistics to summarize the textural features extracted using WTA and is used in this paper.

### 7.5.3 Regression Models for Predicting Alumina Content Based on Image Features

The last step of the proposed methodology consists in building a regression model to predict alumina content of the anode cover material based on a sample image of the corresponding mixture. In the previous section, various methods were proposed to extract color and textural features of the mixture images. For each image, these features are stored row-wise in a regressor matrix $\mathbf{X}$ ($I \times J$), where $I$ is the total number of images in the set used to build the model, and $J$ is the total number of features (color and/or textural) used in the model. As mentioned in section 7.4, for each of the 101 mixture images collected in the sampling campaign corresponds a measurement of alumina content obtained using X-ray spectroscopy. These measurements can be stored in a response matrix $\mathbf{Y}$ ($I \times 1$). One can therefore use any appropriate regression method such as Ordinary Least Squares (OLS), Partial Least Squares (PLS), etc. to build a predictive model for alumina content.

In this paper, PLS regression was used since in most case studied (discussed in next section), the color and/or textural features stored in **X** are highly collinear. Partial Least Squares regression is a latent variable (or multivariate projection) method that relates two groups of variables (i.e. **X** and **Y**) through a set of latent variables **T** (i.e. score vectors) as shown below:

$$\mathbf{X} = \mathbf{T}\mathbf{P} + \mathbf{E} \quad [7.12]$$

$$\mathbf{Y} = \mathbf{T}\mathbf{Q} + \mathbf{F} \quad [7.13]$$

$$\mathbf{T} = \mathbf{X}\mathbf{W}^{*} \quad [7.14]$$

where the **P** and **Q** matrices contain the loading vectors that best represent the **X** and **Y** spaces respectively, whereas **W*** contain the loading vectors that define the relationship between the **X** and the **Y** spaces. The **E** and **F** matrices contain the residuals of each space. PLS is often seen as an extension of PCA for the analysis of two groups of variables having a lower dimensional structure (i.e. colinearity between the columns of **X** and **Y**). However, in PLS, the loading vectors **W*** (linear combinations of the columns of **X**) are chosen to maximise the covariance between **X** and **Y** instead of maximizing the explained variance of each spaces separately as PCA does. The loading and score vectors of each latent dimension (or principal components) are usually calculated sequentially using the Non-linear Iterative Partial Least Squares (NIPALS) algorithm (Kresta et *al.*, 1991). The number of components is typically determined using a cross-validation procedure that aims at selecting the model order that maximizes the predictive power of the model.

## 7.6 Alumina Content Prediction Results

A total of 15 PLS regression models have been studied in this work as shown in Table 7.2, each using a different combination of color and/or textural features extracted from the mixture images. The image database described in section 7.4 has been randomly divided into two sub-sets: a training set (71 images) and a test set (30 images). The training set was used to build the regression models whereas the test set was used to select the number of principal components (PCs) and to compare the predictive power of the models. The Root Mean Squared Error of Prediction (RMSEP) statistics obtained from predictions of the test set was used for both selecting the PCs and comparing predictive powers. The number of

PCs of each model was selected to be the one leading to the smallest RMSEP statistics on the test set.

Table 7.2: Combinations of color and/or textural features in each of the 15 PLS models.

| Type of features | Description | Model ID |
|---|---|---|
| Color | RGB means and stds | 1 |
| | RGB histograms | 2 |
| | PCA loadings | 3 |
| Texture | WTA level 1-6 | 4 |
| | WTA level 1-3 | 5 |
| | WTA level 2-5 | 6 |
| | WTA level 2-6 | 7 |
| | GLCM 1 pixel | 8 |
| | GLCM 2 pixel | 9 |
| | GLCM 5 pixel | 10 |
| | GLCM 10 pixel | 11 |
| | GLCM multiresolution | 12 |
| Color and texture | WTA 2-6 + PCA loadings | 13 |
| | GLCM multi + PCA loadings | 14 |
| | GLCM multi + mean and std | 15 |

The predictive power of the models is compared in Table 7.3, where the RMSEP statistics are reported for both the training and test sets. The percentage of predictions on the test set falling within +/- 1 $\sigma$ and +/- 2 $\sigma$ of the laboratory analysis standard-deviations is also shown. These measurement uncertainties were obtained from Alcoa's laboratory personnel. Based on current operating policies, operators would not react to variations within +/- 2 $\sigma$ of the laboratory analysis, but would follow very closely when approaching that limit. Control decisions are made when sustained deviations, significantly beyond +/- 2 $\sigma$ occur. Finally, Figure 7.7 shows the prediction results for models 1, 12, and 15, which correspond to the best models using color features only, textural features only, and both color and textural features, respectively.

Table 7.3: Comparison of the predictive power of the 15 PLS models investigated.

| Type of features | Model ID | Number of features | Number of PC | RMSEP ($x10^4$) | | % Prédiction inside +/- 1 σ | % Prédiction inside +/- 2 σ |
|---|---|---|---|---|---|---|---|
| | | | | Training | Test | | |
| Color | 1 | 6 | 2 | 35 | 40 | 26.7 | 56.7 |
| | 2 | 768 | 3 | 3 | 44 | 23.3 | 40.0 |
| | 3 | 9 | 7 | 163 | 113 | 20.0 | 36.7 |
| Texture | 4 | 18 | 11 | 19 | 42 | 56.7 | 70.0 |
| | 5 | 9 | 4 | 22 | 42 | 46.7 | 66.7 |
| | 6 | 12 | 8 | 26 | 33 | 30.0 | 66.7 |
| | 7 | 15 | 11 | 25 | 39 | 30.0 | 66.7 |
| | 8 | 4 | 3 | 16 | 32 | 36.7 | 56.7 |
| | 9 | 4 | 2 | 18 | 30 | 36.7 | 53.3 |
| | 10 | 4 | 2 | 19 | 31 | 20.0 | 50.0 |
| | 11 | 4 | 2 | 20 | 34 | 30.0 | 53.3 |
| | 12 | 16 | 10 | 7 | 12 | 63.3 | 80.0 |
| Color and texture | 13 | 24 | 13 | 20 | 44 | 30.0 | 50.0 |
| | 14 | 25 | 10 | 8 | 11 | 60.0 | 76.7 |
| | 15 | 22 | 12 | 6 | 9 | 63.3 | 83.3 |

The results show that color features alone are not sufficient to adequately predict alumina content. Model 1, which is the best model among those using color features only, has a test set RMSEP of 0.0040 compared to 0.0012 for the best model using textural features only (model 12). Furthermore, most models based on textural features extracted using WTA and GLCM (models 4-11) do not perform much better than models using color only (models 1-3); the RMSEP obtained from the test set is almost double the value obtained from the training set. The multi-resolution GLCM algorithm is clearly the best model among those tested using textural features only. This supports the assumption that the size distribution of the mixture is a good indicator of the proportions of alumina/crushed bath in the mixture. Combining both color and textural features only, results in small improvements in model predictions (models 13-15). This confirms again that textural features are the most important for predicting alumina content.

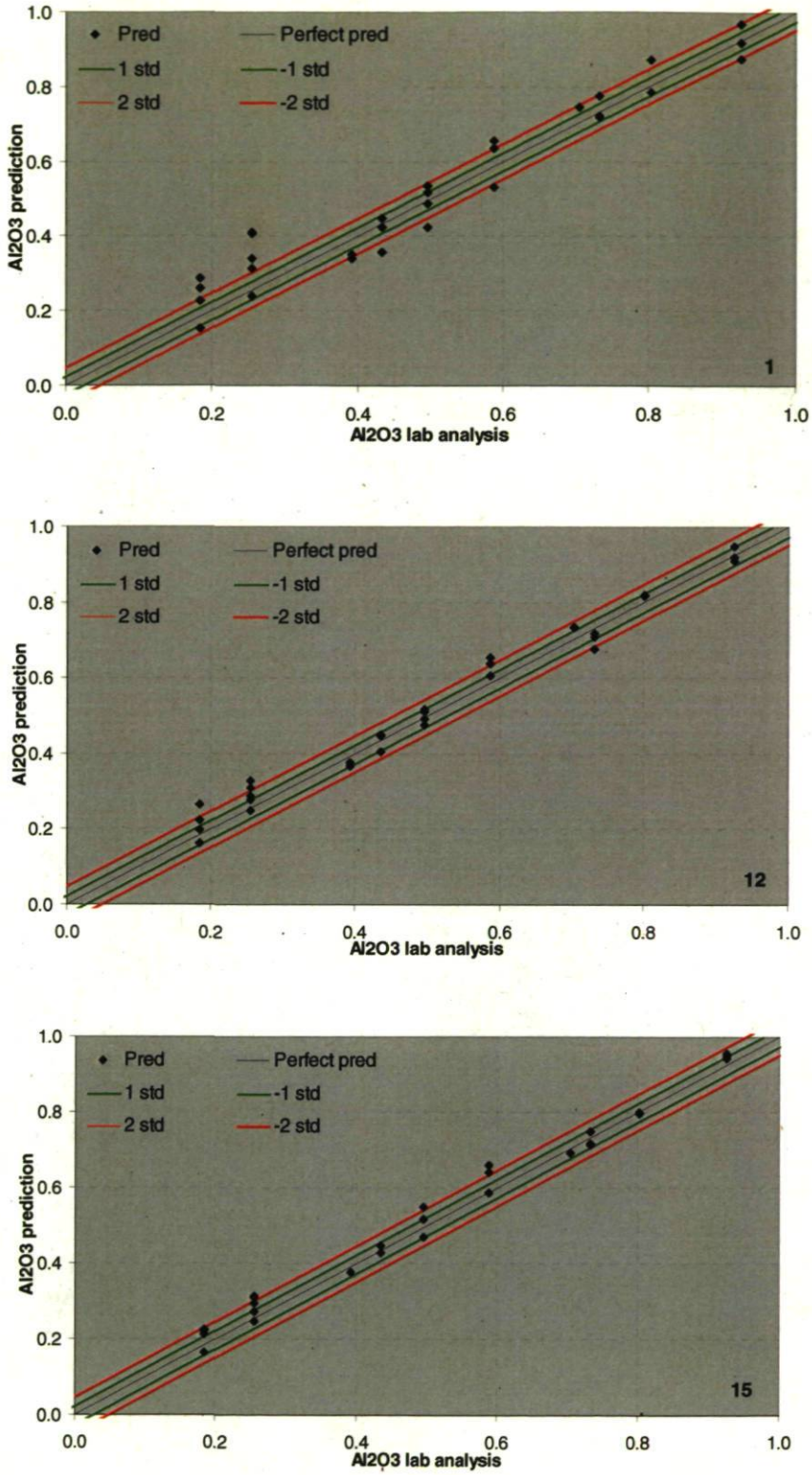


Figure 7.7: Predictions of $Al_2O_3$ content vs. laboratory analysis for models 1, 12, and 15.

The lower performance of models using color features only might be explained, on one hand, by a lack of color contrast at lower alumina concentrations as shown on Figure 7.7(a). It appears that images of mixtures of less than 40% alumina are more difficult to discriminate using color only. On the other hand, another reason for the poorer performance of color features is a lack of robustness to irrelevant features present in the images such as the waves shown on Figure 7.8.

These waves have an effect on color distributions by modifying the way light is reflected. The top of these waves are lighter and shadows surrounding them are darker. The texture algorithms, however, should be more robust to the presence of waves since by selecting the number of decomposition levels in WTA, or the distance between pixels ($L$) in GLCM, one is actually filtering the images. An additional smoothing is performed in the GLCM algorithm since the images are reduced to 32 gray-levels, thus locally reducing high pixels variations and noise. To illustrate how texture algorithms filter out the waves, Figure 7.9 presents the results of a typical WTA analysis decomposition. Using a colormap to enhance contrast, this figure shows an original image of anode cover material and the approximations and details images of a three levels decomposition. From these pictures, it can be seen that wave patterns are seen in the approximations images and not in the details images. Hence, using energy from details images only, major light effects from the presence of waves will not be accounted since they will remain in the approximation of the image at the higher level of decomposition. However, these waves will start to appear in the details at levels four and five.

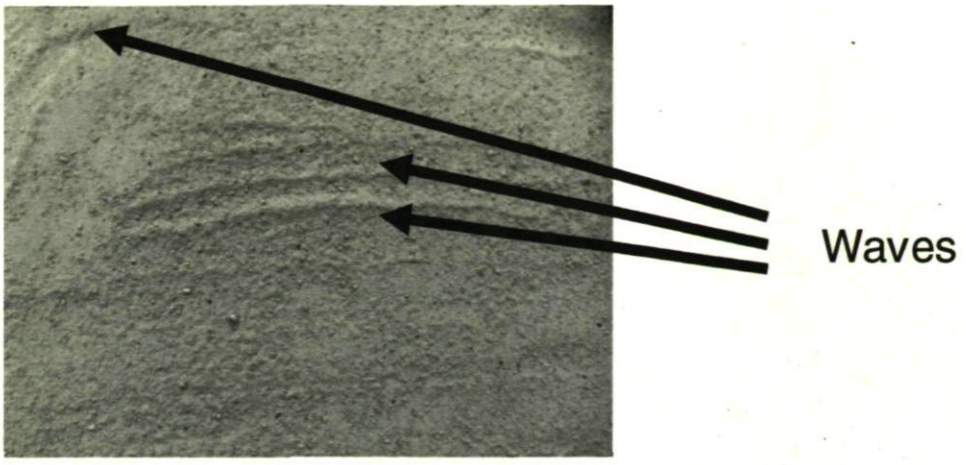


Figure 7.8: The presence of waves within an image.

Finally, in spite of the fact that some authors found that WTA was superior to GLCM for image texture classification (Bharati et *al.*, 2004), it seems that this is very application dependent. In this study, multi-resolution GLCM was found to be superior to WTA in terms of extracting textural features that are relevant for predicting alumina content. This might be due to the greater frequency resolution provided by the GLCM algorithm. In the latter method, the user decides on the frequencies by selecting the pixel distances ($L$) with steps of one pixel. In WTA, the analyzed frequencies are constrained to a down sampling by a factor of two. Some useful information may be lost in between two frequencies, but may be captured by the GLCM algorithm which offers a greater frequency resolution.

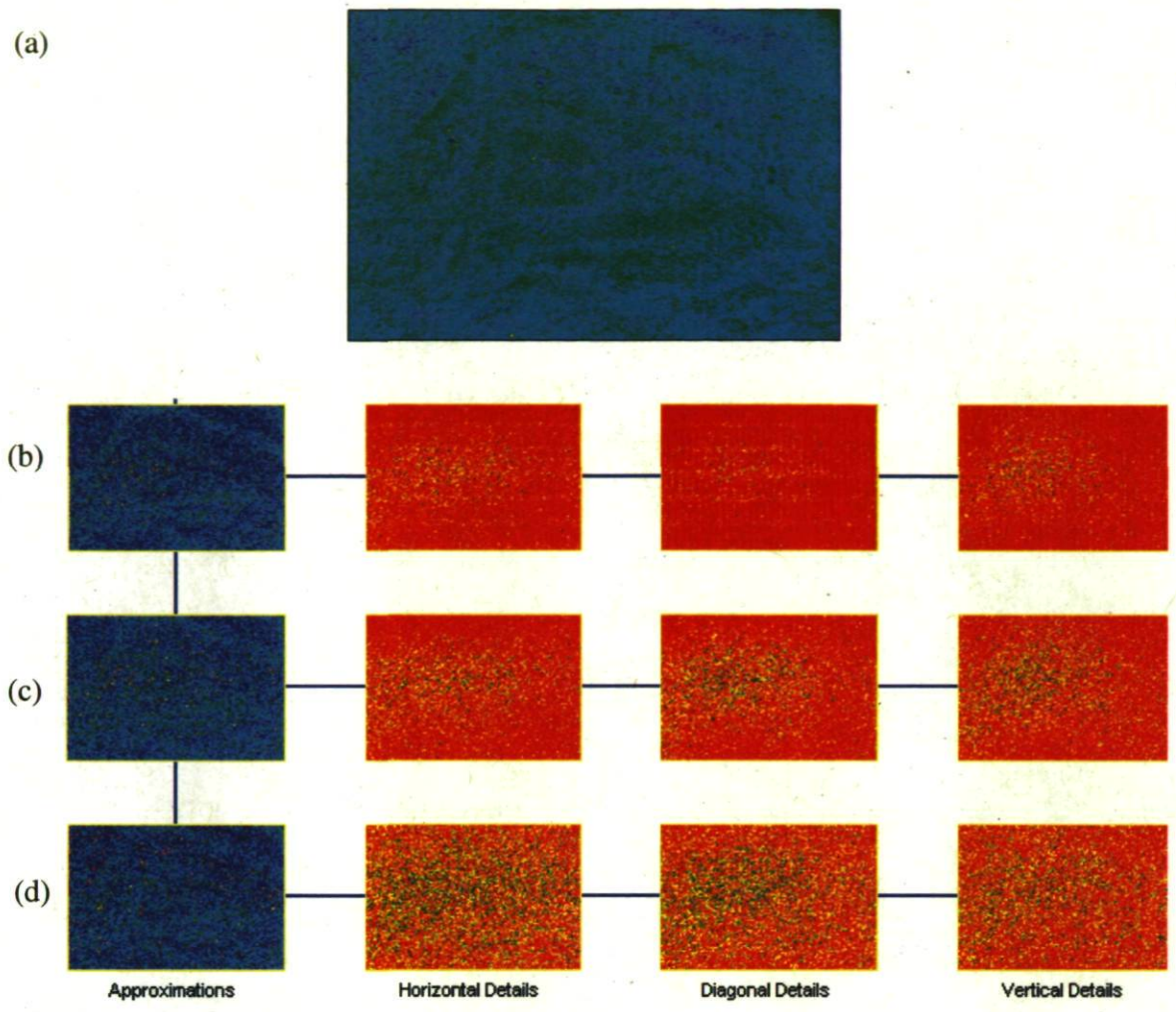


Figure 7.9: (a) Original cover product image displayed in a color map and its WTA for three levels of decomposition; (b) Level one, (c) level 2 and (d) level 3.

## 7.7 Conclusions

The main objective of this paper was to investigate whether it is possible to predict alumina content within anode cover mixtures used in primary aluminum production using a machine vision approach. A secondary objective was to compare various ways of extracting information from images and to select the most promising approach. In total, fifteen different PLS regression models were built and compared, each using a different combination of color and/or textural features to predict alumina content of anode cover mixture images. Color features were extracted both in the original RGB space of the images

and from a projection space obtained after applying Principal Component Analysis (PCA) to the images. Textural features were extracted using two different methods: Wavelet Texture Analysis (WTA) and Gray Level Co-ocurrence Matrices (GLCM). Very promising results were obtained for the prediction of alumina content. It was also found that multi-resolution textural features led to the best predictive power since they extract information related to the size distribution of the product which, in turn, is monotonically related to the percentage of alumina within the binary mixture. Furthermore, it was also shown that textural features are more robust to irrelevant information present in the images, such as waves. Finally, the multi-resolution GLCM algorithm was found to be superior to WTA in this particular application, most probably due to a greater frequency resolution. Color features were found to be less robust and there seems to be a lack of color contrast in the images of mixtures having less than 40% alumina.

Future work involves a larger experimental plan covering several weeks of operation to simulate on-line application of the machine vision approach. Predictions results will allow establishing a relationship between alumina content in the anode cover material and reduction cell performance, and to develop effective feedback control strategies to reduce variations. Finally, this vision-based sensor will be part of contingency plan in case of failure of the X-ray spectroscopy equipment.

## 7.8 Acknowledgements

Part of the funding of this project was available from NSERC Industrial Postgraduate Scholarships program. The authors would like to thank Alcoa Inc. for funding and granting permission to publish these results. Special thanks also go to Pierre Mineau and his Technical Staff at Alcoa Aluminerie Deschambault for performing the lab analysis and their good councils.

# 8 General Conclusion

## 8.1 Conclusion

Aluminum reduction cells are complex multivariate processes which performance is affected by many sources of variations. An important part of this thesis is devoted to the investigation of sources and variables leading to cell performance variations:

- The impact of preheating, start-up and early operation was investigated, with respect to potlife, in chapter 4. Based on a multiway PLS models, it was demonstrated that these three steps alone can explain up to 73% of the potlife variance and that potlife can be predicted within 84 days after only 60 days of operation. Considering these cells were in operation for more than 2000 days, and the uncertainties associated with the decision to stop a pot, these predictions were found more than acceptable from an operational point of view. Bearing in mind the many sources of disturbances pots sustain during their life cycle, this study demonstrates the importance of carefully monitoring and performing preheating, start-up and early operation since these steps explain more variance of the potlife metric than the variations sustained during normal operation.

- The effect of variations in alumina and anode properties, as well as pot manipulated and state variables and start-up conditions, were studied with respect to current efficiency and energy consumption in chapter 5. Based on a multi-block PLS model, built using data over complete potlife cycles, it was demonstrated that 54.21% of the variance of current efficiency and 50.87% of the variance of energy consumption can be explained from the available information about the process. Considering that alumina and anode properties are not available on a pot basis, but rather as population average and standard deviations estimates, these results are judged satisfactory.

- In chapter 5, it was demonstrated that bath level plays an important role in pot performance variations. Therefore, an investigation of variables affecting bath level

was conducted in chapter 6. The analysis of the root causes of weekly bath level averages and standard deviation was performed using two separate PLS models. These models explained 69.23% and 66.42% of the variance of bath level averages and standard deviations, respectively. Among the variables considered in this analysis, anode cover material composition was ranked first in terms of correlation with bath level fluctuations. Unfortunately, as demonstrated, this composition is not well controlled because grabbed samples sent to laboratory are not necessarily representative of the population composition due to the mixture heterogeneity. Therefore, there is a need to analyze more samples which would come at increased costs and labour from the laboratory department.

- However, in chapter 7, a novel method for estimating anode cover material composition was proposed based on image analysis. Presented results demonstrate that it is possible to estimate cover material composition as 83% of the predictions fall within +/- $2\sigma$ of the laboratory confidence intervals. The use of image analysis would overcome the limitations from laboratory analysis as many anode cover material samples could easily be imaged. Therefore, composition prediction of these samples could be used to get a better estimation of the average anode cover composition used in the potroom or even on a pot basis.

Nevertheless, the most important conclusion from the work presented here is that reduction cells are truly multivariate processes and that monitoring or investigating performance drop should be done using multivariate statistical analysis techniques, as opposed to the univariate or bivariate statistical analysis used throughout the industry. These methods are better suited for the analysis of these types of processes as;

- They can simultaneously use all available variables, in spite of the fact of the correlations among them,

- They can split the systematic and stochastic variations enclosed in the investigated data by carefully selecting the number of principal components to use,

- Through the computation of variables importance in the prediction, it is possible to assess the model structure, based on process knowledge,

- Through the computation of variables contributions, it is possible to investigate and isolate, among the hundreds of variables used in the analysis, variables statistically linked with performances variations.

Moreover, multivariate statistical analysis techniques are well suited for the development of multivariate statistical control charts. These charts are advantageous as only few statistics have to be computed to efficiently summarize process behaviour and hence determine if a pot is in control or not, based on a model built from good operation. Examples of these charts were presented in chapters 3 and 4 through the use of $T^2$ and Q statistics. These statistics include the in-model and out-of-model variations, respectively. In the event these statistics violate their statistical limits, the contributions of the variables can be used to help isolate possible causes for the process disturbance.

## 8.2 Recommendations and Future Work

Alcoa Deschambault is a modern smelter where the database structure is considered good, compared to older smelters. In spite of this, the work presented in this thesis pointed out that not enough information is available around reduction cells to completely assess their behaviour and thus their performances variations:

- Alumina properties are only available as bulk estimates from the certificate of analysis (COA). Unfortunately, due to the inequalities arising from gas treatment center, charging alumina with fluoride, and from the transportation systems, not all the pots are fed with the *same* alumina. Some segregation arises in the alumina handling systems and therefore, some pots are fed with more fine particles while other are fed with coarser ones. This might play a role in the alumina dissolution rate and hence increase or decrease current efficiency and/or energy consumption in particular cells. Characterising this segregation throughout a potline may come handy when performance assessment is made on a pot-to-pot basis.

- In a similar fashion, anode properties are assessed using a few core samples collected on a weekly basis. However, considering the fact that a few thousands anode pieces are produced on a weekly basis, this limited population sample might not always give a representative picture of the anodes average quality. Furthermore, anode quality is not known on a pot basis which is a limitation to better capture the effects of anode quality on pot performance. It is known that pots are operated as a function of the worst anode in the pot. Unfortunately, it is actually impossible to track the properties of each anode and hence properly link their variations to pot performance.

- Moreover, there is room for more information complementing the already available information from each pot. Bath temperature, level and chemistry are only available on a daily basis, or every other day. An industrial device, robust to the daily aggressive conditions inside reduction cells, has yet to be developed in order to measure at least bath level and temperature. Anode cover material composition is not available on a pot basis, in spite of the fact that it is the most influential variable to bath level variations. However, the image analysis technique proposed in this thesis may overcome this situation and give this information on a pot to pot basis. There is only little information indicating manual operation quality, however, heavily instrumented pot tending machines and tapping cranes are now available and are in used in different smelters. Such equipments can transmit information collected during anode setting or metal and bath tapping, and hence give an indication of the manual operation consistency and quality.

- Only a limited amount of information is available from the preheating stage of reduction cells. At best, few thermocouples are embedded in cathodes blocks to monitor temperatures through the preheating phase. Unfortunately, due to variations in contact resistances throughout the anode shadow area, in case of electrical preheating, it is not guaranteed that all cathodes are at a sufficiently high temperature to prevent thermal gradients or cathode cracking. Therefore, not all the effect of preheating temperature is captured here.

Having these data available would greatly improve the results obtained in this thesis as it would give a better idea of the real disturbances affecting each reduction cell. It is believed that the variance explained for current efficiency, energy consumption and potlife would increase.

A new anode cover material imaging prototype is currently in development. The image quality obtained through this set-up is greatly improved compared to images used in the work performed in chapter 7. An industrial validation should be performed soon.

Finally, performing similar studies based on data from different smelter would be of interest. Comparing results obtained here with those from a smelter using the same technology could clarify some of the results. On the other hand, using data from other pot technology might highlight some systematic differences between both technologies.

# References


Adams, A., Cahill, R., Belzile, Y., Cantin, K., Gendron, M., 2009, Minimizing impact of low sulphur coke on anode quality, *Proceedings of The Minerals, Metals & Materials Society, Light Metals 2009*, pp. 957-962.

Banta, L., Dai, C., Biedler, P., 2003, Noise classification in the aluminum reduction process, *Proceedings of The Minerals, Metals & Materials Society, Light Metals 2003*, pp.431-435.

Baron, J.T., McKinney, S.A., Wombles, R.H., 2009, Coal tar pitch - Past, present and future, *Proceedings of The Minerals, Metals & Materials Society, Light Metals 2009*, pp. 935-939.

Bartolacci, G., Pelletier, P., Tessier, J., Duchesne, C., Bossé, P.A., Fournier, J., 2006, Application of numerical image analysis to process diagnosis and physical parameter measurement in mineral processes—Part 1: Flotation control based on froth textural characteristics, *Minerals Engineering*, Vol., 19, No. 6-8, pp. 734-747

Bearne, G.P., 1999, The development of aluminum reduction cell process control, *JOM*, May 1999, pp. 16-22.

Benkahla, B., Caratini, Y., Mezin, H., Renaudier, S., Fardeau, S., 2008, Last development in AP-50 cells, *Proceedings of The Minerals, Metals & Materials Society, Light Metals 2008*, pp.451-455.

Benkahla, B., Martin, O., Tomasino, T., 2009, AP-50 performances and new development, *Proceedings of The Minerals, Metals & Materials Society, Light Metals 2009*, pp.365-370.

Bharati, M .H., 1997, *Multivariate Image Analysis for Real-Time Process Monitoring*, MSc. Thesis, McMaster University, Hamilton, Ontario, Canada, 125 p..

Bharati, M.H., MacGregor, J.F., 2001,Texture analysis of images using principal component analysis, *Proceedings of the SPIE; Process Imaging for Automatic Control*, Vol. 4188, pp. 27-37.

Bharati, M. H., Liu, J., MacGregor, J.F., 2004, Image texture analysis: Methods and comparisons, *Chemometrics and Intelligent Laboratory Systems*; Vol. 72, pp. 57-71.

Bonifazi, G., La Marca, F., Massacci, P., 1999, Imaging and pattern recognition techniques applied to particulate solids material characterization in mineral processing, *Proceedings of Control and Optimization in Minerals, Metals and Materials Processing, MetSoc 99*, pp. 43-57.

Burnham, A.J., Viveros, R., MacGregor, J.F., 1996, Frameworks for latent variable multivariate regression, *Journal of Chemometrics,* Vol. 10, 1996, pp.31-45.

Bruno, M.J., 2003, Aluminum carbothermic technology comparison to Hall-Héroult process, *Proceedings of The Minerals, Metals & Materials Society, Light Metals 2003*, pp.395-400.

Calderon De Anda, J., Wang, X.Z., Roberts, K.J., 2005, Multi-scale segmentation image analysis for the in-process monitoring of particle shape with batch crystallizers, *Chemical Engineering Science*, Vol. 60, pp. 1053-1065.

Chandan, C., Sivakumar, K., Masad, E., Fletcher, T., 2004, Application of imaging techniques to geometry analysis of aggregate particles, *Journal of Computing in Civil Engineering*, Vol. 18, No. 1, pp. 75-82.

Choate, W., Green, J., 2006, Thenoeconomic assessment of the carbothermic reduction processfor aluminum production, *Proceedings of The Minerals, Metals & Materials Society, Light Metals 2006*, pp.445-450.

Chong, I.-G., Jun, C.H., 2005, Performance of some variable selection methods when multicollinearity is present, *Chemometrics and Intelligent Laboratory Systems*, Vol. 78, pp. 103-112.

Conlin, A.K., Martin, E.B., Morris, A.J., 2000, Confidence limits for contribution plots, *Journal of Chemometrics,* Vol. 10, pp.725-736.

D'Amours, G., Fafard, M., Gakwaya, A., Mirchi, A.A., 2003, Mechanical behaviour of carbon cathode: Understanding, modeling and identification, *Proceedings of The Minerals, Metals & Materials Society, Light Metals 2003*, pp.633-639.

Dando, N., Xu, W., Nichols, R, Rusche, S., Neimer, M., 2008, Comparison of PFC emission rates for operating and newly started pots at a horizontal Söderberg smelter, *Proceedings of The Minerals, Metals & Materials Society, Light Metals 2008*, pp.233-237.

Dewing, E.W., Loss of current efficiency in aluminum electrolysis cells, *Metallurgical and Materials Transactions B*, Vol. 22B, April 1991, pp.177-182.

Doiron, P., Lindsay, S.J., 2009, Pure metal production and methodology: The Alcoa Deschambault experience, *Proceedings of The Minerals, Metals & Materials Society, Light Metals 2009*, pp.499-503.

Duchesne, C., Kourti, T., MacGregor, J.F., Multivariate SPC for startups and grade transitions, *AIChE Journal, 2002*, pp.2890-2901.

Duchesne, C., Bouajila, A., Bartolacci, G., Pelletier, P., Breau, Y., Fournier, J., Girard, D., 2003, Application of Multivariate Image Analysis (MIA) to Predict Concentrate

Grade in Froth Flotation Processes, *Proceedings of the 35th Annual Meeting of the Canadian Mineral Processors, CMP 2003*, pp. 511-526.

Dunn, M.R., Galadari, Q.M.I., 1997, An analysis of the electrical preheat technique based on the start-up of the CD200 prototypes at Dubai Aluminum Co. Ltd., *Proceedings of The Minerals, Metals & Materials Society, Light Metals 1997*, pp.247-251.

Edwards, J., 1955, *The Immortal Woodshed: The story of the inventor who brought aluminum to America*, New York,USA, Dodd, Mead & Company, 244p.

*Encyclopædia Britannica (a),* Retrieved July 22, 2009, from Encyclopædia Britannica Online: http://www.britannica.com/EBchecked/topic/17944/aluminum

*Encyclopædia Britannica (b),* Retrieved September 15, 2009, from Encyclopædia Britannica Online: http://www.britannica.com/EBchecked/topic /564172/statistics#

Entner, P.M., 1992, Control of AlF3 concentration, *Proceedings of The Minerals, Metals & Materials Society, Light Metals 1992*, pp.369-374.

Eriksson L., Johansson E., Kettaneh-Wold N., Trygg J., Wikstrom C., Wold S., 2006, *Multivariate and Megavariate Data Analysis: Part I - Basic Principles and Applications.* Umetrics, Umeå, Sweden, 307p.

Fisher, W.K, Mannweiler, U., Keller, F., Perruchoud, R.C., Bühler, U., 1995, *Anodes for the Aluminum Industry*, Sierre, Switzerland, R&D Carbon, 394p.

Geladi, P., Kowalski, B.R., 1986, Partial least squares regression: A tutorial, *Analytica Chimica Acta*, Vol. 186, pp.1-17.

Geladi, P., Grahn, H., 1996, *Multivariate Image Analysis*, John Wiley and Sons, Chichester, England, 316 p..

Geladi, P., Manley, M., Lestander, T., 2003, Scatter plotting in multivariate data analysis, *Journal of Chemometrics*, Vol. 17, pp.503-511.

Grjotheim, K., Kvande, H., 1993, *Introduction to Aluminum Electrolysis,* Düsseldorf, Germany, Aluminum-Verlag, 260p.

Haralick, R.M., 1979, Statistical and structural approaches to texture, *Proceedings of the IEEE*, Vol.67, No.5, pp. 786-804.

Haugland, E., Børset, H., Gikling, H., Høie, H., 2003, Effects of ambient temperature and ventilation on shell temperature, heat balance and side ledge of an alumina reduction cell, *Proceedings of The Minerals, Metals & Materials Society, Light Metals 2003*, pp.269-276.

Haupin, W.E., 1991, A challenging task to improve potlife in aluminum industry, *10th International Course on Process Metallurgy of Aluminum,* Institute of Inorganic Chemistry, Trondheim, Norway.

Haupin, W.E., Kvande, H., 1993, Mathematical model of fluoride evolution from Hall-Héroult cells, *Proceedings of The Minerals, Metals & Materials Society, Light Metals 1993*, pp.257-263.

Haupin, W.E., 1995, Principles of aluminum electrolysis, *Proceedings of The Minerals, Metals & Materials Society, Light Metals 1995*, pp.195-203.

Haupin, W.E., 2003, History of Aluminum Production: What is its significance to today?, *Industrial Aluminum Electrolysis: Theory & Practice of Primary Aluminum Production,*The Minerals, Metals and Materials Society, Quebec City, Canada

Homsi, P., Peyneau, J.-M., Reverdy, M., 2000, Overview of process control in reduction cells and potlines, *Proceedings of The Minerals, Metals & Materials Society, Light Metals 2000*, pp.223-230.

Höskuldsson, A., 1988, PLS regression methods, *Journal of Chemometrics*, Vol. 2, pp. 211-228.

Höskuldsson, A., Svinning, K., 2006, Modelling of multi-block data, *Journal of Chemometrics,* Vol. 20, pp. 376–385.

Jackson, J.E., 1991, *A User's Guide to Principal Component Analysis*, John Wiley and Sons, New-York, United States of America, 592 p..

Jain, R.K., Tricklebank, S.B., Welch, B.J., Williams, D.J., 1983, Interaction of aluminas with aluminum smelting electrolytes, *Proceedings of The Minerals, Metals & Materials Society, Light Metals 1983*, pp.609-622.

Jentoftsen, T., Linga, H., Aga, B., Christensen, V., Hoff, F., Holden, I., 2009, Correlation between anode properties and cell performance, *Proceedings of The Minerals, Metals & Materials Society, Light Metals 2009*, pp.301-304.

Johnson, A.R., 1981, Alumina crusting and dissolution in molten electrolyte, *Proceedings of The Minerals, Metals & Materials Society, Light Metals 1981*, pp.373-387.

Keniry, J., 2001, The economics of inert anodes and wettable cathodes for aluminum reduction cells, *JOM*, Vol. 52, No. 2, pp.22-28

Kolas, S., Støre, T., 2009, Bath temperature and $AlF_3$ control of an aluminum electrolysis cell, *Control Engineering Practice,* In Press, 9p.

Kourti, T., MacGregor, J.F., 1995, Process analysis, monitoring and diagnosis, using multivariate projection methods, *Chemometrics and Intelligent Laboratory Systems*, Vol. 28, pp. 3-21.

Kourti, T., 2002, Process analysis and abnormal situation detection: From theory to practice, *IEEE Control Systems Magazine*, October 2002, pp.10-25.

Kourti, T., 2005, Application of latent variable methods to process control and multivariate statistical process control in industry, *International Journal of Adaptive Control and Signal Processing*,Vol. 19, No. 4, 2005, pp.213-246.

Kresta, J.V., MacGregor, J.F., Marlin, T.E., 1991, Multivariate statistical monitoring of process operating performance, *The Canadian Journal of Chemical Engineering*, Vol. 69, pp. 35-47.

Kvande, H., 1994, Bath chemistry and aluminum cell performance – Facts, fictions and doubts, *JOM*, Vol. 52, No. 2, pp.22-28.

Kvande, H., 1998, Alumina, In *Fundamentals of Aluminum Production 1998 Course*, Institute of Inorganic Chemistry, Trondheim, Norway.

Larsen, P.A., Rawling, J.B., Ferrier, N.J., 2006, An algorithm for analyzing noisy, in situ images of high-aspect-ratio crystals to monitor particle size distribution, *Chemical Engineering Science*, Vol. 61, pp. 5326-5248.

Lepistö, L., Kunttu, I., Autio, J., Visa, A., 2003, Rock image classification using non-homogeneous textures and spectral imaging, *Proceedings of the WSCG 2003*, 5 p.

Li, J., Lü, X.-j., Lai, Y.-q., Li, Q-y, Liu, T.-x., 2008, Research progress in $TiB_2$ wettable cathode for aluminum reduction, *JOM*, August 2008, pp. 32-37.

Lindsay, S.J., 2005, SGA requirements in coming years, *Proceedings of The Minerals, Metals & Materials Society, Light Metals 2005*, pp.429-434.

Liu, J., 2004, *Machine Vision for Process Industries: Monitoring, control, and Optimization of Visual Quality of Process and Products*, PhD. Thesis, McMaster University, Hamilton, Canada, 170 p..

Liu, J., McGregor, J.F., Duchesne, C., Bartolacci, G., 2005, Flotation froth monitoring using multiresolutional multivariate image analysis, *Minerals Engineering*, Vol. 18, No.1, pp. 65-76.

Liu, D., Zhang, G., Li, J., Ostrovski, O., 2009, Solid start carbothermal of alumina, *Proceedings of The Minerals, Metals & Materials Society, Light Metals 2009*, pp.429-434.

MacGregor, J.F., Yu, H., Munoz, S.G., Flores-Cerrillo, J., 2005, Data-based latent variable methods for process analysis, monitoring and control, *Computers & Chemical Engineering*, Vol. 29, pp. 1217-1223.

Maeda, H., Matsui, S., Era, A., 1985, Measurement of dissolution rate of alumina in cryolite melt, *Proceedings of The Minerals, Metals & Materials Society, Light Metals 1985*, pp.763-780.

Maharaj, D., Imery, J., Zárate, J., Lazarde, J., 1991, Investigation of early cathode failure, *Proceedings of The Minerals, Metals & Materials Society, Light Metals 2009*, pp.429-434.

Majid, N.A.A., Young, B.R., Taylor, M.P., Chen, J.J.J., 2009, Detecting abnormalities in aluminium reduction cells based on process events using multi-way principal component analysis (MPCA), *Proceedings of The Minerals, Metals & Materials Society, Light Metals 2009*, pp. 589-593.

Martens, H., 2001, Reliable and relevant modelling of real world data: a personal account of the development of PLS Regression, *Chemometrics and Intelligent Laboratory Systems,* Vol. 58, pp. 85-95.

Martin, O., Jolas, J.M., Benkahla, B., Rebouillat, O., Richard, C., Ritter, C., 2006, The next stop to the AP3X-HALE technology: Higher amperage, lower energy and economical performances, *Proceedings of The Minerals, Metals & Materials Society, Light Metals 2006*, pp.249-254.

Meier, M.W., Fisher, W.K., Perruchoud, R.C., Thermal shock of anodes – A solved problem?, *Proceedings of The Minerals, Metals & Materials Society, Light Metals 1994*, pp.685-694.

Metson, J.B., Haverkamp, R.G., Hyland, M.M., Chen, J., 2002, The anode effect revisited, *Proceedings of The Minerals, Metals & Materials Society, Light Metals 2002*, pp.239-244.

Miletic, I., Quinn, S., Dudzic, M., Vaculik, V., Champagne, M., 2004, An industrial perspective on implementing on-line applications of multivariate statistics, *Journal of Process Control,* Vol. 14, pp. 821-836.

Moolman, D.W., Aldrich, C., Van Deventer, J.S.J., Stange, W.W., 1994, Digital image processing as a tool for on-line monitoring of froth in flotation plants, *Minerals Engineering*, Vol. 7, No. 9, pp. 1149-1164.

Moore, K.L., Urata, N., 2001, Multivariable control of aluminum reduction cells, *Proceedings of The Minerals, Metals & Materials Society, Light Metals 2001*, pp.1243-1249.

Nomikos, P., MacGregor, J.F., 1995, Multivariate SPC charts for monitoring batch processes, *Technometrics,* Vol. 37, 1995, pp.41-59.

Patnaik, P., 2002, *Handbook of Inorganic Chemicals*, McGraw-Hill, New York, USA 1086 p..

Paulino, L., Yamamoto, J., Camilli, R.A., Araujo, J.C., 2006, Bath ration control improvements at Alcoa Poços de Caldas-Brazil- an update, *Proceedings of The Conference of Metallurgists, Aluminum 2006*, pp.359-368.

Petersen, K.R.P, Aldrich, C., Van Deventer, J.S.J., 1998, Analysis of ore particles based on textural pattern recognition, *Minerals Engineering*, Vol. 11, No. 10, pp. 959-977.

Proulx, G., Doiron, P., Champoux, P., Paquin, J., 2006, Step changes in potroom operation schedule at the Alcoa Deschambault smelter, *Proceedings of The Conference of Metallurgists, Aluminum2006*, pp.333-343.

Richard, D., 2004, *Aspects Thermomécaniques de la Modélisation par Éléments Finis du Préchauffage Électrique d'une Cuve de Hall-Héroult : Lois Constitutives, Conception Orientée-Objets et Validation*, PhD Thesis, Université Laval, Québec, Canada, 183 p. (In French)

Richard, D., D'Amours, G., Fafard, M., Gakwaya, A., Désilets, M., 2005, Development and validation of a thermo-chemo-mechanical model of the baking of ramming paste, *Proceedings of The Minerals, Metals & Materials Society, Light Metals 2005*, pp.733-738.

Rieck, T., Iffert, M., White, P., Rodrigo, R., Kelehtermans, R., 2003, Increased current efficiency and reduced energy consumption at the Trimet Smelter Essen, using 9 box matrix control, *Proceedings of The Minerals, Metals & Materials Society, Light Metals 2003*, pp.449-456.

Rolots, B., Wai-Poi, N., 2000, The effect of anode spike formation on operational performance, *Proceedings of The Minerals, Metals & Materials Society, Light Metals 2000*, pp.189-193.

Schmidt-Hatting, W., Perruchoud, R., Durgnadt, J.M., 1986, Influence of vanadium on anode quality and pot performances, *Proceedings of The Minerals, Metals & Materials Society, Light Metals 1986*, pp.623-625.

Smilde, A.K., Westerhuis, J.A., Jong, S. de., 2003, A framework for sequential multiblock component methods, *Journal of Chemometrics*, Vol. 17, pp.323-337.

Sorlie, M., Øye, H.A., 1989, *Cathodes in Aluminum Electrolysis*, Düsseldorf, Germany, Aluminum-Verlag, 294p.

Sterten, A., Solli, P.A., Skybakmoen, E., 1998, Influence of electrolyte impurities on current efficiency in aluminum electrolysis cells, *Journal of Applied Electrochemistry*, Vol. 28, 1998, pp.781-789.

Stevens McFadden, F.J., Welch, B.J., Austin, P.C., 2006, The multivariable model-based control of the non-alumina electrolyte variables in aluminum smelting cells, *JOM*, February 2006, pp. 42-47.

Szatvanyi, G., Duchesne, C., Bartolacci, G., 2006, Multivariate Image Analysis of Flames for Product Quality and Combustion Control in Rotary Kilns, *Industrial & Engineering Chemistry Research*, Vol. 45, No. 13, pp. 4706-4715.

Tabereaux, A. T., 2000, Prebake Cell Technology: A Global Review, *JOM*, Vol. 52, No. 2, pp.22-28.

Tabereaux, A. T., 2007, Maximum anode effect voltage, *Proceedings of The Minerals, Metals & Materials Society, Light Metals 2007,* pp.405-410.

Tabsh, I., Dupuis, M., Gomes, A., 1996, Process simulation of aluminum reduction cells, *Proceedings of The Minerals, Metals & Materials Society, Light Metals 1996*, pp. 451-457.

Tabsh, I., Dupuis, M., 1997, Simulation of the dynamic response of aluminum reduction cells, *Proceedings of The Minerals, Metals & Materials Society, Light Metals 1996*, pp. 443-447.

Tarcy, G.P., DeCapite., 1990, Controlled potential coulometry as a tool for the determination of current efficiency in commercial Hall cells, *Proceedings of The Minerals, Metals & Materials Society, Light Metals 1990*, pp.275-283.

Tarcy, G.P., Sorensen, J., 1991, Determination of factors affecting current efficiency in commercial Hall cells using controlled potential coulometry and statistical experiments, *Proceedings of The Minerals, Metals & Materials Society, Light Metals 1991*, pp.453-459.

Tarcy, G.P., Strategies for maximizing current efficiency in commercial Hall-Héroult cells, *Proceedings of the 5th Australasian Aluminum Smelting Technology Workshop*, Sydney, Australia, 1995, pp.139-160.

Taylor, M. P., Johnson, G. L., Andrews, E. W., Welch, B. J., 2004, The impact of anode cover control and anode assembly design on reduction cell performance, *Proceedings of The Minerals, Metals & Materials Society, Light Metals 2004*, pp. 199-206.

Tessier, J., 2006, Détermination de la Composition de l'Alimentation des Circuits de Broyage par Analyse d'Images Multivarié, MSc. Thesis , Université Laval, Quebec City, Canada, 97 p.., In French

Tessier, J., Duchesne, C., Bartolacci, G., 2006, On-line multivariate image analysis of run-of-mine ore for control of grinding and mineral processing plants, *Proceedings of Mineral Process Modelling, Simulation and Control,* pp. 175-189.

Tessier, J., Duchesne, C., Tarcy, G.P., Gauthier, C., Dufour, G., 2008, Analysis of a potroom performance drift, from a multivariate point of view, *Proceedings of The Minerals, Metals & Materials Society, Light Metals 2008*, pp. 319-324.

Tessier, J., Zwirz, T.G., Tarcy, G.P., Manzini, R.A., 2009, Multivariate statistical process monitoring of reduction cells, *Proceedings of The Minerals, Metals & Materials Society, Light Metals 2009*, pp. 305-310.

Thonstad, J., Fellner, P., Haarberg, G.M., Hives, J., Kvande, H., Sterten, A., 2001, *Aluminum Electrolysis: Fundamentals of the Hall-Héroult Process*, 3rd edition, Aluminum-Verlag, Düsseldorf, Germany, 360p.

Vanvoren, C., 2001, The PECHINEY reduction cell family: 25 years of development in design and process control, *Proceedings of The Conference of Metallurgists, COM 2001; Light Metals*, pp.49-62.

Venetski, S., 1969, Silver form clay, *Metallurgist*, Vol. 13, No. 7, July, 1969, pp. 44–46.

Wang, X., Tabereaux, A.T., Richards, N.E., 1994, The electrical conductivity of cryolite melts containing aluminum carbide, *Proceedings of The Minerals, Metals & Materials Society, Light Metals 1994*, pp.177-185.

Wang, X., 2009, Alumina dissolution in aluminum smelting electrolyte, *Proceedings of The Minerals, Metals & Materials Society, Light Metals 2009*, pp.383-388.

Welch, B.J., 1999, Aluminum production paths in the new millennium, *JOM*, May 1999, pp. 24-28.

Welch, B.J., 2009, Inert anodes- The status of the materials science, the opportunities they present and the challenges that need resolving before commercial implementation, *Proceedings of The Minerals, Metals & Materials Society, Light Metals 2009*, pp. 971-978.

Westerhuis, J.A., Coenegracht, P.M.L., 1997, Multivariate modelling of the pharmaceutical two-step process of wet granulation and tableting with multiblock partial least squares, *Journal of Chemometrics*, Vol. 11, pp. 379-392.

Westerhuis, J.A., Kourti, T., MacGregor, J.F., 1998, Analysis of multiblock and hierarchical PCA and PLS models, *Journal of Chemometrics*, Vol. 12, pp. 301-321.

Westerhuis, J.A., Kourti, T., MacGregor, J.F., 1999, Comparing alternative approaches for multivariate statistical analysis of batch process data, *Journal of Chemometrics*, Vol. 13, pp. 397-413.

Westerhuis, J.A., Gurden, S.P., Smilde, A.K., 2000, Generalized contribution plots in multivariate statistical process monitoring, *Chemometrics and Intelligent Laboratory Systems*, Vol. 51, pp. 95-114.

Wilkening, S., Reny, P., Murphy, B., 2005, Anode cover material and bath level control, *Proceedings of The Minerals, Metals & Materials Society, Light Metals 2005*, pp. 367-372.

Wilkening, S., 2009, Maintaining consistent anode density using varying carbon raw materials, *Proceedings of The Minerals, Metals & Materials Society, Light Metals 2009*, pp. 991-998.

Wold, S., 1978, Cross-validation estimation of the number of components in factor and principal components models, *Technometrics*, Vol. 20, pp.397-405.

Wold, S., Esbensen, K., Geladi, P., 1987, Principal component analysis, *Chemometrics and Intelligent Laboratory Systems*, Vol. 2, pp.37-52.

Wold, S., Sjöström, M., Eriksson, L., 2001, PLS-Regression: a basic tool of chemometrics, *Chemometrics and Intelligent Laboratory Systems*, Vol. 58, pp.109-130.

Yu, H., MacGregor, J.F., Haarsma, G., Bourg, W., 2003, Digital Imaging for Online Monitoring and Control of Industrial Snack Food Processes, *Industrial & Engineering Chemistry Research*, Vol. 42, pp. 3036-3044.

Yu, H., MacGregor, J.F., 2004, Monitoring flames in an industrial boiler using multivariate image analysis, *AIChE Journal*, Vol. 50, No. 7, pp. 1474-1483.

Yurkov, V., Mann, V., Nikandrov, K., Trebukh, O., 2004, Development of aluminum reduction process supervisory control system, *Proceedings of The Minerals, Metals & Materials Society, Light Metals 2004*, pp.263-267.

Yurkov, V., Mann, V., 2005, A simple dynamic realtime model for aluminum reduction cell control system, *Proceedings of The Minerals, Metals & Materials Society, Light Metals 2005*, pp.423-428.

Zangiacomi, C., Pandolfelli, V., Paulino, L., Lindsay, S., Kvande, H., 2005, Preheating study of smelting cells, *Proceedings of The Minerals, Metals & Materials Society, Light Metals 2005*, pp.333-336.

Zangiacomi, C., Pandolfelli, V., Paulino, L., 2006, A challenging task to improve potlife in aluminum industry, *Proceedings of The Conference of Metallurgists COM 2006, Aluminum*, p.653-666.